
Electronic Thesis and Dissertation Repository

6-10-2019 9:00 AM

Structural Optimization of Cable-Stayed Bridges Considering the Action of Permanent and Transitory Loads

Carolina Almeida Novaes dos Santos, *The University of Western Ontario*

Supervisor: El Damatty, Ashraf, *The University of Western Ontario*

Joint Supervisor: Pfeil, Michele S., *Federal University of Rio de Janeiro, Brazil*

A thesis submitted in partial fulfillment of the requirements for the Doctor of Philosophy degree in Civil and Environmental Engineering

© Carolina Almeida Novaes dos Santos 2019

Follow this and additional works at: <https://ir.lib.uwo.ca/etd>



Part of the [Civil Engineering Commons](#)

Recommended Citation

Almeida Novaes dos Santos, Carolina, "Structural Optimization of Cable-Stayed Bridges Considering the Action of Permanent and Transitory Loads" (2019). *Electronic Thesis and Dissertation Repository*. 6505. <https://ir.lib.uwo.ca/etd/6505>

This Dissertation/Thesis is brought to you for free and open access by Scholarship@Western. It has been accepted for inclusion in Electronic Thesis and Dissertation Repository by an authorized administrator of Scholarship@Western. For more information, please contact wlsadmin@uwo.ca.

Abstract

Cable-stayed bridges are complex structures with several advantages such as aesthetical appeal, economic use of materials, and efficient construction method. Due to these advantages and the extensive knowledge gained from projects over the years, longer cable-stayed bridges are being constructed. As span lengths increase, structures become more flexible, which makes the accurate evaluation of wind loads critically important in the design of cable-stayed bridges. A large number of variables are involved in the design of cable-stayed bridges. Those include overall geometric dimensions, cross-sectional dimensions, number of stay-cables and pre-tensioning forces to be applied to the cables. Taking all variables into account, and considering the need to conduct multiple moving load analyses and to calculate accurately aerodynamic wind forces, a design optimization process for such bridges becomes challenging. In this thesis, a numerical model capable of achieving this design optimization task is developed. The numerical model uses a structural system in which the deck is composite steel-concrete with two I main girder. The developed numerical model is based on the Finite Element Method (FEM), the Real Coded Genetic Algorithm (RCGA), and the Discrete-Phases Design Approach. The latter classifies variables into two categories: (i) main variables: number of stay-cables, I-girder inertia, concrete slab thickness, tower cross-section external dimensions, tower height above the deck; (ii) secondary variables: I-girder dimensions, stay-cable areas and pre-tensioning forces. The main variables are design variables optimized directly by the RCGA, while the secondary variables are indirectly optimized by the discrete phases. Buffeting wind loads are considered as equivalent static forces, which were validated through a theoretical-experimental correlation. This powerful tool is used to assess the importance of considering truck versus lane loads, as well as wind buffeting loads and various aeroelastic instabilities in the design optimization process. Results show that the most critical load combination include the wind effect, and that the critical wind velocities of aeroelastic phenomena play a significant role for high values of basic wind speeds.

Keywords

Cable-stayed Bridge, Composite Deck, Finite Element Method, Real Coded Genetic Algorithm, Pre-tensioning Forces, Live Loads, Buffeting Wind Loads, Critical velocities for Aeroelastic Phenomena, Theoretical-Experimental Correlation, Optimization

Co-Authorship Statement

This thesis has been prepared in accordance with the regulation for an Integrated-Article format thesis stipulated by the School of Graduate and Postdoctoral Studies at the University of Western Ontario and has been co-authored as:

Chapter 2: Structural optimization of two I-girder composite cable-stayed bridges under the action of dead and live loads

The analyzes were conducted by C.A.N. Santos under supervision of A.A. El Damatty and M.S. Pfeil. Drafts of Chapter 2 were written by C.A.N. Santos and modifications were done under supervision of A.A. El Damatty, M.S. Pfeil and R.C. Battista. A version of this work co-authored by C.A.N. Santos, A.A. El Damatty, M.S. Pfeil and R.C. Battista was submitted to the *Canadian Journal of Civil Engineering* and currently is under revisions.

Chapter 3: Comparison between the theoretical and experimental wind responses of a full aeroelastic model test of a cable-stayed bridge

The analyzes were conducted by C.A.N. Santos under supervision of A.A. El Damatty and M.S. Pfeil. Drafts of Chapter 3 were written by C.A.N. Santos and modifications were done under supervision of A.A. El Damatty and M.S. Pfeil. A preliminary version of this work co-authored by C.A.N. Santos, A.A. El Damatty and M.S. Pfeil was presented by C.A.N. Santos at the 4th *American Association for Wind Engineering Workshop, Miami - USA, 2016*.

Chapter 4: Structural optimization of two I-girder composite cable-stayed bridges under the action of dead, live and wind loads

The analyzes were conducted by C.A.N. Santos under supervision of A.A. El Damatty and M.S. Pfeil. Drafts of Chapter 4 were written by C.A.N. Santos and modifications were done under supervision of A.A. El Damatty and M.S. Pfeil. A version of this work co-authored

by C.A.N. Santos, A.A. El Damatty and M.S. Pfeil will be submitted to the journal *Engineering Structures*.

Dedication

To my grandmother Severiana (in memoriam).

Acknowledgments

I would like to express my gratitude to my research supervisors Dr. El Damatty and Dr. Michele Pfeil for their dedication, valuable guidance and willingness to share their knowledge along these years.

I wish to acknowledge the National Council for Scientific and Technological Development (CNPq), Brazil for the financial support; and Compute Canada for its supercomputer facility.

I would also like to express my appreciation to my colleagues and staff that have helped me through my thesis research.

A special thanks to my family, outstandingly to my mother and brother, for all their unconditional support.

At last but not the least, I want to thank my husband for his kind words and constant encouragement.

Table of Contents

Abstract	iii
Co-Authorship Statement.....	v
Dedication	vii
Acknowledgments.....	viii
Table of Contents	ix
List of Tables	xiii
List of Figures	xv
List of Symbols	xx
List of Appendices	xxiv
Chapter 1	1
1 Introduction	1
1.1 Cable-stayed bridges	1
1.1.1 A brief history	1
1.1.2 Structural system.....	3
1.1.3 Structural components	4
1.1.4 Main characteristics	9
1.2 Optimization of cable-stayed bridges	11
1.2.1 Significance.....	11
1.2.2 Literature review	12
1.3 Research Objectives.....	22
1.3.1 Methodology and Relevance.....	23
1.3.2 Organization of the Thesis	24
References	26
Chapter 2	29

2	Structural optimization of two I-girder composite cable-stayed bridges under the action of dead and live loads	29
2.1	Introduction	29
2.2	Description of numerical tool	32
2.2.1	Optimization procedure	36
2.2.2	Case study	43
2.2.3	Numerical results for design <i>Objective-1</i> considering dead load and truck plus lane live load	46
2.2.4	Numerical results for design <i>Objective-1</i> considering dead load and lane live load	51
2.2.5	Numerical results for design <i>Objective-1</i> considering dead load only	52
2.2.6	Numerical results for design <i>Objective-2</i>	54
2.2.7	Comparison of costs from <i>Objective-1</i> and <i>Objective-2</i> considering dead load and truck plus lane live load	61
2.3	Validation of the discrete phases design approach	63
2.4	Conclusions	65
	References	67
	Chapter 3	69
3	Comparison between the theoretical and experimental wind responses of a full aeroelastic model test of a cable-stayed bridge	69
3.1	Introduction	69
3.2	Wind loads and bridge responses	70
3.3	Methodology	77
3.4	Case study	78
3.4.1	Theoretical approach	80
3.4.2	Experimental Approach	84
3.4.3	Results	84

3.5 Conclusions.....	90
References	92
Chapter 4.....	94
4 Structural optimization of two I-girder composite cable-stayed bridges under the action of dead, live and wind loads.....	94
4.1 Introduction.....	94
4.2 Description of numerical tool	97
4.2.1 Design variables.....	97
4.2.2 Design constraints	99
4.2.3 Objective function.....	103
4.2.4 Finite element model.....	104
4.2.5 Design methodology	105
4.2.6 Optimization technique.....	109
4.2.7 Cable-stayed bridge optimum design algorithm.....	111
4.3 Case of study.....	112
4.3.1 Cable-stayed bridge optimum design algorithm.....	112
4.3.2 Results and Discussion	115
4.4 Conclusions.....	122
References	124
Chapter 5.....	128
5 Conclusions and Recommendations	128
5.1 Structural optimization of two I-girder composite cable-stayed bridges under the action of dead and live loads.....	129
5.2 Comparison between the theoretical and experimental wind responses of a full aeroelastic model test of a cable-stayed bridge.....	131
5.3 Structural optimization of two I-girder composite cable-stayed bridges under the action of dead, live and wind loads.....	132

5.4 Recommendations for future research	133
Appendices.....	135
Appendix A: Examples of cable-stayed bridges constructed in the last 40 years.....	135
Appendix B: I-girder dimensions for width-to-thickness limit ratio of Class 3 in order to minimize the cross-section area.	137
Appendix C: I-girder dimensions for width-to-thickness limit ratio of Class 2 in order to minimize the cross-section area.	138
Appendix D: Finite element modelling of concrete-steel composite two I-girders deck	139
Appendix E: Aerodynamic coefficients and flutter derivatives	140
Curriculum Vitae	144

List of Tables

Table 1. 1: Record main spans for cable-stayed bridges (Svensson, 2012; Pedro & Reis, 2016).	7
Table 1. 2: Relation between main span length and cross-section material and geometry. 9	
Table 2. 1: Material properties and costs used in the study.	45
Table 2. 2: Lower and upper bounds of the design variables.	46
Table 2. 3: Deck masses obtained for Objective-1 normalized by the minimum mass....	47
Table 2. 4: Deck mass ratio (DL + lane LL)/(DL + truck and lane LL) obtained for <i>Objective-1</i>	52
Table 2. 5: Deck mass ratio (DL)/(DL + truck and lane LL) obtained for <i>Objective-1</i>	53
Table 2. 6: Design variables obtained for the considered case study.	55
Table 2. 7: Constraint values (Equations 2.7 to 2.18) obtained for the considered case study.	55
Table 2. 8: Maximum longitudinal displacements at the top of towers (SLS).	56
Table 2. 9: Material costs for the optimal solutions with minimum deck mass (TL ₁ =6m and TL ₂ =3m).	61
Table 2. 10: Comparison of material costs for <i>Objective-1</i> (H _b =30m, H _a =50m, TL ₁ =3.0m, and TL ₂ =1.5m) and <i>Objective-2</i> (H _b =30m) optimal solutions in London-ON.	62
Table 2. 11: Comparison of material costs for <i>Objective-1</i> (H _b =30m, H _a =40m, TL ₁ =3.0m, and TL ₂ =1.5m) and <i>Objective-2</i> (H _b =30m) optimal solutions in North Bay-ON.	62
Table 2. 12: Comparison of material costs and design variables for validation of the Discrete Phases Design Approach.	64

Table 3. 1: Geometric properties of the structural elements.....	80
Table 3. 2: Frequencies and mode shapes.....	81
Table 3. 3: Aerodynamic coefficients and theirs slopes for a wind attack of 0°	81
Table 4. 1: Design variables: lower and upper bounds.....	113
Table 4. 2: Hourly mean basic wind velocities adapted from CAN/CSA-S6-14.	114
Table 4. 3: Main cases of analysis.	114
Table 4. 4:: Load factor combinations.....	114
Table 4. 5: Deck limiting design constraint and material cost for cases A1, B1 and C1.	118
Table 4. 6: Design variables, frequencies and damping ratios for optimized cable-stayed bridges considering critical wind velocity $V_{0,2}$	121
Table A. 1: Concrete cross-section cable-stayed bridges (Svensson, 2012).....	135
Table A. 2: Steel cross-section cable-stayed bridges (Svensson, 2012).	135
Table A. 3: Composite steel-concrete cross-section cable-stayed bridges (Svensson, 2012; Pedro & Reis, 2016).....	136

List of Figures

Figure 1. 1: First bridges designed, but not constructed, with the concept of cable-stayed bridge: (a) Bridge designed by Verantius in 1617 (Verantius, 1617 apud Svensson, 2012); (b) Bridge designed by Löscher in 1784 (Löscher, 1784 apud Svensson, 2012).	2
Figure 1. 2: First proven constructed cables-stayed bridge: Kings Meadow Bridge, 1817 (Stephenson, 1821 apud Svensson, 2012).....	2
Figure 1. 3: First modern cable-stayed bridge: Strömsund, 1956 (Wenk, 1954 and Ernst, 1956 apud Svensson, 2012).	3
Figure 1. 4: Flow of forces in a cable-stayed bridge (Svensson, 2012).....	4
Figure 1. 5: Longitudinal cable arrangement systems (Svensson, 2012).	5
Figure 1. 6: Tower shapes for (a) double-plane and (b) single-plane cable arrangements (Svensson, 2012).....	6
Figure 1. 7: Concrete cross-sections: (a) thin concrete beams (Koppel, 1984 apud Svensson, 2012); (b) 2 concrete girders (Leonhardt, 1980 apud Svensson, 2012); (c) box girder (Battista, 2011).....	8
Figure 1. 8: Composite steel-concrete cross-section: two main plate girders (Battista, 2013).	8
Figure 1. 9: Steel cross-section: box girder (You et al., 2008 apud Svensson, 2012); two box girders (Morgenthal, 2008 apud Svensson, 2012).	8
Figure 2. 1: Cable-stayed bridge geometry: (a) longitudinal view; (b) tower dimensions; (c) tower cross-section; (d) deck cross-section; (e) steel I-girder dimensions. Dimensions in meter.	35
Figure 2. 2: Flow chart for the optimization scheme.	37
Figure 2. 3: Finite element model.	40

Figure 2. 4: Deck mass due to dead plus live loads as a function of Hb and tower dimensions TL1 x TL2.....	48
Figure 2. 5: Steel I-girder inertia about major axis due to dead plus live loads as a function of Hb and tower dimensions TL1 x TL2.	48
Figure 2. 6: Stay-cables mass as a function of Hb and tower dimensions TL1 x TL2.	49
Figure 2. 7: Relation between deck rigidity and tower longitudinal stiffness to obtain lightest deck mass.	50
Figure 2. 8: Deck mass, stay-cables mass, and steel I-girder inertia due to dead and lane live loads as a function of tower dimensions TL1 x TL2.	52
Figure 2. 9: Deck mass, stay-cables mass, and steel I-girder inertia due to dead load as a function of tower dimensions TL1 x TL2.....	53
Figure 2. 10: Comparison of material costs for the considered case study.....	54
Figure 2. 11: Deflections, axial forces, and vertical bending moments at the deck spine due to dead loads for the considered case study.	57
Figure 2. 12: Deflections, axial forces and vertical bending moments at the deck spine due to dead and live loads for the considered case study.	58
Figure 2. 13: Axial forces and longitudinal bending moments in one of the tower's legs due to dead loads for the considered case study.	59
Figure 2. 14: Axial forces and longitudinal bending moments in one of the tower's legs due to dead and live loads for the considered case study.	59
Figure 2. 15: Cables areas and pre-tensioning forces for the considered case study.....	60
Figure 3. 1: Scheme of deck cross-section dimensions, mean and turbulent wind speeds, and axis representation.....	72

Figure 3. 2: Flowchart of the comparison between theoretical and experimental approaches.	77
Figure 3. 3: Bridge geometry, cross-section of the side span, and finite element model of the cable-stayed bridge.	79
Figure 3. 4: Longitudinal turbulence intensity profile and mean wind speed profile obtained experimentally from the full aeroelastic model test and the ones used in the theoretical approach.	82
Figure 3. 5: Comparison of mean drag displacements: (a) at $\frac{1}{2}$ -point of main span; (b) at $\frac{1}{4}$ -point of main span.	85
Figure 3. 6: Comparison of mean lift displacements: (a) at $\frac{1}{2}$ -point of main span; (b) at $\frac{1}{4}$ -point of main span.	86
Figure 3. 7: Comparison of mean rotations: (a) at $\frac{1}{2}$ -point of main span; (b) at $\frac{1}{4}$ -point of main span.	86
Figure 3. 8: Comparison of mean lateral displacements at the top of the 1st tower.	87
Figure 3. 9: Comparison of peak drag displacements: (a) at $\frac{1}{2}$ -point of main span; (b) at $\frac{1}{4}$ -point of main span.	88
Figure 3. 10: Comparison of peak lift displacements: (a) at $\frac{1}{2}$ -point of main span; (b) at $\frac{1}{4}$ -point of main span.	88
Figure 3. 11: Comparison of peak rotations: (a) at $\frac{1}{2}$ -point of main span; (b) at $\frac{1}{4}$ -point of main span.	89
Figure 3. 12: Comparison of peak lateral displacements at the top of the 1st tower.	89
Figure 4. 1: Main and secondary variables.	98

Figure 4. 2: Deck mode shapes: (a) 1st symmetric vertical mode; (b) 1st antisymmetric vertical mode; (c) 1st symmetric lateral mode; (d) 1st antisymmetric lateral mode; (e) 1st symmetric torsional mode; (f) 1st antisymmetric torsional mode.	109
Figure 4. 3: Optimized material cost for distinct load combinations and different basic wind velocities.	116
Figure 4. 4: (a) Relation between deck rigidity and tower longitudinal stiffness; (b), (c), (d) proportion of elements material cost for cases of analysis (A1), (B1), and (C1).	119
Figure 4. 5: Material total cost optimized for the six main cases of analysis: A1, B1, C1, A2, B2 and C2.....	120
Figure B. 1: I-girder depth as a function of the Class3 I-girder inertia.	137
Figure B. 2: Bottom flange width as a function of the Class3 I-girder inertia.	137
Figure B. 3: Web thickness as a function of the Class3 I-girder inertia.	137
Figure C. 1: I-girder depth as a function of the Class3 I-girder inertia.	138
Figure C. 2: Bottom flange width as a function of the Class3 I-girder inertia.	138
Figure C. 3: Web thickness as a function of the Class3 I-girder inertia.	138
Figure D. 1: Finite element modelling of concrete-steel composite two I-girders deck according to Wilson et al. (1991).....	139
Figure E. 1: Geometry of plate girder section model evaluated by Lin et al. (2005).	140
Figure E. 2: Drag coefficients (Lin et al., 2005).....	140
Figure E. 3: Lift coefficients (Lin et al., 2005).....	141
Figure E. 4: Torsional coefficients (Lin et al., 2005).....	141
Figure E. 5: Flutter derivative $H1^*$ (Lin et al., 2005).	142

Figure E. 6: Flutter derivative A_2^* (Lin et al., 2005). 142

List of Symbols

$[m]$	Influence matrix
$\{x\}$	vector of design variables
$\{X\}$	Vector of stay-cables pre-tensioning force corrections
A	Steel total cross-section area of stay-cable
$A_{1\phi}$	Steel nominal cross-section area for 1 strand
A_2^*	Flutter derivative function of the torsional frequency
B	Deck width
b_1	Deck I-girder top flange width
b_2	Deck I-girder bottom flange width
C_f	Factored compressive force at ULS
$C_{Fx}, C_{Fz}, C_{M\theta}$	Static force coefficients
C_i	Constants specified by the design for determining maximum displacements allowed
C_r	Factored compressive resistance
D	Deck I-girder depth
$\frac{dC_{Fx}}{d\alpha}, \frac{dC_{Fz}}{d\alpha}, \frac{dC_{F\theta}}{d\alpha}$	Slopes of static force coefficients
DL	dead load
E_{cs}	Stay-cable effective modulus of elasticity
E_{eq}	Stay-cable equivalent tangent modulus of elasticity
f	Frequency of vibration
f^*	Reduced frequency
$F'_x(\eta, t)$	Quasi-steady horizontal force (wind direction)
$F'_z(\eta, t)$	Quasi-steady vertical force
$M'_\theta(\eta, t)$	Quasi-steady pitching moment
$F\{x\}$	Fitness value
F_B	Breaking force of stay-cable
f_B	First vertical bending mode frequency
$F_{B,1\phi}$	Steel nominal breaking load for 1 strand
f_{max}	Fitness value of the worst feasible solution that has been observed
f_T	First torsional bending mode frequency
g	Design constraint
G	Shear modulus of the material

GEN	number of generations
H	Horizontal projection of the stay-cable
H _a	Tower height above the deck level
H _b	Tower height below the deck level
H _t	Tower total height
$ H ^2$	Mechanical admittance
I	Moment of inertia of the deck steel I-girder about its major axis
I _u	Wind longitudinal turbulence intensity
I _w	Wind vertical turbulence intensity
I _m	Deck mass moment of inertia
J _t	Torsional moment of inertia
$ J ^2$	Joint acceptance function
L	Total length of the bridge
L ₁	Main span length
L ₂	Side span length
LL	live load
l_u	Turbulence length scale
m	Mass per length
M ₀	Desired bending moments at deck control points
M _{DL}	Bending moment at SLS due to dead load
M _f	Factored bending moment at ULS
M _{fx}	Factored bending moment at ULS about x-axis
M _{fy}	Factored bending moment at ULS about y-axis
M _{LL}	Bending moment at SLS due to live load
M _p	Bending moments at the control points due to dead and superimposed loads obtained from the cable-stayed bridge complete 3D FEM
M _r	Factored bending moment resistance
M _{rx}	Factored bending moment resistance about x-axis
M _{ry}	Factored bending moment resistance about y-axis
M _{SL}	Bending moment at SLS due to superimposed load
N	Number of stay-cables in the side spans or in half of the main span, in one plane of cables.
POP	number of samples in the population
$\overline{Q'^2_{X,j}}$	Mean-square fluctuating generalized horizontal force
$\overline{Q'^2_{Z,j}}$	Mean-square fluctuating generalized vertical force

$\overline{Q'^2_{\theta,j}}$	Mean-square fluctuating generalized pitching moment
R	Vertical reaction of continuous beam FEM
r	Mass of gyration
$R_{F'1,F'2}$	Cross spectrum of forces
S	Elastic section modulus of the steel section
S'	Elastic section modulus of the steel section and reinforcement within the effective width of the slab
S_c	Scruton number
SL	superimposed load
S_n, S_{3n}	Elastic section modulus of the steel girder and the concrete slab using a modular ratio n and $3n$
$S_{Q'_{x,j}}$	Power spectral density of the fluctuating generalized force in X direction
$S_{Q'_{z,j}}$	Power spectral density of the fluctuating generalized force in Z direction
$S_{Q'_{\theta,j}}$	Power spectral density of the fluctuating generalized moment about η axle
S_t	Strouhal number
S_{uu}	Power spectral density for longitudinal wind velocity
S_{ww}	Power spectral density for vertical wind velocity
$S_{X',j}$	Power spectral density of displacements in X direction
$S_{Z',j}$	Power spectral density of displacements in Z direction
$S_{\theta',j}$	Power spectral density of rotations about η axle
T	Stay-cable final pre-tensioning force
T_0	Stay-cable initial pre-tensioning force
t_1	Deck I-girder top flange thickness
t_2	Deck I-girder bottom flange thickness
t_c	Thickness of concrete slab
T_f	Factored axial forces at ULS
$T_{f,DL+SL}$	Factored axial forces at ULS due to dead and superimposed loads
$T_{f,LL}$	Factored axial forces at ULS due to live load
TL_1	External dimension of the tower cross-section in the longitudinal direction
TL_2	External dimension of the tower cross-section in the transverse direction
\bar{U}	Mean wind speed at the deck height
$u(t)$	Horizontal velocity fluctuation
$U_{cr,divergence}$	Torsional divergence critical velocity
$U_{cr,flutter}$	Classical flutter critical velocity

$U_{cr,galloping}$	Galloping critical velocity
$U_{cr,vortex}$	Vortex shedding excitation critical velocity
$U_{m,k}$	Mean wind velocity for return period $T_R=k$ years
U_0	Basic wind velocity
V_f	Factored shear force at ULS
V_r	Factored shear resistance
w	Deck I-girder web thickness
$w(t)$	Vertical velocity fluctuation
w_{cs}	Weight per unit length of the stay-cable
WL	wind load
X	Deck transversal direction
Z	Deck vertical direction
z_0	Roughness length
\bar{z}	Effective height
α	Wind tunnel test angle of attack
δ_{DL+SL}	Displacements at the deck due to dead and superimposed loads
Δ_{DL+SL}	Displacements at the towers due to dead and superimposed loads
δ_{LL}	Displacements at the deck due to live load
Δ_{LL}	Displacements at the towers due to live load
η	Deck longitudinal direction
η'	Reduction factor for calculating classical flutter critical velocity
θ	Stay-cable horizontal angle of inclination
ξ_a	Aerodynamic damping ratio
ξ_s	Structural damping ratio
ρ	Air mass density
σ_u	Standard deviation of longitudinal wind velocity fluctuations
σ_w	Standard deviation of vertical wind velocity fluctuations
$\sigma_{\bar{F}'_{X,j}}^2, \sigma_{\bar{F}'_{Z,j}}^2, \sigma_{\bar{F}'_{\theta,j}}^2$	Mean-square value of the equivalent static forces
$\sigma_{X'}^2, \sigma_{Z'}^2, \sigma_{\theta'}^2$	Mean-square value of fluctuating generalized deflections
$\sigma_{\bar{F}'_{B,X}}^2, \sigma_{\bar{F}'_{B,Z}}^2, \sigma_{\bar{F}'_{B,\theta}}^2$	Background mean-square equivalent static forces
$\sigma_{\bar{F}'_{R,X}}^2, \sigma_{\bar{F}'_{R,Z}}^2, \sigma_{\bar{F}'_{R,\theta}}^2$	Resonant mean-square equivalent static forces
ϕ	Mode shape function
$ \chi ^2$	Aerodynamic admittances

List of Appendices

Appendix A: Examples of cable-stayed bridges constructed in the last 40 years.	135
Appendix B: I-girder dimensions for width-to-thickness limit ratio of Class 3 in order to minimize the cross-section area.	137
Appendix C: I-girder dimensions for width-to-thickness limit ratio of Class 2 in order to minimize the cross-section area.	138
Appendix D: Finite element modelling of concrete-steel composite two I-girders deck	139
Appendix E: Aerodynamic coefficients and flutter derivatives.....	140

Chapter 1

1 Introduction

1.1 Cable-stayed bridges

1.1.1 A brief history

One of the first projects designed with features that resemble a modern-day cable-stayed bridge was dated in 1617 and attributed to Faustus Verantius. The bridge consisted of a timber beam deck suspended by inclined eye bars and a suspended cable in the middle as shown in Figure 1. 1(a) (Verantius, 1617 apud Svensson, 2012). Over one-hundred and fifty years later, the concept of considering only inclined stays in a cable-stayed bridge was developed for the first time by the German carpenter Immanuel Löscher in 1784. As shown in Figure 1. 1(b), the 44.3m cable-stayed bridge was conceived with all structural members – deck, stays and towers - constructed with timber. Although the structural designs for these two projects were completed, neither bridge was fully constructed as originally planned (Löscher, 1784 apud Svensson, 2012).

In 1817 two Scottish ironworkers, James Redpath and John Brown, designed the first constructed permanent cable-stayed bridge. The Kings Meadow Bridge was constructed as a pedestrian walkway over the River Thames with stays made of iron wires (Figure 1. 2), and partially collapsed in the winter of 1822/1823 (Stephenson, 1821 apud Svensson, 2012). It was later repaired by using an additional number of stays but failed again in 1954 due to flood waters. Also in 1817, John and William Smith constructed the first bridge over the Tweed River in Scotland. This bridge had similar geometry to the Kings Meadow Bridge and shared the same fate as serious dynamic problems led to its collapse in 1818 after a thunderstorm (Stephenson, 1821 apud Svensson, 2012).

The accidents and collapses described previously (and many others) were due to the lack of knowledge of the real behavior of cable-stayed bridges and the availability of adequate materials to build the structural components. For these reasons, the development of cable-stayed bridges was slow until the end of World War II when many bridges needed reconstruction following the war. Advances in the technology of steel production made

cable-stayed bridges ideal for many of these projects because they have the advantages of efficient use of materials and high-speed construction.

The Strömsund Bridge with central span of 182m, designed by the German engineer Franz Dischinger and constructed in Sweden in 1956, is considered by many authors as the first modern cable-stayed bridge. Although it contains a concrete roadway, the Strömsund Bridge is classified as steel bridge (rather than composite) because the concrete slab only distributes local wheel loads and is not integrated with the main steel girders (Figure 1. 3) (Wenk, 1954 and Ernst, 1956 apud Svensson, 2012).

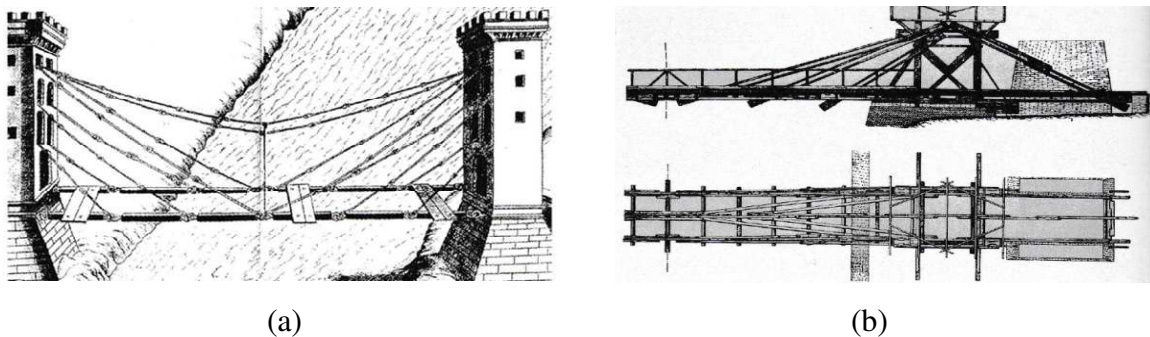


Figure 1. 1: First bridges designed, but not constructed, with the concept of cable-stayed bridge: (a) Bridge designed by Verantius in 1617 (Verantius, 1617 apud Svensson, 2012); (b) Bridge designed by Löscher in 1784 (Löscher, 1784 apud Svensson, 2012).

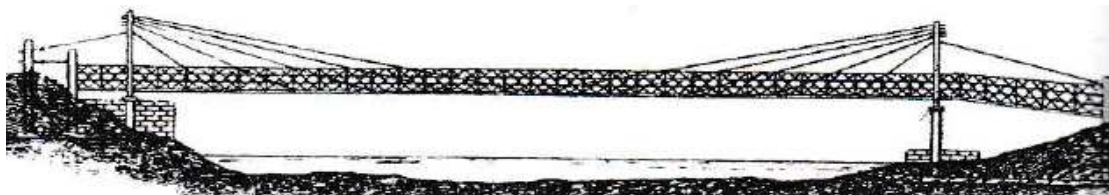


Figure 1. 2: First proven constructed cables-stayed bridge: Kings Meadow Bridge, 1817 (Stephenson, 1821 apud Svensson, 2012).

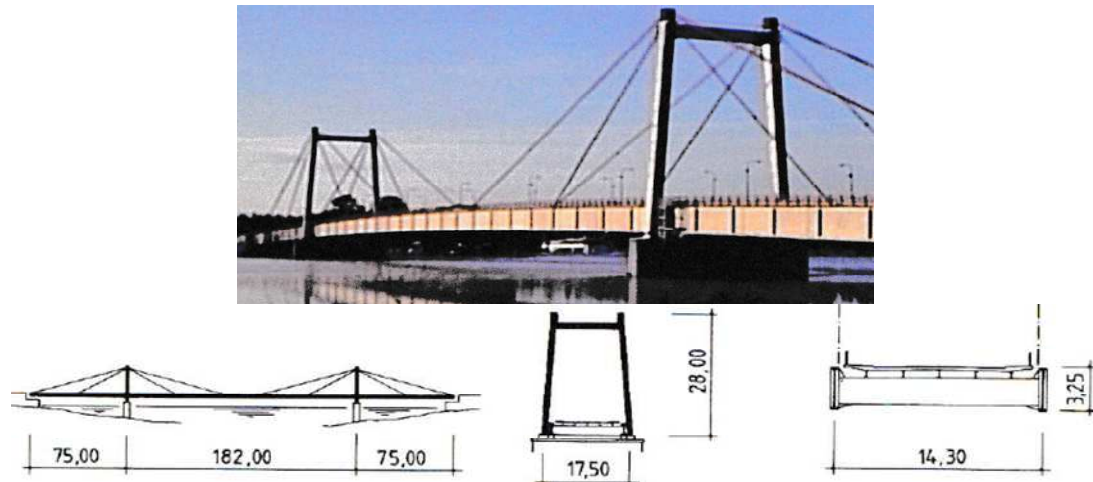


Figure 1. 3: First modern cable-stayed bridge: Strömsund, 1956 (Wenk, 1954 and Ernst, 1956 apud Svensson, 2012).

1.1.2 Structural system

In a cable-stayed bridge, the deck is supported at numerous points along its length by pre-tensioning cables, in a way that the beam spans large distances without the need of intermediary rigid supports.

The flow of forces in a cable-stayed bridge, in the static configuration due to dead loads and superimposed loads, is detailed in the Figure 1. 4 and shows that stay cables transfer their forces directly to the deck. The horizontal components are introduced to the deck as compression forces on the girders achieving maximum value at the position of the tower. This is explained by the fact that compression forces in the deck produced by the pre-tensioned cables in the main and side spans act in opposite directions. The vertical components of the stay cable-forces are upward on the deck anchorages and downward on the towers anchorage, while the dead, superimposed and live loads act downward.

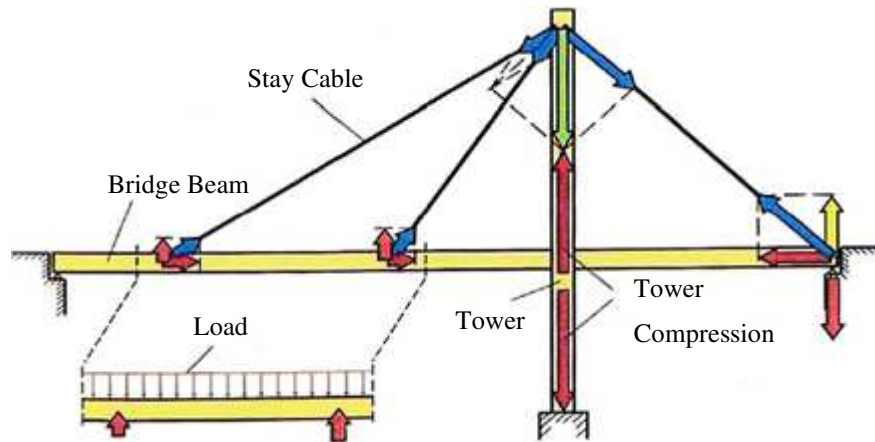


Figure 1. 4: Flow of forces in a cable-stayed bridge (Svensson, 2012).

1.1.3 Structural components

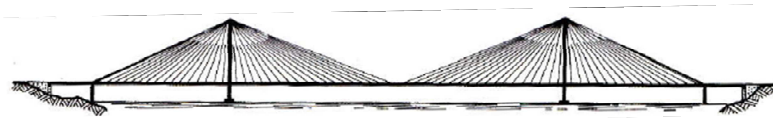
When a cable-stayed bridge is chosen to span over an obstacle, there is a vast number of possible geometric configurations that must be considered. These include, but are not limited to: (i) cable arrangement; (ii) type of deck cross-section; and (iii) shape of towers. When these three parameters are defined it is then necessary to determine: (i) number of cables, their cross-section areas and pre-tensioning forces; (ii) dimensions of the girder; (iii) thickness of the roadway slab; (iv) height of the towers; and (v) cross-section dimensions of the tower components. In addition, other parameters must be carefully adopted such as proportion between the side span and main span that should be selected in accordance with the terrain topography, width of the deck required for number of traffic lanes, and the support conditions.

1.1.3.1 Cable arrangement systems

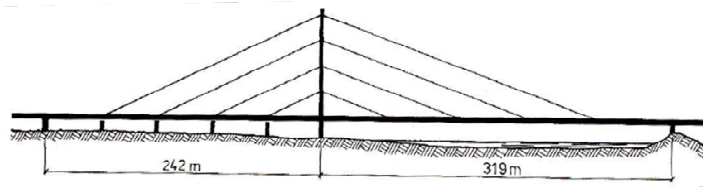
Choosing a small number of stay-cables results in greater forces on the cables and consequently requires a complex anchorage system and robust beams to span the distance between anchorage points. A better and lighter structural system is achieved by increasing the number of stay-cables. This provides a uniform distribution of forces along the deck and eliminates the need for temporary cables during construction stages (Podolny, 1976).

There are three basic types of longitudinal cable arrangements for cable-stayed bridges: fan systems, harp systems, and semi-fan systems as illustrated in Figure 1. 5. In the fan

arrangement system, all the cables are attached to a single point at the top of the towers. This is not a practical option because damage in one of the cables may destabilize the structure. For this reason, all cables should have individual anchorage points and be able to withstand additional forces until the problem is solved. In the harp arrangement system, cables are parallel and anchored equally spaced to the towers to distribute the forces. However, this means that increasing the number of cables requires higher towers to accommodate all anchorages. Finally, the semi-fan arrangement is an intermediate system between the fan and harp arrangements, that does not present the disadvantages previously mentioned.



(a) Fan system



(b) Harp system



(c) Semi-fan system

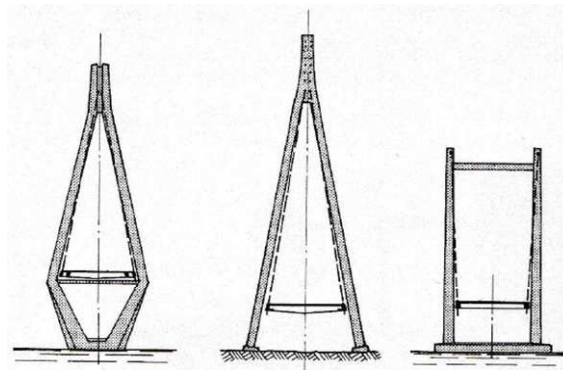
Figure 1. 5: Longitudinal cable arrangement systems (Svensson, 2012).

The transversal cable arrangements can be single-plane or double-plane. In the single plane arrangement, cables are anchored under the roadway slab dividing it in the middle. This means they do not have transversal component forces and should only be used with box girder cross sections. For cross-sections with low torsional rigidity, such as thin concrete

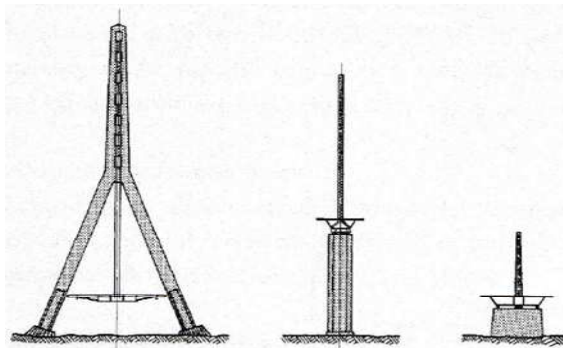
beam cross-sections, double-plane arrangements are required to carry additional loads (ex. loads generated from asymmetric traffic of vehicles).

1.1.3.2 Towers

Given that towers are primarily subjected to compression forces, the most common and economic material to be used for their construction is concrete. The type of tower will depend mainly on the transversal arrangement systems as illustrated in Figure 1. 6. In addition, short and medium spans may have towers with vertical legs connected with cross beams, while long spans should have tower legs connected at the top to increase torsional rigidity (Podolny, 1976 and Svensson, 2012).



(a)



(b)

Figure 1. 6: Tower shapes for (a) double-plane and (b) single-plane cable arrangements (Svensson, 2012).

1.1.3.3 Deck cross-sections

Deck cross-sections are classified by the type of material used in the construction: concrete, steel, and composite steel-concrete (Podolny, 1976). In addition, deck cross-sections may also be classified as a hybrid deck when the main and side spans have different materials. In this case, the main span is usually made of steel in order to be lighter in weight, and the side spans are in concrete and work as a counterweight to provide stability for the main span. Figure 1. 7 to Figure 1. 9 show some deck cross-section geometries that are used depending on the type of material.

Besides the geometry, the value of the cable-stayed bridge main span has a direct relation to the type of material. Svensson (2012) compared deck costs for different main span lengths and concluded that concrete decks are the most economic for main span under 400m, composite decks for main spans between 400m and 900m, and steel decks for main spans over 900m. Essentially, concrete decks are for short spans, steel decks are for long spans and composite steel-concrete are used for intermediate spans. These guidelines are exemplified by the record of longest main span of cable-stayed bridges (Table 1. 1) with 530m, 616m and 1104m for concrete, composite and steel deck cross-sections, respectively.

Considering the example of over 40 cable-stayed bridges constructed in the last 40 years, Table 1. 2 shows the relation between type of cross-section and main span size. To develop this relation, it was assumed that short and medium main span lengths are under 200m and 450m, respectively, while long spans are over 450m. Importantly, it is necessary to emphasize that Table 1. 2 represents the most common situations observed in the literature and so unique cable-stayed bridges would not be covered in these relations. Details of the bridges used in Table 1. 2 are presented in the Appendix A.

Table 1. 1: Record main spans for cable-stayed bridges (Svensson, 2012; Pedro & Reis, 2016).

Material	Bridge	Country	Year	Main Span (m)
Concrete	Skarnsundet Bridge	Norway	1991	530
Composite	Erqi Yangtze River Bridge	China	2011	616
Steel	Russky Island Bridge	Russia	2012	1104

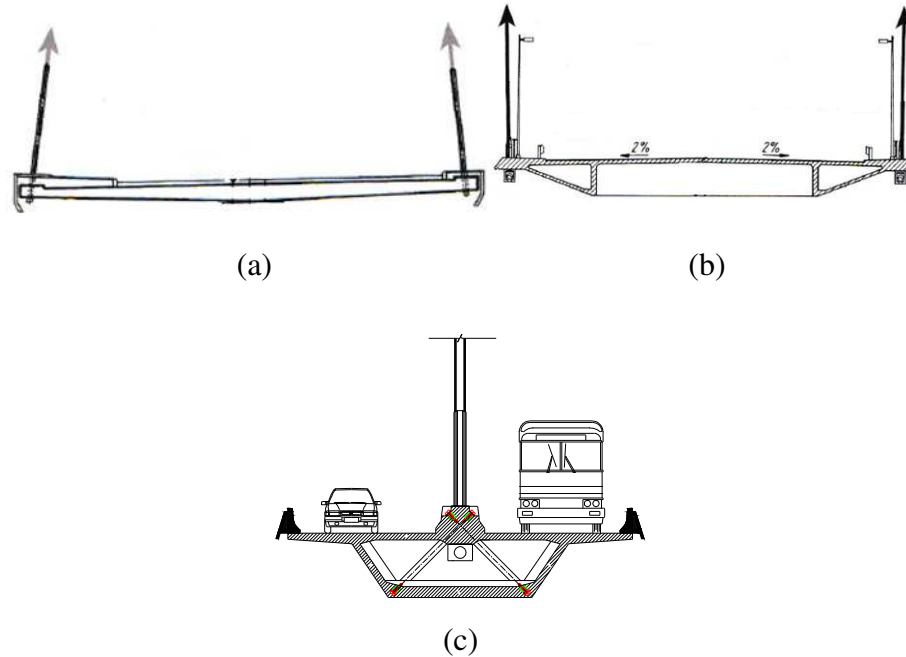


Figure 1. 7: Concrete cross-sections: (a) thin concrete beams (Koppel, 1984 apud Svensson, 2012); (b) 2 concrete girders (Leonhardt, 1980 apud Svensson, 2012); (c) box girder (Battista, 2011).



Figure 1. 8: Composite steel-concrete cross-section: two main plate girders (Battista, 2013).

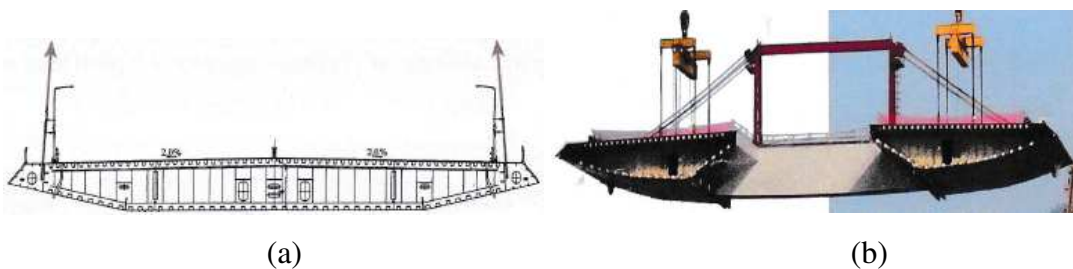


Figure 1. 9: Steel cross-section: box girder (You *et al.*, 2008 apud Svensson, 2012); two box girders (Morgenthal, 2008 apud Svensson, 2012).

Table 1. 2: Relation between main span length and cross-section material and geometry.

Material	Geometry	Main Span Length		
		Short	Medium	Long
Concrete	Thin concrete beams	✓		
	2 concrete girders	✓	✓	
	Box girder		✓	
Composite	2 plate girders	✓	✓	✓
	3 plate girders		✓	
	4 plate girders		✓	
	Truss deck		✓	
	2 box girders			✓
	Hybrid			✓
Steel	Box girder		✓	✓
	2 box girders		✓	✓

1.1.4 Main characteristics

The main goals in bridge design were listed in the following order of importance by Menn (1991): structural integrity and resilience, maintenance, economics, and aesthetics. While structural integrity, resilience, and maintenance are vital requisites for the design project, the costs and aesthetics are control criteria to define the geometry. In addition, the project must also consider the topography, geology, span length, clearance, design codes, and planned routes for the roadway or railway.

After evaluating all the components of a cable-stayed bridge given in Section 1.1.3, as well as their structural system behavior provided in Section 1.1.2, one may state the following (Nazmy, 1990; Svensson, 2012; Troitsky, 1988; Podolny, 1976):

- Cable-stayed bridges provide an efficient and economical use of materials because:
 - (i) the cables subjected to tension are composed by multi-parallel strands formed by 5 or 7 helical wires of 5mm diameter made of low relaxation high strength steel;
 - (ii) the towers subjected to compression and bending moments are generally constructed with reinforced or prestressed concrete; and (iii) there are many alternative design solutions for the deck cross-section.

- Cable-stayed bridges result in reduced bending moments on the deck because the girders work as a continuous supported beam and due to the flow of loads on the deck, bending moments along the girders are minimized.
- Cable-stayed bridges have an efficient construction method. The balanced cantilever construction method widely used for cable-stayed bridges eliminates the need for temporary supports because the flow of loads is the same during construction and in the completed structure. Conversely, temporary supports may be needed in construction of long span arch bridges which are not stable during erection and also of suspension bridges.
- Cable-stayed bridges have greater stiffness than suspension bridges. This is because the main cables of a suspended bridge find equilibrium by small increases in cable stress, while cable-stayed bridges always have cables stresses increased substantially to support the applied load. Consequently, the frequencies of cable-stayed bridges tend to be higher than suspension bridges.
- Cable-stayed bridges have an aesthetical appeal due to the variety of cable arrangements and towers, slender decks and large spans with reduced number of supports.

Despite all these advantages, the combination of long spans with light and slender decks increases the flexibility of cable-stayed bridges. Consequently, these bridges are highly susceptible to environmental loads (such as wind and rain) and traffic loads.

1.2 Optimization of cable-stayed bridges

1.2.1 Significance

As detailed previously in Section 1.1, the construction of cable-stayed bridges involves choosing one of many deck cross-section options, towers shapes and cable arrangements. In this way, the optimization of cable-stayed bridge is important not only economically, but also to exploit new possibilities.

Regarding the economical perspective, optimization aims to identify the optimum geometry to fulfill all the requisites from the Ultimate Limit State and Serviceability Limit State as well as to provide the lowest cost. Regarding the new possibilities, optimization offers the opportunity to fix certain parameters (ex. ratio between tower and main span, ratio between deck depth and main span length, etc.) to check if they result in feasible design solutions.

The optimization of cable-stayed bridges may be classified into three different levels:

1. Optimization of stay-cable pre-tensioning forces: The optimum distribution of cable pre-tensioning forces corresponding to the complete bridge affects the structure stiffness and is paramount to a successful project design.
2. Optimization of some geometries together with cable pre-tensioning forces. At this level, general features of the bridge have already been defined, such as span lengths, deck material and cross-section type, shape of the towers, cable arrangements, etc. The remaining parameters to be optimized are: thickness of slab, dimensions of main girders, dimension of tower cross-sections, number of stay cables, stay-cables cross-sectional areas, and pre-tensioning forces.
3. Optimization of all bridge features: (i) number of spans and towers; (ii) constraints; (iii) material and type of deck cross-section; (iv) material, shape, and height of towers; (v) longitudinal and transversal arrangement of cable system; (vi) number of stay-cables; (vii) quantity of strands and pre-tensioning forces of each stay-cable.

1.2.2 Literature review

The main studies found during the literature review for this thesis are presented below according to the classifications levels introduced in Section 1.2.1. No example of cable-stayed bridge level 3 was found in the literature.

1.2.2.1. Level 1 optimization of cable-stayed bridges

- Shape Finding Procedure / Zero Displacement Method

Wang *et al.* (1993) developed a procedure for calculating the pre-tensioning forces of cable-stayed bridges that attend deck displacements requirements. In this procedure, two-dimensional finite element models that consider cable-sag, beam-column, and large displacement non-linear effects are were developed. All bridge materials were considered to behave linearly. The Newton Raphson Method was chosen to iteratively determine the equilibrium configuration of the cable-stayed bridge models under the action of deck dead loads and pre-tensioning stay-cable forces.

In the first step, stay-cables pre-tensioning forces are set equal to zero, which results in very large displacements and bending moments values. The second step considers the deformed shape and cable pre-tensioning forces obtained in the first step. The deck displacements at control points (nodes of stay-cable anchorage at the deck) obtained from the second step are compared to the tolerance to check if convergence is achieved (Equation 1.1). This procedure is repeated until the tolerance (ϵ) is attended.

$$\left| \frac{\text{deflection at control point}}{\text{span}} \right| \leq \epsilon \quad (1.1)$$

When convergence is achieved, the pre-tensioning forces of stay-cables for the deck self-weight are determined. The authors showed that the Shape Finding Procedure converted monotonously for three cable-stayed bridge examples: (i) unsymmetrical; (ii) symmetric harp; and (iii) symmetric radiating. The Shape Finding Procedure is also called Zero

Displacement Method because the objective of the problem is to minimize displacements at the control points.

- Force Equilibrium Method

Instead of minimizing displacements, Chen *et al.* (2000) minimized the bending moments diagram by considering a three-stage method. To establish the target bending moments vector $\{\mathbf{M}^0\}$ due to dead load, the first stage considers only the deck by substituting the tower and cables by rigid supports.

In the second stage, bending moments vector $\{\mathbf{M}^d\}$ due to dead loads are obtained considering a model of the deck and tower, whereas the cables are substituted by internal forces. The matrix $[\mathbf{m}]$ of influence and initial pre-tensioning forces vector $\{\mathbf{T}^0\}$ were also calculated in this stage:

$$\{\mathbf{M}^0\} = [\mathbf{m}]\{\mathbf{T}^0\} + \{\mathbf{M}^d\} \quad (1.2)$$

$$\{\mathbf{T}^0\} = [\mathbf{m}]^{-1}(\{\mathbf{M}^0\} - \{\mathbf{M}^d\}) \quad (1.3)$$

where $\{\mathbf{M}^0\}$ is the target bending moments vector obtained from the first stage; $[\mathbf{m}]$ is a $N \times N$ matrix of m_{ij} coefficients; m_{ij} is the i th control section bending moment due to a unit force applied at the j th stay cable; $\{\mathbf{M}^d\}$ is the bending moments vector due to dead loads from the second stage; $\{\mathbf{T}^0\}$ is the initial vector of pre-tensioning forces.

In the third stage, the same second stage FEM is considered, and the initial estimate of cable forces $\{\mathbf{T}^0\}$ is used as input to calculate the new deck bending moments vector $\{\mathbf{M}^1\}$. Adjustments of cable forces $\{\Delta\mathbf{T}^1\}$ are calculated as follow:

$$\{\Delta\mathbf{T}^1\} = [\mathbf{m}]^{-1}(\{\mathbf{M}^1\} - \{\mathbf{M}^0\}) \quad (1.4)$$

$$\{\mathbf{T}^1\} = \{\mathbf{T}^0\} + \{\Delta\mathbf{T}^1\} \quad (1.5)$$

where $\{\mathbf{T}^1\}$ is the vector of pre-tensioning forces obtained from the first iteration of the third stage. This procedure is repeated until the updated deck bending moments vector $\{\mathbf{M}^k\}$ of the k th iteration converge to the target bending moments $\{\mathbf{M}^0\}$ by the tolerance δ .

$$\|\{\mathbf{M}^k\} - \{\mathbf{M}^0\}\| < \delta \quad (1.6)$$

Chen *et al.* (2000) evaluated 2D linear-elastic structure behaviour of cable-stayed bridges with three different deck vertical profiles and compared to the Zero Displacement Method from Wang *et al.* (1993). The authors demonstrated that for bridge deck with a vertical slope the Force Equilibrium Method is preferred.

- Unit Load Method

Janjic *et al.* (2003) developed the Unit Load Method with experience acquired in the Uddevalla cable-stayed bridge (Sweden) design project. Similar to the Force Equilibrium Method presented by Chen *et al.* (2000), the Unit Load Method also considers bending moments as constraints. Janjic *et al.* (2003) concisely described the method by the equation below:

$$M^K = M_P^K + \sum_{m=1}^n M_{T_m}^K \cdot X_m \quad (1.7)$$

where M^K is the desired moment distribution at the k th control point; n is the total number of control points for which the desired bending moments are known; M_P^K is the bending moment due to dead loads at the k th control point; $M_{T_m}^K$ is the bending moment at the k th control point due to a unit load applied to the m th stay-cable; X_m is the unknown multiplication factor, i. e. the m th stay-cable pre-tensioning force. The M_P^K and $M_{T_m}^K$ variables are calculated through a FEM that includes deck, towers and stay-cables.

- Two-step Method

Lee *et al.* (2008) applied the Unit Load Method to the Wando cable-stayed bridge (Korea). According to the authors, the cable forces and bending moments obtained were not well distributed due to the lack of symmetry in the structure. Besides that, the authors obtained stay-cables forces that were exceeding maximum working load values. To avoid increasing the cable cross-section areas, the authors added a new step to the Unit Load Method. In this new step, an additional constraint related to the lower and upper bound of stay-cable forces is added and the Unit Load Method becomes the Two-step Method.

- B-spline Method

Hassan *et al.* (2012) observed that the distribution of cable pre-tensioning forces along the spans, provided by Simões & Negrão (2000), Chen *et al.* (2000) and Lee *et al.* (2008), follow an arbitrary polynomial function. According to the authors, B-spline curves were chosen for representing the pre-tensioning forces distribution because they are able to represent complex curves with low degree polynomials. The p th degree B-spline curve were presented in Hassan *et al.* (2012) work as follow:

$$C(u) = \sum_{i=0}^n N_{i,p}(u)P_i; \quad 0 \leq u \leq 1 \quad (1.8)$$

$$N_{i,0}(u) = \begin{cases} 1 & \text{if } u_i \leq u \leq u_{i+1} \\ 0 & \text{otherwise} \end{cases} \quad (1.9)$$

$$N_{i,p}(u) = \frac{u-u_i}{u_{i+p}-u_i} N_{i,p-1}(u) + \frac{u_{i+p+1}-u}{u_{i+p+1}-u_{i+1}} N_{i+1,p-1}(u) \quad (1.10)$$

$$U = \left\{ \underbrace{0, \dots, 0}_{p+1}, u_{p+1}, \dots, u_{m-p-1}, \underbrace{1, \dots, 1}_{p+1} \right\} \quad (1.11)$$

$$m = n + p + 1 \quad (1.12)$$

where $C(u)$ is the B-spline curve; u is the independent variable; $(n + 1)$ is the number of control points; P_i are the control points; p is the basic function degree; $N_{i,p}(u)$ are the p th

degree B-spline basis functions; U is the knot vector with $(m + 1)$ elements. The horizontal coordinate (x) of the control points represents a deck side span or half of the main span, while the vertical coordinate (y) characterizes pre-tensioning forces.

The optimization of pre-tensioning stay-cable forces was obtained by combining B-spline curves, finite element modelling and real coded genetic algorithm. The three-dimensional finite element models considered cable sag, the P- Δ and the large displacements nonlinear effects. The optimization of pre-tensioning forces was obtained under the self-weight of deck and towers, considering as constraints the vertical deflection of the deck and the horizontal deflection of the towers. The authors expressed the objective function by the equation below:

$$F = \sqrt{(\delta_1^2 + \delta_2^2 + \dots)_{deck} + (\delta_{1t}^2 + \delta_{2t}^2 + \dots)_{towers}} \quad (1.13)$$

where F is the objective function; δ_i is the vertical deflection of the i th deck node; $\delta_{j,t}$ is the longitudinal deflection of the j th tower node.

Hassan *et al.* (2012) considered the optimization of pre-tensioning stay-cables forces for a symmetric cable-stayed bridge with composite steel-concrete two I-girder deck, H-shape towers, and semi-fan double plane cables arrangement. An example with total number of stay-cables equal to 80, being 10 cables in one plane of the side span or half of the main span was evaluated. Among other solutions, two cases were compared: (i) optimization considering the concept of B-spline curves; (ii) direct optimization of pre-tensioning stay-cable forces.

As the bridge is symmetrical, a total of 20 pre-tensioning forces were optimized in the second case. For the first case, the authors considered four control points ($n + 1 = 4$). The horizontal coordinate of the first and forth control points that represent the beginning and end of the side span or half of the main span are known. Again, considering symmetry, 12 variables were optimized. Results showed that the first case presented more uniform distribution of pre-tensioning forces and exemplified the efficacy of the B-spline curve method. The authors also conclude that cable sag effect was the only source of non-linearity that slightly contributed to the results.

1.2.2.2. Level 2 optimization of cable-stayed bridges

- Entropy Based Optimization Method

Simões & Negrão (1994) developed a multi-objective optimization method for determining sizing and geometric variables of a cable-stayed bridge constituted by a steel box girder deck cross-section, H-shape towers with steel box section, and semi-fan cables arrangement. The vector of sizing variables (\mathbf{x}) included distance between pier and cable anchorages and height of the first stay-cable at the tower. The geometric variables vector (\mathbf{y}) consisted of equivalent plate thickness of tower elements, equivalent plate thickness of the upper and bottom flanges of main girder elements, and cross-sectional area of each stay-cable. The constraints included stay-cables cost, lower limit of sizing variables, lower and upper limit of geometric variables, spacing between cables and strength requirements.

In comparative analysis performed by the authors, they concluded that the P- Δ and the large displacement nonlinear had less than 1% effect when compared to linear analysis and, thereby, they recommended disregarding these effects. The non-linear axial force elongation of the cables was expected to be very small and consequently disregarded. The material behavior of the structural steel was assumed linear elastic. The modelling of the cable-stayed bridges was accomplished through a two-dimensional finite element model. Regarding the loads, dead loads were evaluated in the erection stage analysis, while dead and uniform live loads were considered in the service stage analysis.

The method presented by Simões & Negrão (1994) determines the variables (\mathbf{x} and \mathbf{y} vectors) that minimize all goals by using a minimax optimization problem. The minimax was solved indirectly by minimizing a continuously differentiable function based on entropy. This technique measures the amount of disorder in a system, with a small value indicating that the solution is in order. The unconstrained and differentiable equation solved by the optimization method is presented below.

$$\text{Min} \left(\frac{1}{\rho} \right) \ln \left\{ \sum_{j=1, J} e^{\rho [g_j(\mathbf{x}, \mathbf{y})]} \right\} \quad (1.14)$$

where g are constraint functions; and ρ is the control parameter that has to be increased through the iterations. As stresses are obtained numerically throughout the analysis, the Taylor series is applied for providing explicit algebraic form. Pareto solution was also applied for determining the minimum solution that attends both objectives.

Simões & Negrão (2000) used the Entropy Based Optimization Method for optimizing a steel box-girder deck cable-stayed bridge with goals of cost, strength requirements and displacements. The three-dimensional finite element model considered plate membrane elements for representing the deck. The variables included equivalent thickness of top, bottom and side plates of the box-girder in different parts of the bridge, length, width, and thickness of towers below and above the deck, cross-sectional area of cables, pre-tensioning forces of cables, and cable anchorages positioning at deck and towers. The completed bridge configuration was evaluated due to dead loads, uniform live loads, and uniform lateral wind loads at the deck. The sag effect of the cables was the only source of non-linearity considered in the optimization process, through the use of Ernst modulus of elasticity.

▪ Power Search Optimization Methodology

Neves (1997) applied a multi-objective nonlinear programming optimization method to the design procedure of cable-stayed bridges. Power search routines to find optimal Pareto solutions were employed within the formulation of the multi-objective problem. A three-dimensional finite element modelling of the structural system was used within the framework to reach an optimized solution for the completed bridge structure as well for the construction stages.

The optimization process considered cable sag, beam column and large displacements nonlinear effects and aimed to minimize: (i) displacements, shear and bending moments in towers and deck, (ii) stay-cable cross-section areas and stresses in all elements, (iii) geometric deviations of deck grade during construction stages, and (iv) overall weight. The variables optimized included: (i) stay-cables quantity, cross-section areas, and pre-

tensioning forces, (ii) I-girder composite deck or box girder deck dimensions, and (iii) height of towers and cross-section dimensions.

- Powell's Direct Search Method

Long *et al.* (1999) optimized composite box girder cable-stayed bridges to minimize cost of the structure by applying the Powell's Direct Search Method, which does not make use of the functions derivatives. Two-dimensional finite element models considered non-linearity effects and optimized the final configuration of the structure under the action of dead and live loads. Optimized design variables included: (i) thickness of concrete slab, (ii) width and thickness of flanges and webs of the steel box girder, (iii) dimensions and spacing of stiffeners, (iv) area of stay-cables cross-sections, and (v) towers dimensions.

- Hybrid Genetic Algorithm (GA) and Support-vector Machine (SVM) Method

Although the GA is very efficient for finding global optimum, it may require a large number of analyses. By considering the extra analysis due to the nonlinearities, the optimization becomes impractical due to the high computational cost. In order to consider the nonlinear effects in the cable-stayed bridge optimization process, and at the same time to avoid the massive number of analysis, Lute *et al.* (1999) proposed a hybrid GA and SVM method.

SVM is a supervised machine learning algorithm that generalizes the input/output relation of experiments (also called training set) in order to predict unseen examples. The inputs are the side to main span ratio, tower height to bridge length ratio, girder top and bottom flange widths, girder overall depth, tower box width and depth, and cables diameter. The corresponding outputs are maximum vertical girder deflection, maximum longitudinal tower deflection, maximum girder positive and negative bending moments, maximum girder compression force, maximum tower moment, and maximum stay-cable force. The authors evaluated around 4,000 FEM with different values of input, and the outputs were

obtained through ANSYS analyses. The inputs described above are considered design variables, while the outputs are used for calculating constraint functions. These functions are related to the strength of cables, stiffness of deck and towers, and stability due to critical buckling load. The overall objective is to obtain the minimum material cost.

The framework proposed by Lute *et al.* (1999) has two main phases. In the first phase, training data is generated via ANSYS, and posteriorly SVM is used as a regression machine. In the second phase, GA and SVM are used together for the optimization. While GA generates random design variables, apply operators and calculate fitness values, the SVM predicts outputs based on the same probability distribution as the training data. Two-dimensional box-girder deck cross-section cables-stayed bridges with fan cable arrangement were considered considering total length ranging from 300 and 500m. The comparisons between outputs obtained by SVM and ANSYS provided less than 5% error. According to the authors, results showed that the hybrid GA and SVM method is efficient computationally and can be used for preliminary design of cable-stayed bridges.

- Surrogate function Method

Hassan *et al.* (2013a), continuing their work described above as B-spline Method (Hassan *et al.*, 2012), developed surrogate polynomial functions for evaluating pre-tensioning cable-forces in semi-fan cable-stayed bridges under the action of dead loads. This way, during the optimization of bridge geometric variables, the pre-tensioning forces are directly estimated through surrogate functions instead of being considered as design variables.

In order to minimize the deflections at the deck and towers, Hassan *et al.* (2013a) considered that the follow main variables for the optimization of pre-tensioning cable forces: the number of stay-cables, main span length, and height of the towers. The authors adopted the ordinary least square method (OLS) as the technique of fitting data, responsible for determining the regression coefficients that compose the surrogate polynomial function of the pre-tensioning stay-cable forces. The vector of stay-cable forces was defined as follow:

$$F_{N \times 1} = X_{N \times p} \beta_{p \times 1} + \varepsilon_{N \times 1} \quad (1.15)$$

where N is the number of stay-cables, $F_{N \times 1}$ is the vector of stay-cable pre-tensioning forces, p is the number of constants that compose the surrogate function, $X_{N \times p}$ is the matrix of constants, $\beta_{p \times 1}$ is the vector of unknown parameters to be determined from the regression analysis, $\varepsilon_{N \times 1}$ is the vector of independent random variables with expectation. The constants depend on the following parameters: (γ_1) the ratio of main span length and the total length of bridge, (γ_2) the ratio of the upper strut height of tower and the total length of bridge, (γ_3) the total length of the bridge divided by 1000.

A total of 1800 bridges covering different number of cables and parameters (γ_1 , γ_2 and γ_3) were analyzed in a parametric study performed by the authors. The stay-cable pre-tensioning forces of each one of these bridges were optimized to minimize deck and towers deflections. The adequacy of the surrogate functions was proved by comparing the results with pre-tensioning forces obtained through surrogate functions to “exact solutions”. The latter solutions were obtained via finite element analysis and RCGA optimization as described by the B-spline Method (Hassan *et al.*, 2012). The coefficients obtained through the parametric study were stored in a built-in library of the optimization program.

Hassan *et al.* (2013b) optimized two I-girder composite cable-stayed bridges with semi-fan cable arrangements. The considered design variables were: (i) number of stay-cables and their diameters, (ii) main span length, (iii) height of the tower upper strut, (iv) thickness of concrete slab and I-girder dimensions, (v) depth, width, and thickness of tower cross-section. The pre-tensioning forces were estimated using the surrogate polynomial functions developed by Hassan *et al.* (2013a). Dead load, uniformly distributed live load, and mean wind loads at the deck were applied to the FEM. The structures were optimized using RCGA with the objective of minimizing the total cost of the structure.

1.2.2.3. Optimization of other types of cable-supported bridges

Studies have also been dedicated to the structural optimization of arch bridges and suspended bridges. Lonetti *et al.* (2014a) proposed a two-step interaction algorithm for the

optimization of the cable system of hybrid cable-stayed suspension bridges with the objective of minimizing the amount of steel used in the cable system. The first iteration considers an initial configuration based in practical rules. In the first step, the FEM is assessed under the action of dead loads in order to evaluate the cables cross-sectional areas and post-tensioning forces. In the second step, live load analysis is performed and the maximum stresses of the cable elements are determined. If the tolerance conditions are not satisfied, a new iteration is performed considering the updated stresses. Lonetti et al. (2014b) performed a parametric study applying the two-step iteration algorithm verifying the convergent behaviour of the method.

Regarding arch bridges, Bruno et al. (2016) presented a Three-steps algorithm model for the optimization of hangers with multiple intersections (network) of arch bridges. The hanger post-tensioning forces are calculated in the first step, while in the second step the hangers, the arch and girder cross-sections are evaluated. In the third and last step, the tolerance conditions are checked. If these tolerances are not satisfied the variables are updated and a new iteration is performed.

1.3 Research Objectives

The subject of this thesis is level 2 (stay-cables pre-tensioning forces and geometric variables) optimization of highway composite steel-concrete two I-girder cable-stayed bridges considering the action of dead, live and wind loads.

Similarly to Hassan *et al.* (2013b), the RCGA is used for the structural optimization of cable-stayed bridges. The aim objective is to develop an optimization procedure that performs truck moving load and buffeting wind forces evaluation with a reduced number of design variables in order to avoid excessive computational effort. The resulting procedure called Discrete Phases Approach is based on classifying the variables to be optimized into two categories; main and secondary variables. Instead of the secondary variables being considered as design variables for the RCGA, they are optimized indirectly by the discrete phases.

1.3.1 Methodology and Relevance

Optimization of cable-stayed bridges is a powerful tool for design because it provides the optimum solution from the structural and economic points of view. This optimization will focus on medium span cable-stayed bridges (rather than long span bridges) because longer bridges have challenges that may require unique solutions.

Considering the background information presented in Section 1.1, composite steel-concrete cross section is one of the best options for medium span cable-stayed bridges. This is because steel girders are lightweight and offer high strength, while the concrete slab improves deck resistance to axial loads and provides a proper platform for vehicles or trains. The record main span for this type of bridge was established in 2011 by the Erqi Yangtze River Bridge in China, which has 616m of main span and two-plate girder cross-section. According to Pedro *et al.* (2016), the competitiveness of composite cable-stayed bridges is explained by two facts: (i) the cost of the deck per square metre does not show great sensitivity to span increases, (ii) none of the bridge's main components – deck, towers or cables – have reached their limit application. Given these facts, the following work is focused on a two I-girder composite steel-concrete cable-stayed bridge with semi-fan double plane cable configuration and H tower shape.

In the literature review presented in Section 1.2 for level 2 optimization of cable-stayed bridges, one may observe that previous efforts have considered live loads as a simple uniform distributed load and wind loads as basic mean wind loads. Given that engineers are adopting thinner and lighter decks, a deeper analysis of dynamic loads (specifically live and wind loads) is essential for the design and optimization of cable-stayed bridges.

In this study, live loads, truck and lane loads are evaluated according to the Canadian Highway Bridge Design Code. The envelope of displacements and internal forces are calculated by considering different configurations of loading on the main and side spans. For each configuration, several analyses will be done to consider the five truck axles moving along the roadway.

For the wind loads, critical wind speeds for aeroelastic phenomena will be investigated. Once the structure is considered stable, emphasis is put in the buffeting phenomenon. According to Davenport (1966), buffeting loads lead to the estimative of envelope of maximum bending moment and shear force, and, consequently have an important role in determining the dimensions of structural components in the optimization process.

A Discrete Phases Approach is developed for performing the design and verification of finite element models in this study. The different phases that compose the approach are responsible for: (i) calculating deck I-girder dimensions, (ii) determining stay-cable cross-sectional areas, (iii) calculating pre-tensioning stay-cable forces, (iv) computing live loads, (v) performing free vibration analysis, (vi) estimating wind loads acting on the structure, (vii) assessing critical wind velocities due to aeroelastic phenomena such as flutter, torsional divergence and vortex shedding, (viii) and checking the design criteria to attend the Ultimate Limit State and Serviceability Limit State. The considerable advantage of the Discrete Phases Approach is the ability of adding new phases in the future for considering further effects.

1.3.2 Organization of the Thesis

Chapter 2 provides the optimization of composite concrete-steel two I-girder cable-stayed bridge considering the action of dead, superimposed and live loads. The structural optimizations are performed using RCGA to minimize the deck weight or the material cost of deck, towers and stay-cables. In this chapter, the methodology for design and verification denominated Discrete Phases Approach is introduced and explained in details. The following main design variables are directly optimized through the RCGA: (i) number of cables, (ii) deck I-girder inertia, (iii) deck concrete slab thickness, (iv) tower cross-section external dimensions, and (v) tower height above the deck. The following secondary variables are optimized by the discrete phases: (i) deck I-girder dimensions, (ii) stay-cable cross-section areas and pre-tensioning forces. The influence of considering truck concentrated loads together with lane uniformly distributed loads in the live loads analysis is assessed, and parametric studies are performed to evaluate the integrated behavior of number of cables, deck inertia, and tower height.

Chapter 3 presents a comparison between theoretical and experimental approaches to validate the mean and buffeting wind load analysis implemented in the numerical tool. The theoretical approach is mainly function of: (i) coefficients obtained from wind tunnel sectional model tests, (ii) equivalent static forces due to buffeting loads based on Davenport and King (1984) and implemented in the numerical tool, and (iii) a finite element model of the cable-stayed bridge. The experimental approach is based on the results from a full aeroelastic model, tested in wind tunnel, of the same bridge investigated in the numerical approach. The results show a good agreement between the theoretical and experimental approaches, allowing the validation of the theoretical approach that is later used in Chapter 4.

Chapter 4 provides the optimization of composite concrete-steel two I-girder cable-stayed bridge considering the action of dead, superimposed, live, and wind loads. Similar to Chapter 2, the structural optimizations are performed based on FEM, RCGA, and on the Discrete Phases Design Approach. For considering the action of mean and buffeting wind loads, three discrete phases are added to the numerical tool presented in Chapter 2. These discrete phases are responsible for: (i) determining the deck modes of vibration and their respective frequencies, (ii) performing the theoretical approach, validated in Chapter 3, for the calculation of displacements and internal forces due to the mean and buffeting wind loads, (iii) checking the critical wind velocities for aerodynamic phenomena in order to assure that the structure is stable. Three different basic wind speeds are considered for studying the connected behavior of structural elements. The results show the importance of considering not only wind loads, but also of evaluating critical wind velocities in the structural optimization process of cable-stayed bridges.

Chapter 5 summarizes the main analyzes performed in the data chapters and the most significant conclusions drawn for the exploration of their results. With the intention of continuing and complementing the work presented in this thesis, suggestions for future works are presented.

References

- Battista, R. C., *et al.* 2011. Technical report. Structural Dynamic Analysis of the Cable-stayed Bridge crossing the Cunha Cannal (in Portuguese). CL-539A/10-RT02, CONTROLLATO – Projeto, Monitoração e Controle de Estruturas Ltda, Rio de Janeiro, Brasil.
- Battista, R. C., *et al.* 2013. Technical report. Aerodynamic Analysis of the Structural System of the Guanabara Bay Cable-stayed Bridge (in Portuguese). CL-711D/12-RT01, CONTROLLATO – Projeto, Monitoração e Controle de Estruturas Ltda, Rio de Janeiro, Brasil.
- Bruno, D., Lonetti, P., Pascuzzo, A., 2016. An optimization model for the design of network arch bridges. *Computers and Structures*, 170: 13–25. doi: 10.1016/j.compstruc.2016.03.011.
- CAN/CSA-S6-14, 2014, Canadian Highway Bridge Design Code.
- Chen, D.W., Au, F.T.K., Tham, L.G., and Lee, P.K.K. 2000. Determination of initial cable forces in prestressed concrete cable-stayed bridges for given design deck profiles using the force equilibrium method. *Computers and Structures*, 74(1): 1–9.
- Davenport, A. G. 1966. The action of wind on suspension bridges. Keynote Paper, Intl. Symp. Suspension Bridges.
- Davenport, A.G., King, J.P.C. 1984. Dynamic wind forces on long span bridges using equivalent static loads. IABSE, 12th Congress, Vancouver, BC, Canada, pp. 705–712.
- Ernst, H. J. 1956. “Montage eines seilverspannten Balkens im Grob-Brückenbau”. In: *Stahlbau*, pp 101-108 apud Svensson, H., 2012, *Cable-Stayed Bridges, 40 Years of Experience Worldwide*. 1 ed. Ernst & Sohn GmbH & Co.KG.
- Hassan, M.M., Nassef, A.O., and El Damatty, A.A. 2012. Determination of optimum post-tensioning cable forces of cable-stayed bridges. *Engineering Structures*, 44: 248–259.
- Hassan, M.M., Nassef, A.O., and Damatty, A.A. El. 2013a. Surrogate Function of Post-Tensioning Cable Forces for Cable-Stayed Bridges. 16(3): 559–578.
- Hassan, M.M., Nassef, A.O., and Damatty, A.A. El. 2013b. Optimal design of semi-fan cable-stayed bridges. 40: 285–297.
- Janjic, D., Pircher, M., and Pircher, H. 2003. Optimization of cable tensioning in cable-stayed bridges. *Journal of Bridge Engineering*, 8(3): 131–137.

- Köppel, J. 2012. "Buchs and Bacchetta: Rheinbrücke Diepoldsau". In: SchweizerIngenieur und Architekt, pp 1-6, 818-821, apud Svensson, H., 2012, Cable-Stayed Bridges, 40 Years of Experience Worldwide. 1 ed. Ernst & Sohn GmbH & Co.KG.
- Lee, T.Y., Kim, Y.H., and Kang, S.W. 2008. Optimization of tensioning strategy for asymmetric cable-stayed bridge and its effect on construction process. Structural and Multidisciplinary Optimization, 35(6): 623–629.
- Leonhardt, F., et al. 1980. "Die Spannbeton-Schräggabelbrücke über den Columbia zwischen Pasco und Kennewick im Staat Washington". In: Beton und Stahlbetonbau, pp 29-36, 64-70, 90-94, apud Svensson, H., 2012, Cable-Stayed Bridges, 40 Years of Experience Worldwide. 1 ed. Ernst & Sohn GmbH & Co.KG.
- Lonetti, P., Pascuzzo, A., 2014a. Optimum design analysis of hybrid cable-stayed suspension bridges. Advances in Engineering Software, 73: 53–66. doi: 10.1016/j.advengsoft.2014.03.004.
- Lonetti, P., Pascuzzo, A., 2014b. Design analysis of the optimum configuration of self-anchored cable-stayed suspension bridges. Structural Engineering and Mechanics, 51(5): 847–866. doi: 10.12989/sem.2014.51.5.847.
- Long, W. 1999. Optimum design of cable-stayed bridges. Structural Engineering and Mechanics, 7(3): 241–257.
- Löscher, C. T. 1784. "Angabe einer ganz besonderen Hängewerksbrücke, die mit wenigen und schwachen Hölzern, sehrweitübereinen Fluss gespannt werden kann, die größten Lastenträgt und vor den stärksten Eisfahrtsicherist", Leipzig apud Svensson, H., 2012, Cable-Stayed Bridges, 40 Years of Experience Worldwide. 1 ed. Ernst & Sohn GmbH & Co.KG.
- Lute, V., Upadhyay, A., and Singh, K.K. 2009. Computationally efficient analysis of cable-stayed bridge for GA-based optimization. Engineering Applications of Artificial Intelligence, 22: 750–758.
- Menn, C. 1991. An Approach to Bridge Design. Engineering Structures, 13: 106-112.
- Morgenthal, G., et al. 2008. "Montageplanung und Herstellung der Seitenfelder der Stonecutters Bridge". In: Beton und Stahlbeton, pp 766-773 apud Svensson, H., 2012, Cable-Stayed Bridges, 40 Years of Experience Worldwide. 1 ed. Ernst & Sohn GmbH & Co.KG.
- Nazmy, A.S., Abdel-Ghaffar, A.M. 1990. Three-Dimensional Nonlinear Static Analysis of Cable-Stayed Bridges. Computers & Structures, 34: 257-271.
- Neves, F.A. 1997. Multi-objective nonlinear programming applied to the design optimization of cable-stayed (in Portuguese). D.Sc. Thesis, Civil Engineering, COPPE Institute of Engineering, Federal University of Rio de Janeiro.

- Pedro, J.J., and Reis, A.J. 2016. Composite cable-stayed bridges: state of the art. *Proceedings of the Institution of Civil Engineers - Bridge Engineering*, 169(1): 13–38.
- Podolny W., Scalzi, J.B. 1976. *Construction and Design of Cable-Stayed Bridges*. USA, John Wiley & Sons, Inc.
- Simões, L.M.C., Negrão, J.H.J.O. 1994. Sizing and Geometry Optimization of Cable-Stayed Bridges. *Computers & Structures*, 52: 309-321.
- Simões, L.M.C., and Negrão, J.H.J.O. 2000. Optimization of cable-stayed bridges with box-girder decks. *Advances in engineering software*, 31(6): 417–423.
- Stephenson, R. 1821. Description of Bridges of Suspension. In: *The Edinburgh Philosophical Journal*, pp 237-256 apud Svensson, H., 2012, *Cable-Stayed Bridges, 40 Years of Experience Worldwide*. 1 ed. Ernst &Sohn GmbH & Co.KG.
- Svensson, H. 2012. *Cable-Stayed Bridges. 40 Years of Experience Worldwide*. 1 ed. Ernst & Sohn GmbH & Co.KG.
- Troitsky MS. 1988. *Cable-stayed bridges: theory and design*. 2nd Ed. Oxford, BSP.
- Verantius, F. 1617. “*Machinae Novae Fausti*”, Venedig apud Svensson, H. 2012, *Cable-Stayed Bridges, 40 Years of Experience Worldwide*. 1 ed. Ernst &Sohn GmbH & Co.KG.
- Wang, P.H, Tseng, T.C, Yang, C.G. 1993. Initial shape of cable-stayed bridges. *Pergamon Press Ltd*, 47(1): 111–123.
- Wenk, H. 1954. “*Die Strömsundbrücke*”. In: *Stahlbau*, pp 73-76 apud Svensson, H., 2012, *Cable-Stayed Bridges, 40 Years of Experience Worldwide*. 1 ed. Ernst &Sohn GmbH & Co.KG.
- You, Q., et al. 2008. Sutong Bridge – The longest cable-stayed bridge in the World. In: *Structural Engineering International* 4, pp 390-395, apud Svensson, H., 2012, *Cable-Stayed Bridges, 40 Years of Experience Worldwide*. 1 ed. Ernst &Sohn GmbH & Co.KG.

Chapter 2

2 Structural optimization of two I-girder composite cable-stayed bridges under the action of dead and live loads

2.1 Introduction

Cable-stayed bridges have several advantages over comparable designs (Podolny et al. 1976; Troitsky 1988; Svensson 2012; Pedro and Reis 2016) as they (1) span large distances without the need of intermediary supports; (2) have reduced bending moments at the deck and superior rigidity compared to suspension bridges; (3) have an aesthetic appeal. In addition, their construction can be economical through the use of the free cantilever method. In particular, steel-concrete composite cable-stayed bridges offer an efficient use of materials. The concrete slab provides a good surface for the roadway and works well in resisting the axial compression imposed by the stay-cables, while the steel girders provide flexural strength.

On the other hand, cable-stayed bridges are complex structures due to the distribution of forces among the structural elements; deck, stay-cables and towers. The stay-cable pre-tensioning forces play an important role in the behavior of the bridges. As such, many studies have been directed towards to the optimization of the stay-cable pre-tensioning forces. Wang et al. (1993) proposed a procedure for finding the initial shape of cable-stayed bridge due to dead loads of the deck and pre-tensioning forces of the cables. The procedure uses Newton-Raphson iteration method to obtain vertical displacements of deck control points that satisfy the convergence tolerance. Chen et al. (2000) proposed the force equilibrium method, which considers bending moments as parameters to be controlled rather than the displacements. Janjic et al. (2003) proposed the unit load method, which also considers bending moments as parameters of control, and the expanded unit load method that includes constructions stage analysis and time-dependent material behavior. Lee et al. (2008) proposed the two-step approach that is based on the unit load method. Beside the displacement constraints of the unit load method, there are also constraints for the cables forces to find the optimum pre-tensioning forces for asymmetrical bridges under construction. Hassan et al. (2012, 2013a) proposed an approach that combines the finite

element method, the B-spline function, and the Real Code Genetic Algorithm to determine the optimum distribution of stay-cables forces for the final configuration of the bridge. The authors noticed that the stay-cables pre-tensioning forces may be described by a high order polynomial function with a large number of coefficients. B-spline function which uses low-degree polynomials for representing complex functions is then applied to describe the pre-tensioning forces function (Hassan *et al.*, 2012). The same authors proposed surrogate polynomial functions to evaluate stay-cables forces that depend on the bridge geometry and the number of stay-cables. They stored those functions as a database in a design optimization Software.

In relation to the optimization of the dimensions of the structural elements, Simões and Negrão (1994) and Negrão and Simões (1997) adopted an entropy-based approach to solve a multi-objective problem, and to determine optimum variables like distance between cables anchorages and deck girder dimensions under dead and lane live load. Hassan et al. (2013b, 2014) optimization of composite steel-concrete cable stayed bridges. The independent variables considered were: (i) the six dimensions that define the deck I-girder geometry, (ii) number of stay-cables, (iii) cross-sectional area of stay-cables, (iv) tower height, and (v) tower cross-section dimensions. The pre-tensioning cable forces were determined by using surrogate polynomial functions developed by Hassan *et al.* (2013a). Their numerical tool involved the use of the Finite Element Method (FEM) to discretize the structure and predict its structural performance and the Real Coded Genetic Algorithm (RCGA) technique as the optimization tool. The structural analysis/optimization numerical model accounted for the effects of dead load, lane live load, and mean wind load.

Because of the large number of variables included in the optimization scheme adopted by Hassan et al. (2013b), it is almost impossible to consider the moving traffic load as well as to conduct dynamic analysis under wind loads using this model.

In this chapter, a procedure is developed to optimize the design of cable-stayed bridges and obtain optimum dimensions and cable pre-tensioning forces. The procedure developed in this chapter is also based on the FEM and RCGA methods. The design variables are divided

to main and secondary variables and the optimization procedure is accomplished through five consecutive phases.

The chapter starts by introducing the developed Finite Element/optimization procedure including a description of the five analysis phases. In order to illustrate the procedure, a case study for the design optimization of a cable-stayed bridge is considered under two different objective functions.

The research significance of this study and the main advantages of the 5-Phase approach compared to Hassan et al. (2013b) can be stated as follows:

1. The 5-Phase approach considers dead and live loads in the final configuration of the cable-stayed bridge. The way the numerical tool is structured, other phases can be easily added by considering construction stages or other loads such as wind and earthquake during the optimization process, to become a 6, 7, and/or 8-Phase strategy.
2. In Phase-1, the optimization of the steel I-girder is accomplished by using only one design variable (inertia about major axis) instead of optimizing all six dimensions that define its geometry. This and also the determination of the stay-cables areas in Phase-2 reduce considerably the number of design variables, decrease the number of samples required to obtain a reliable optimal solution, and substantially reduce computational time required to perform the analyzes.
3. In Phases-2 and 3, the unit force method (based on Janjic et al. 2003) can be used to determine pre-tensioning forces for both the final configuration and different stages of construction (Lee et al. 2008). Although the unit force method requires computational time to generate an influence matrix, once the method is implemented in the numerical tool, it can be used for any configuration of bridge, and there is no need to generate a new database if the bridge characteristics are changed.

4. A comparison between optimal solutions for the structural optimization considering dead plus live loads and dead load only is performed to estimate the significance of taking live loads into account in the optimization process of a cable-stayed bridge considered as a study case.
5. A correlation between the optimal solutions considering truck plus lane live load, and lane live load only is executed to assess the importance of considering the truck in the analyses.
6. Two design objective functions are evaluated separately and then compared. Objective-1 obtains the lightest deck that attends all design constraints, while Objective-2 determines the lowest material cost of all structural elements.

2.2 Description of numerical tool

The study considers composite steel concrete cable-stayed bridges with two steel I-girders deck, H-shaped towers, and intermediate fan-harp system arranged in two outer plans. Figure 2. 1 shows all the dimensions that describe the bridge. The dimensions shown in bold are those considered as variables in the optimization scheme. The other dimensions are kept constant and are defined by the user. Those are the total length of the bridge (L), the middle span (L_1), the side span (L_2), and the tower height below the deck (H_b), which are governed by the topography and navigation conditions. The width of the deck including the distance between barriers are also kept constant as they are governed by the traffic requirements and the number of lanes. It should be mentioned that the number between parentheses in Figure 2. 1 correspond to the values of the fixed dimensions considered in the case study example reported later. The cross-section of the tower is assumed to be a hollow reinforced concrete box, with the thickness of the section taken as a ratio of the outer dimensions as shown in Figure II. 1.c.

The I-girder area depends on six dimensions (b_1 , t_1 , b_2 , t_2 , D , w) considered in this study as secondary variables. Instead of optimizing the six I-girder dimensions, the I-girder main inertia is optimized in order to minimize its area. The other secondary variables are the

cables pre-tensioning forces and cross-sectional areas, which are easier to be determined when the deck and towers cross-sections are already defined. Otherwise, a great number of samples are necessary for obtaining the optimum area and pre-tensioning force for each one of the stay-cables. The accurate prediction of those pre-tensioning forces is important in order to achieve small displacements and well distributed moments at the deck and towers. As such, there are six main variables to be optimized, which are:

- (1) Total number of cables ($2 \times 4 \times N$), where N is the number of cables in the side spans (or in half of the main span) in one plan of cables;
- (2) Moment of inertia (I) of the deck steel I-girder about its major axis;
- (3) Thickness of concrete slab (t_c);
- (4) Height of the tower above the deck level (H_a);
- (5) External dimension of the tower cross-section in the longitudinal direction (TL_1);
- (6) External dimension of the tower cross-section in the transverse direction (TL_2).

While (2) and (3) define the deck total area and inertias, (1) and (6) define the towers total height that together with (4), (5) determine the towers longitudinal and transversal stiffnesses. For example, if the number of cables increases, the tower stiffness is changed and the deck inertia may be reduced. The complexity of cable-stayed bridge can be attributed to the fact that all these parameters are strongly correlated and have significant importance on the final results. The procedure for obtaining the secondary variables from the main variables is explained in the next section.

If the concept of main and secondary variables is not considered, the total number of design variables would vary between 23 and 35 variables for number of cables $N=6$ and $N=12$, respectively, when taking advantage of the bridge symmetry. For longer spans, and consequently greater number of stay-cables, the number of design variables is even higher. According to Michalewicz *et al.* (2000), many efforts have been put towards determining the proper population size, but this parameter is highly dependent on the particularities of the problem to be solved, and is better defined by empirical trials. According to

Sivanandam *et al.* (2008), the population should be large enough to be able to explore the whole search space and to avoid bad diversity and consequently difficulties for finding the global optimum. This way, it can be established by the considerations above that by reducing the number of variables from 23(N=6) or 35(N=12) to 6 the number of samples to be analyzed will be significantly reduced. Compared to Hassan *et al.* (2013b), the number of independent variables has been reduced from 14 to 6, making the process feasible to handle moving traffic loads as well as other load cases. Also the process involves the evaluation of the proper pre-tensioning forces without relying on surrogate functions. The present model can be easily extended to include as a design variable any of the constant dimensions. For example, if the topography allows a ratio β of side (L_2) and main (L_1) spans varying between 0.40 and 0.60, the total number of design variables would become equal to seven. In this case, the bridge total length L will be fixed, and the ratio β will be randomly determined between the lower (0.40) and upper (0.60) bounds with $L_1 = L / (2\beta + 1)$ and $L_2 = (L - L_1) / 2$. In addition, different stay-cables arrangements may be evaluated by adding some restrictions to the cable anchorages at the towers. Deck vertical profiles and radius of curvature can be considered as input parameters to be considered in the calculation of the deck nodes coordinates.

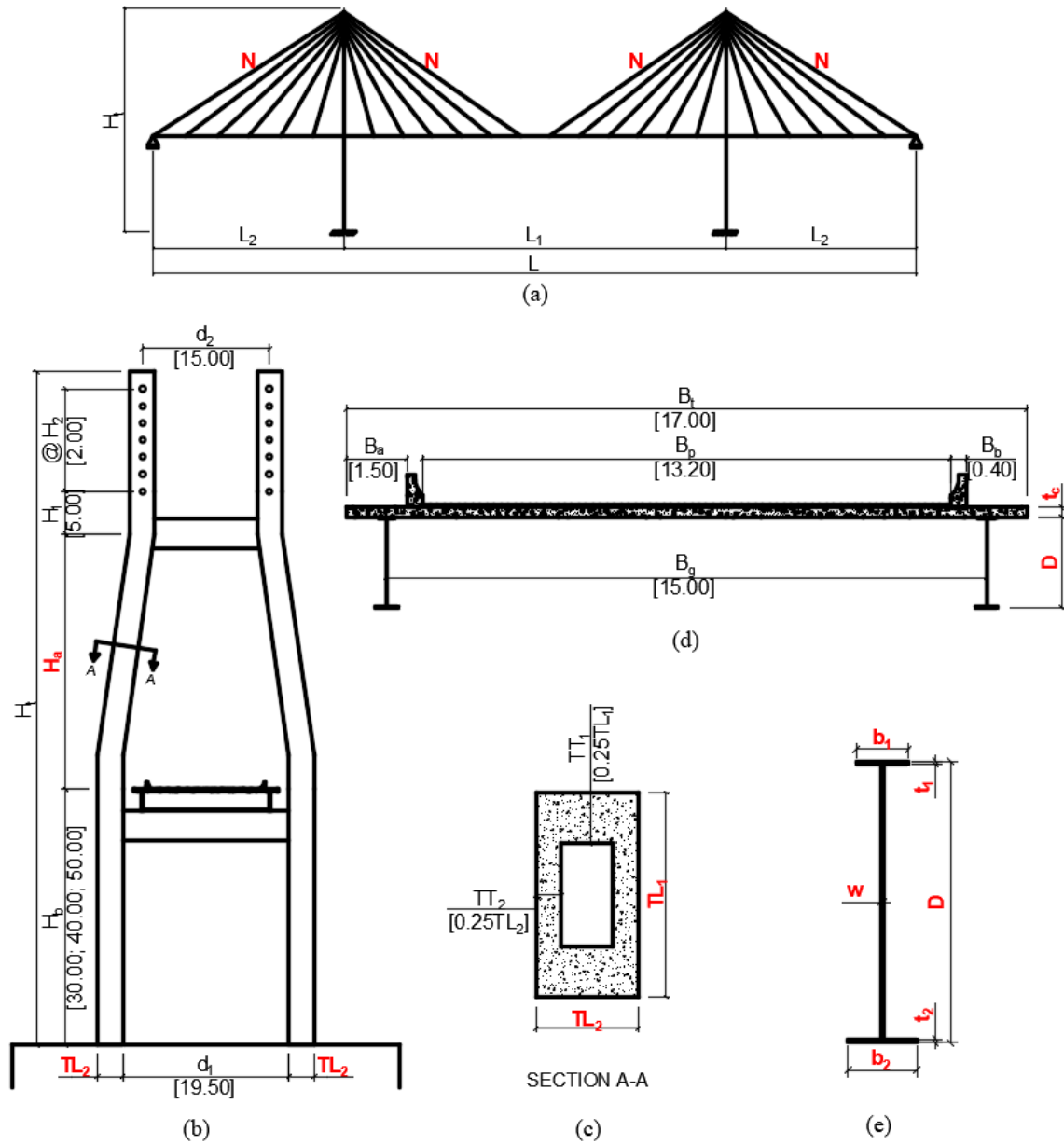


Figure 2. 1: Cable-stayed bridge geometry: (a) longitudinal view; (b) tower dimensions; (c) tower cross-section; (d) deck cross-section; (e) steel I-girder dimensions. Dimensions in meter.

2.2.1 Optimization procedure

The structural optimization is conducted using a numerical model developed in-house and coded using the Fortran language. The numerical model is a modification to the Code developed by Hassan et al. (2013b). The model combines finite element discretization, the Real Coded Genetic Algorithm (RCGA) procedure for optimization, and design criteria based on the Canadian Highway Bridge Design Code CAN/CSA-S6-06. The overall numerical scheme can be described through the flowchart presented in Figure 2. 2. The numerical scheme is controlled by the RCGA. The following two objectives functions are considered in the optimization.

Objective-1 – Lightest deck weight.

Objective-2 – Lowest material cost for the entire bridge.

After the selection of random values for the main design variables, I , N , t_c , TL_1 , TL_2 , and H_a , the numerical procedure go through the following five phases described below. If the solution is feasible, *i. e.* attend all the design criteria, the fitness value is equal to the objective function value, which is the deck weight or the material cost of the bridge, depending on the objective that has been chosen. Otherwise, if any of the design constraints is violated, the solution is considered infeasible and the fitness value is calculated based on Deb (2000):

$$F(\vec{x}) = f_{max} + \sum_{j=1}^m g_j(\vec{x}) \quad (2. 1)$$

where $\vec{x} = \{N, I, t_c, TL_1, TL_2, H_a\}$ is the vector of design variables; $F(\vec{x})$ is the fitness value; m is the total number of design constraints; f_{max} is the fitness value of the worst feasible solution that has been observed; $g_j(\vec{x})$ are the normalized design constraints that have been violated. Preliminary tests should be performed for obtaining some of the RCGA parameters. For optimizing the six design variables showed in red in Figure 2. 1, the RCGA parameters are defined as follows: (i) the total of 90 samples compose the population, (ii) 20 generations, (iii) 3 samples are saved in each generation, for considering elitism in the next one, (iv) 3 crossover operations and 5 mutation operations are applied in each generation, and (v) mutation rate is equal to 0.1.

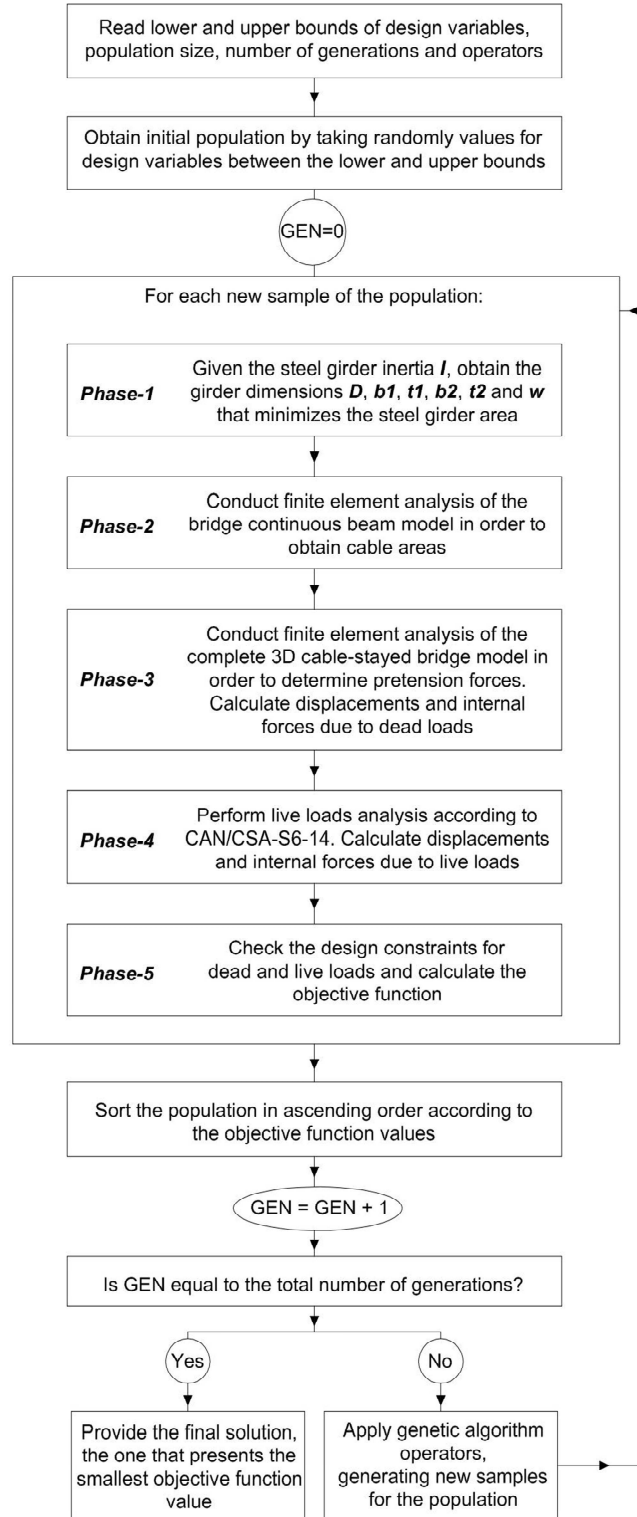


Figure 2. 2: Flow chart for the optimization scheme. GEN is the current generation of analysis.

2.2.1.1 Phase 1

The purpose of this phase is determine the dimensions of the I-girder that leads to minimum value for the cross section area “A” of the girder for a given value of I selected by the random generation RCGA process. The cross-section area of the girder is defined by the following variable: b_1 , t_1 , b_2 , t_2 , D , w (see Figure 2. 1.e). Those variables can be reduced by relating the flange width to thickness ratio (i.e. b_1 to t_1 and b_2 to t_2) and the web depth to thickness ratio (D to w). For classes 2, 3, 4, the upper limit of classes 1, 2, and 3 are used, respectively. By applying those limits, the number of independent variables is reduced to 3. A parametric study is conducted by varying the ratio (b_1/b_2) of the top and bottom flanges. It is found for a given value of I, this ratio has a minor effect on the minimum value of “A”. As such a value of $b_1/b_2=0.75$ is selected as it was found to be used in a number of bridges design. This reduces the number of design variables to two (b_2 , D). The cross-sectional area A is found to be reduced by decreasing the ratio b_2/D . However it was found that the minimum ratio b_2/D in real bridges varies between 0.20 and 0.25. As such, a limit of $b_2/D \geq 0.20$ is adopted in this study.

For a given value of I and assuming a certain class section, this phase determines the dimensions of the I-girder cross section (b_1 , t_1 , b_2 , t_2 , D , w) which lead to a minimum value of the cross section area “A”. The I-girder depth (D), bottom flange width (b_2) and web thickness (w) for width-to-thickness limit ratio of Classes 2 and 3 are presented in Appendices B and C, respectively.

The determination of minimum area for the I-girder is required since the overall objective function of the optimization process is either minimum cost or minimum deck weight.

2.2.1.2 Phase 2

In this phase the deck is simulated using three-dimensional frame elements. A single spine approach, similar to that used by Wilson et al. (1991) is adopted to simulate the slab and the girders (Appendix D). Adeli and Zhang (1995) considered full non-linear analysis of a steel-concrete composite cable-stayed bridge. The authors concluded that for dead and live loads, the geometric nonlinearity had an effect of 4% on the maximum deflection. Given the large number of analysis needed for conducting the design optimization, and the minor

effect of the geometric nonlinearity, the analysis is conducted linearly. In this phase the deck is modelled as a continuous beam with pinned support at each cable-anchorage location. The model is analyzed under the effect of dead and superimposed loads. This model simulates the intended deflection configuration of the bridge where the pre-tensioning cable forces tend to counterbalance the effect of dead and superimposed loads. The model is used to obtain the reaction at the supports from which the cables pre-tensioning forces are obtained using the following relation:

$$T_{0,i} = \frac{R_i}{\sin\theta_i} \quad (2.2)$$

where $T_{0,i}$ is the initial pre-tensioning force for the i -th cable; R_i is the reaction of i -th stay-cable obtained from the continuous beam model; and, θ_i is the angle between the i -th stay-cable direction and longitudinal direction.

It is assumed that the initial pre-tensioning forces are equal to 25% of the cables breaking load. This leads to the evaluation of the cross sectional area of the cables using the following relation:

$$A_i = \left[\frac{T_{0,i}}{0.25 \times F_{B,1\phi}} \right] \times A_{1\phi} \quad (2.3)$$

where A_i is the steel total cross-section area of the i -th cable; $F_{B,1\phi}$ is the steel nominal breaking load for 1 strand; and, $A_{1\phi}$ is the steel nominal cross-section area for 1 strand.

Also in this phase, the bending moments at the cable anchorages points are recorded and are called desired bending moments (M_0).

2.2.1.3 Phase 3

In this phase, the entire bridge, including deck, towers and cables, is modelled using an assembly of finite elements (Figure 2. 3). Three-dimensional frame elements are used to model the deck and the towers, while three-dimensional truss elements are used to model the cables. Hassan et al. (2012) concluded that the cables sag is a source of nonlinear behaviour that affects the response of cable-stayed bridges. The sag effect is taken into

account by replacing each cable with a truss element of an equivalent cable stiffness. The equivalent tangent modulus of elasticity (E_{eq}) was derived by Ernst (1965) and is given by:

$$E_{eq} = \frac{E_{cs}}{1 + \frac{(w_{cs}H)^2 AE_{cs}}{12T^3}} \quad (2.4)$$

where E_{cs} is the cable material effective modulus of elasticity; A is the cross-sectional area of the cable; H is the horizontal projection of the cable; w_{cs} is the weight per unit length of the cable; and T is the tension in the cable.

This model is used to determine the final values of the pre-tensioning forces based on Janjic et al. (2003) and summarized by the following:

$$\{M_0\} = \{M_P\} + [m]\{X\} \quad (2.5)$$

$$\{T\} = \{T_0\} + \{X\} \quad (2.6)$$

where $\{M_0\}$ is the vector of desired bending moments at control points, or cable-anchorage at the deck, obtained in Phase 2; $\{M_P\}$ is a vector of bending moments at the control points due to dead and superimposed loads obtained from the cable-stayed bridge complete 3D FEM – i.e. deck, towers, and non-tensioned cables; $[m]$ is the influence matrix, $m_{i,j}$ is the bending moment at the i -th control point due to a unit force applied to the j -th cable. The influence matrix is obtained employing the same FEM used to obtain $\{M_P\}$. The vector $\{X\}$, obtained from Equation 2.5, is added to the vector of initial pre-tensioning force $\{T_0\}$ to produce the final vector of pre-tensioning forces $\{T\}$.

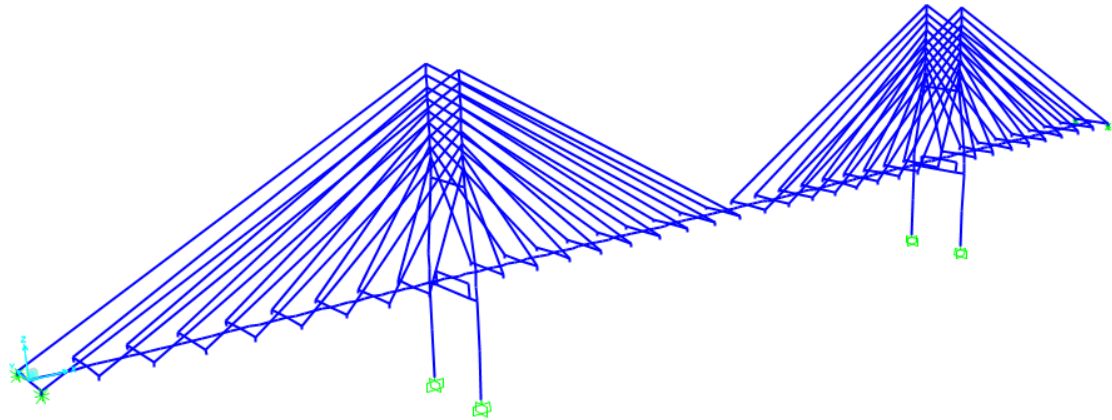


Figure 2. 3: Finite element model.

2.2.1.4 Phase 4

By this phase, all the cross-sectional dimensions of the bridge are assumed, the dead loads are calculated, and the pre-tensioning forces counterbalancing the effects of dead and superimposed loads are calculated. This phase considers finite element analysis of the entire bridge under the effect of live loads which are determined using the Canadian Highway Bridge Design Code (CAN/CSA-S6-14). For the province of Ontario, the CL-625-ONT Lane Load is composed of a 500kN truck with 5 axles and a 9kN/m uniformly distributed load. The number of design lanes is dependent upon the deck width, and a modification factor for multi-lane loading is also considered.

2.2.1.5 Phase 5

In this final phase, the displacements and internal forces due to dead and superimposed loads, and live loads obtained through Phases 3 and 4, respectively, are combined. One Ultimate Limit State (ULS) load combination is considered: $(DL+SL) + 1.7(LL)$, with α equal to 1.10 for factory produced components, 1.20 for cast-in-place concrete, and 1.50 for wearing surfaces (CAN/CSA-S6-14). While two Serviceability Limit State (SLS) combinations are considered: $1.0(DL+SL) + 0.90(LL)$, and $0.90(LL)$. The objective function, which can be the lightest deck weight (*Objective-1*) or the lowest material cost of the entire structure (*Objective-2*) is calculated. If one or more of the design constraints are not satisfied, penalties are applied to the objective function value. The design constraint functions (g_j) at the Serviceability Limit State (SLS) and Ultimate Limit State (ULS) are as follow:

- Displacements at the deck due to dead and superimposed loads (δ_{DL+SL}) at SLS:

$$g_1 = \frac{5000 \times \delta_{DL+SL}}{\text{span length}} - 1.0 \leq 0 \quad (2.7)$$

- Displacements at the deck due to live loads (δ_{LL}) at SLS (AASHTO 2012):

$$g_2 = \frac{800 \times \delta_{LL}}{\text{span length}} - 1.0 \leq 0 \quad (2.8)$$

- Displacements at the towers due to dead and superimposed loads (Δ_{DL+SL}) at SLS:

$$g_3 = \frac{1700 \times \Delta_{DL+SL}}{H_t} - 1.0 \leq 0 \quad (2.9)$$

where H_t is the total length of tower.

- Displacements at the towers due to live loads (Δ_{LL}) at SLS:

$$g_4 = \frac{500 \times \Delta_{LL}}{H_t} - 1.0 \leq 0 \quad (2.10)$$

where H_t is the total length of tower.

- Combined shear and moment at the deck at ULS:

$$g_5 = \frac{V_f}{V_r} - 1.0 \leq 0 \quad (2.11)$$

$$g_6 = \frac{M_f}{M_r} - 1.0 \leq 0 \quad (2.12)$$

$$g_7 = 0.727 \frac{M_f}{M_r} + 0.455 \frac{V_f}{V_r} < 0 \quad (2.13)$$

where V_f is the factored shear force at ULS; M_f is the factored bending moment at ULS; V_r is the factored shear resistance; M_r is the factored bending moment resistance.

- Axial compression and bending at the deck at ULS:

$$g_8 = \frac{C_f}{C_r} + \frac{U_{1x}M_{fx}}{M_{rx}} + \frac{U_{1y}M_{fy}}{M_{ry}} - 1.0 \leq 0 \quad (2.14)$$

where C_f is the factored compressive force at ULS; M_{fx} and M_{fy} are the factored bending moment at ULS about x-axis and y-axis; C_r is the factored compressive resistance; M_{rx} and M_{ry} are the factored bending moment resistance about x-axis and y-axis; U_{1x} and U_{1y} are factors to account for moment gradient and second order effects.

- Control of permanent deflections at the deck at SLS:

$$g_9 = \frac{M_{DL}}{S} + \frac{M_{SL}}{S_{3n}} + \frac{M_{LL}}{S_n} - 0.90F_y \leq 0 \quad (\text{positive moment regions}) \quad (2.15)$$

$$g_{10} = \frac{M_{DL}}{S} + \frac{M_{SL}+M_{LL}}{S'} - 0.90F_y \leq 0 \quad (\text{negative moment regions}) \quad (2.16)$$

where M_{DL} , M_{SL} and M_{LL} are the bending moment at SLS due to dead load, superimposed load, and live load; S , S' , S_n , S_{3n} are the elastic section modulus of the steel section only, the steel section and reinforcement within the effective width of the slab, the steel girder and the concrete slab using a modular ratio n and $3n$, respectively.

- Biaxial loading at the towers at ULS:

$$g_{11} = \frac{M_{fx}}{M_{rx}} + \frac{M_{fy}}{M_{ry}} - 1.0 \leq 0 \quad (2.17)$$

where M_{fx} and M_{fy} are the factored bending moment at ULS about x-axis and y-axis; and, M_{rx} and M_{ry} are the factored bending moment resistance about x-axis and y-axis.

- Stay-cables axial forces at ULS:

$$g_{12} = \frac{T_{f,DL+SL}+T_{f,LL}}{F_B} - 0.50 \leq 0 \quad (2.18)$$

where $T_{f,DL+SL}$ and $T_{f,LL}$ are the factored axial forces at ULS due to dead and superimposed loads, and live loads respectively; and, F_B is the breaking force.

2.2.2 Case study

A cable-stayed bridge is analyzed and optimized using the developed model as a case study. The total length (L), mid span (L_1) and side span (L_2) of the bridge are assumed to be equal to 400m, 200m and 100m, respectively. The assumed fixed dimensions for the deck and the towers are shown in Figure 2. 1. A cross-beam is placed at the stay-cable anchorages coordinates and a maximum distance of 8m between cross-beams is adopted. Three different values for the tower height below the deck (H_b) are assumed: 30m, 40m and 50m. The bridge is analyzed under dead and live loads using the loads and load combination factors defined in the CAN/CSA-S6-14 (2014). The material properties are presented in Table 2. 1.

The semi-fan configuration is chosen for this case study because it combines the advantages of both fan and harp configurations (Svensson, 2012). The fan configuration provides higher stay-cable angles of inclination when compared to the harp configuration, but having all the cable anchorages at the top of the towers is not practical from construction point of view. The harp configuration is aesthetically appealing, but requires considerably taller towers than the fan system. Additionally, according to Adeli and Zhang (1995) the semi-fan system provides the highest failure load capacity when compared to the fan and harp configurations.

The traffic loads are considered by moving the truck along the bridge at each 18m, which corresponds to the truck length. Comparisons with the results provided by the moving load from the commercial program SAP2000 demonstrate that moving the truck at each 18m is an adequate choice for this case study.

As described earlier, two objective functions are considered separately for design optimization. The first objective function (*Objective-1*) aims minimizing the mass of the deck. The second objective function (*Objective-2*) targets minimizing the total cost of the bridge. In this case study, the optimization of *Objective-1* is repeated three times, by considering: (i) dead, truck plus lane live load; (ii) dead and lane live load; (iii) dead load alone. The optimization of *Objective-2* is repeated twice by considering two different locations, which reflect different price schemes for the bridge materials.

For *Objective-1*, the concrete slab thickness (t_c) of the deck is assumed to be 0.25m, which is the lower bound for this variable. A parametric study is conducted by considering four different towers cross-sections ($TL_1 \times TL_2$) – 3.0m x 1.5m, 4.0m x 2.0m, 5.0m x 2.5m, and 6.0m x 3.0m – and, five different tower heights above the deck (H_a) – 10m, 20m, 30m, 40m, and 50m. Since t_c , TL_1 , TL_2 , and H_a are assumed fixed values in the parametric study, only two design variables are obtained during the optimization process, which are number of stay-cables (N) and the steel I-girder inertia (I). For *Objective-2*, two cities in Canada, London, ON and North Bay, ON, with different materials cost are considered. The prices of materials are estimated from RSMeans (2013) and from constructor companies (Table 2. 1). City-specific factors are applied on top of material costs to adjust for differences in

price between the two locations. The city-specific factors for concrete and metal materials are 1.45 and 1.25 for London-ON, and 1.50 and 1.06 for North Bay-ON, respectively. In this design objective all six design variables – N , I , t_c , TL_1 , TL_2 and H_a – are determined by the optimization process. The lower and upper bound for the design variables are presented in Table 2.2. Results of all the optimization analyses are presented below.

Table 2. 1: Material properties and costs used in the study.

Elements	Material	Properties and Costs	
Deck	Steel	Modulus of elasticity (E_s)	200 GPa
		Unit weight (γ_s)	77 kN/m ³
		Yield strength (F_y)	350 MPa
		Cost (C_s)	\$3,125/t
	Concrete	Modulus of elasticity ($E_{c, \text{slab}}$)	25.6 GPa
		Unit weight ($\gamma_{c, \text{slab}}$)	24 kN/m ³
		Compressive strength ($f'_{c, \text{slab}}$)	30 MPa
		Cost ($C_{c, \text{slab}}$)	\$1,300/ m ³
Towers	Reinforcement	Yield strength (f_y)	500 MPa
		Cost (C_r)	\$2,400/t
	Concrete	Modulus of elasticity ($E_{c, \text{tower}}$)	28.4 GPa
		Unit weight ($\gamma_{c, \text{tower}}$)	24 kN/m ³
		Compressive strength ($f'_{c, \text{tower}}$)	40 MPa
		Cost ($C_{c, \text{tower}}$)	\$1,200/ m ³
Cables	Steel strands	Yield strength (f_y)	500 MPa
		Cost (C_r)	\$2,400/t
		Modulus of elasticity (E_{cs})	205 GPa
		Unit weight (γ_{cs})	83 kN/m ³
		Ultimate tensile strength (T_{cs})	1.86 GPa
		Cost (C_{cs})	\$7,650/t

Table 2. 2: Lower and upper bounds of the design variables.

Design Variables	Nomenclature	Lower Bound	Upper Bound
Number of cables	N	6	12
Steel I-girder inertia	I (m ⁴)	0.005	0.50
Concrete thickness	t _c (m)	0.25	0.30
Tower cross-section dimensions	TL ₁ (m)	3.00	6.00
	TL ₂ (m)	0.30	0.70
Tower height above deck	H _a (m)	10.0	50.0

2.2.3 Numerical results for design *Objective-1* considering dead load and truck plus lane live load

Optimizing the number of cables (N) and steel I-girder inertia about the major axis (I) with the objective of minimizing the deck mass has revealed observable patterns for dead plus live loads (Figures 2.4 and 2.5). In these figures, three graphs are presented for tower heights below the deck (H_b) of 30m, 40m and 50m and each curve is related to a specific tower cross-section dimension (TL₁ x TL₂). Each one of the curves has been constructed with 5 points. The first point corresponds to H_a=10m (vertical distance between the deck level and the tower upper transverse beam, Figure 2. 1.b), and the other points have H_a values augmented by 10m, resulting in H_a=50m for the last point. As the total tower height (H_t) depends on the number of cables (N), two points on a single curve can present the same value of H_t even though they each have distinct values for H_a.

Curves in the plots for H_b=30m and H_b=40m have similar trends and three different behavioural patterns can be seen. First, when H_a values are small, a higher number of stay-cables are required to support the deck because angles of inclination (θ) values for each cable is also reduced. Second, as H_a increases, and consequently the θ values, the structure stiffness is increased, allowing the reduction of N and I. Third, while the variable N is maintained constant, but again with the increase of H_a and consequently of θ , the variable I reduces until a point when the stiffness cannot reduce anymore for the same number of stay-cables N, resulting in an increase of I value.

For $H_b=50\text{m}$, the curves present analogous behaviours and relationships between the design variables H_a , N and I as presented for $H_b=30\text{m}$ and $H_b=40\text{m}$. However, due to the fact that the towers are higher than in the other two analyses, other factors have to be taken into account. As mentioned before, the augmentation of H_a values allows the increase of deck rigidity, but also might result in the towers becoming excessively flexible depending on their cross sections. This fact can explain the cross between the $4\text{m} \times 2\text{m}$ and the $5\text{m} \times 2.5\text{m}$ curves. Besides that, for the $4\text{m} \times 2\text{m}$ curve, the number of stay-cables N is reduced twice.

For each tower cross-section, 15 different cases are performed. For $TL_1 \times TL_2$ equal to $3.0\text{m} \times 1.5\text{m}$, only 6 of the 15 cases provide feasible solutions that attend all the design constraints: (1) $H_b=30\text{m}$; $H_a=40\text{m}$; (2) $H_b=30\text{m}$; $H_a=50\text{m}$; (3) $H_b=40\text{m}$; $H_a=40\text{m}$; (4) $H_b=40\text{m}$; $H_a=50\text{m}$; (5) $H_b=50\text{m}$; $H_a=40\text{m}$; and (6) $H_b=50\text{m}$; $H_a=50\text{m}$. Among these solutions, case (2) has delivered the lowest deck mass value (5733 tons). The analysis case with $H_b=30\text{m}$, $H_a=50\text{m}$, $TL_1=6.0\text{m}$, and $TL_2=3.0\text{m}$ provides the lightest deck mass (5304 tons) of all examples. Table 2.3 presents the deck mass of 45 cases normalized by the minimum obtained deck mass. In this table, it is noted that all the cases for $TL_1=6.0\text{m}$ and $TL_2=3.0\text{m}$ have lower deck masses than the respective cases with smaller tower cross-sections. It is also noted that the lightest deck mass is obtained for $H_a = 50\text{m}$.

Table 2. 3: Deck masses obtained for Objective-1 normalized by the minimum mass.

$TL_1 \times TL_2$	H_b	$H_a = 10\text{m}$	$H_a = 20\text{m}$	$H_a = 30\text{m}$	$H_a = 40\text{m}$	$H_a = 50\text{m}$
4m x 2m	30m	1.19	1.14	1.09	1.07	1.06
	40m	1.2	1.15	1.12	1.1	1.07
	50m	1.21	1.17	1.12	1.1	1.09
5m x 2.5m	30m	1.14	1.1	1.06	1.04	1.04
	40m	1.17	1.11	1.09	1.06	1.05
	50m	1.2	1.15	1.09	1.07	1.06
6m x 3m	30m	1.09	1.04	1.02	1.01	1.00
	40m	1.12	1.07	1.04	1.02	1.02
	50m	1.18	1.1	1.06	1.04	1.02

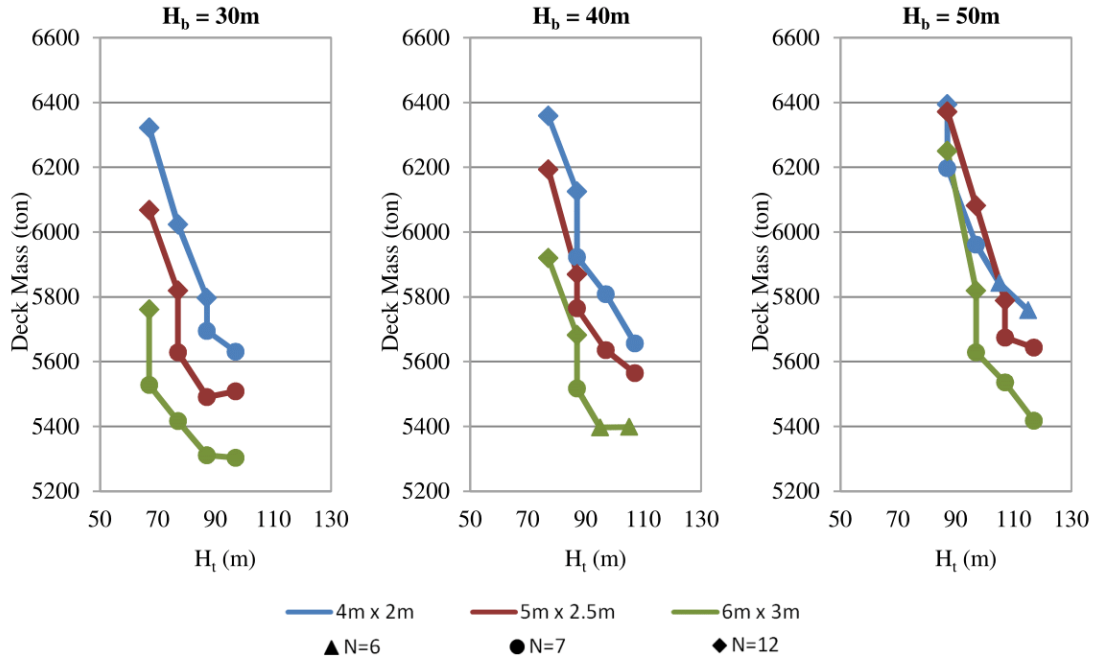


Figure 2. 4: Deck mass due to dead plus live loads as a function of H_b and tower dimensions TL1 x TL2.

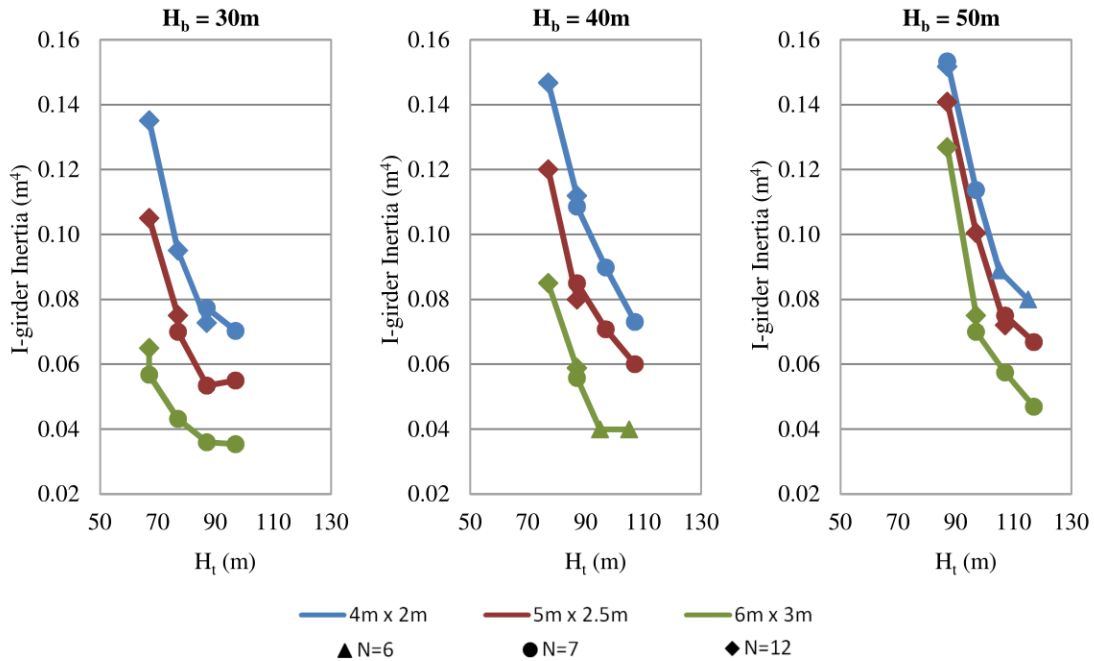


Figure 2. 5: Steel I-girder inertia about major axis due to dead plus live loads as a function of H_b and tower dimensions TL1 x TL2.

Figure 2. 6 shows the values for stay-cable masses that have been obtained by the structural optimization to achieve *Objective-1*. In general, the stay-cable mass curves follow a similar trend as the deck mass curves. In the majority of the cases, an increase/decrease of deck mass is also followed by a proportional increase/decrease of stay-cable mass. The case of analysis with lightest deck mass ($H_b=30\text{m}$; $H_a=50\text{m}$; $TL_1=6.0\text{m}$, and $TL_2=3.0\text{m}$) provides stay-cable mass equal to 128 tons which also presents the minimum stay-cable mass obtained among all the cases.

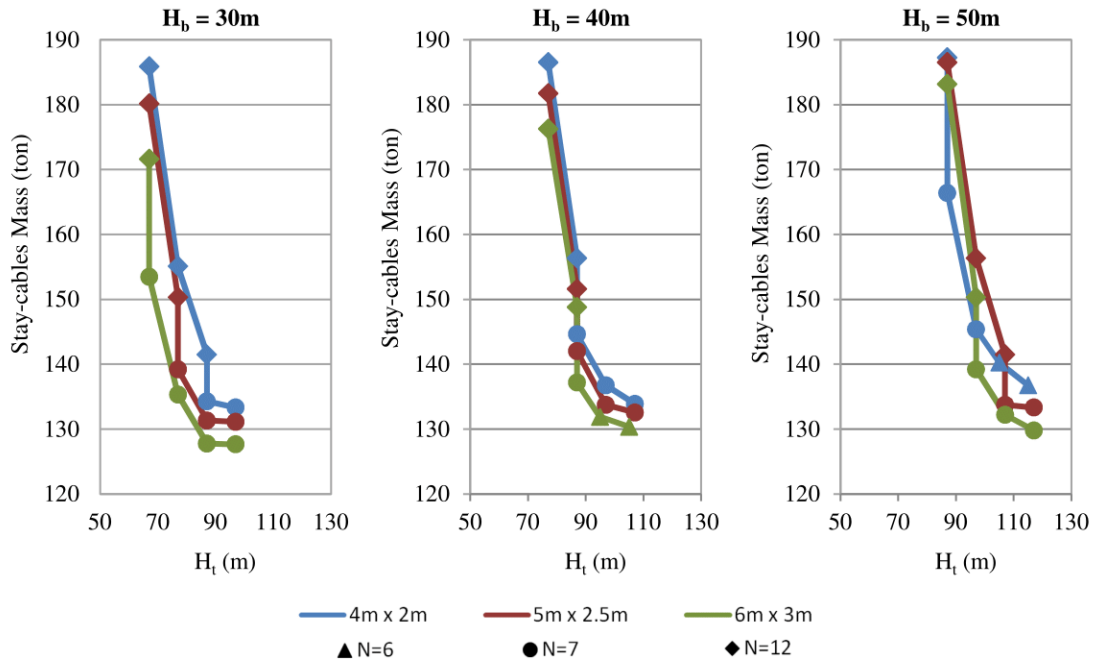


Figure 2. 6: Stay-cables mass as a function of H_b and tower dimensions $TL_1 \times TL_2$.

For all cases, the limiting constraint, for the optimization of the number of cables (N) and inertia of the deck I-girders (I), is the deck displacements due to live loads (Equation 2.8). This means that tower stiffness and deck rigidity relations obtained from these cases may be applied to any cable-stayed bridge deck and towers cross-section (and not only to the composite steel-concrete two I-girder deck and H-shape towers cable-stayed bridges) as a conceptual design tool. Figure 2. 7 presents curves that relate tower total height, tower longitudinal bending stiffness, optimized deck rigidity (EI_{deck}) and number of stay-cables.

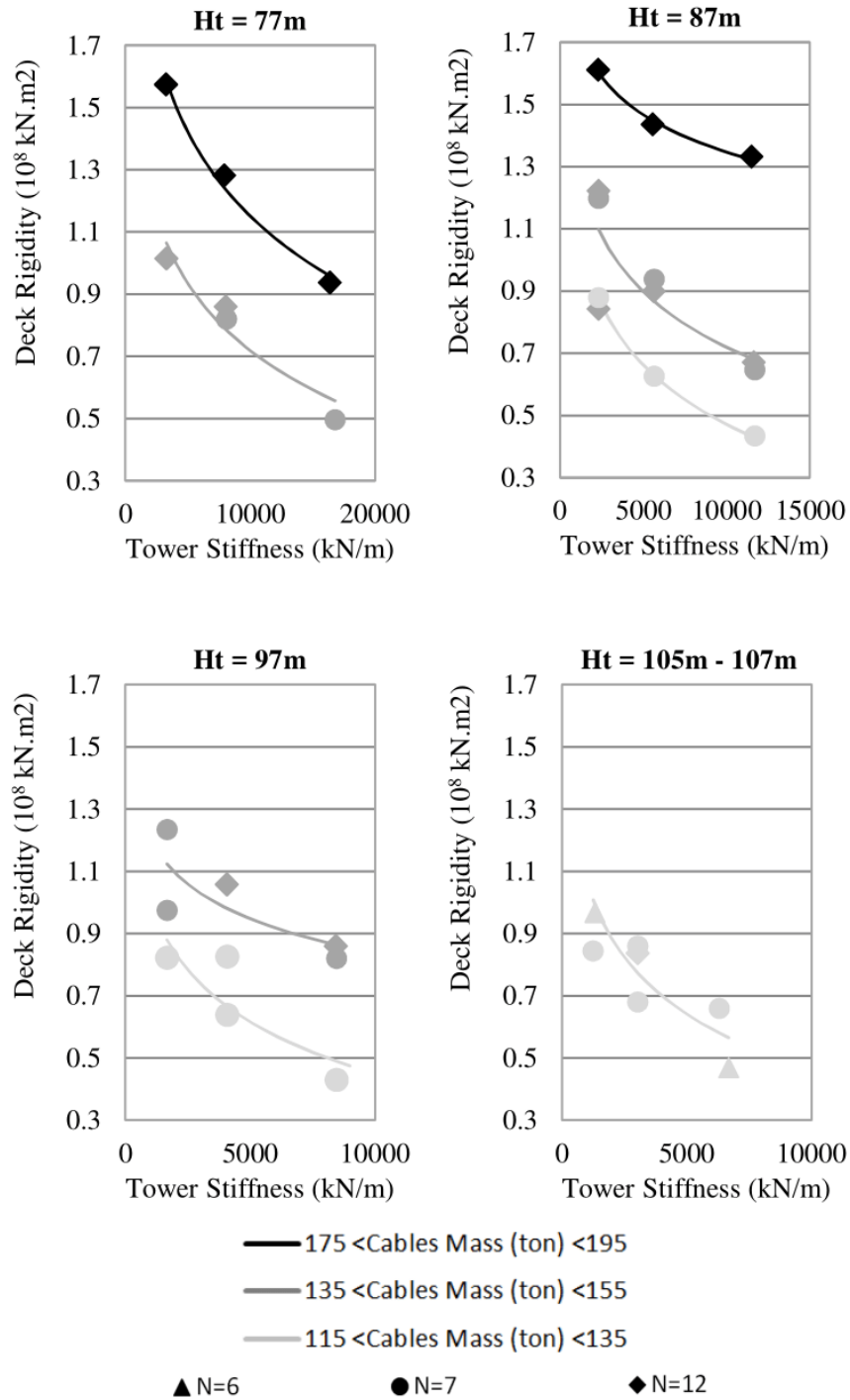


Figure 2. 7: Relation between deck rigidity and tower longitudinal stiffness to obtain lightest deck mass.

The data is presented as a function of ranges of stayed-cable masses: 115-135 tons; 135-155 tons; and 175-195 tons. The stay-cable mass range 155-175tons is not considered because only one sample, related to the tower total height, has been observed. By analyzing Figure 2. 7, it is easily noticed that an increase in tower total height corresponds to a decrease in tower stiffness. Besides that, the stay-cables mass range tends to reduce with the increase of tower total height, and the consequent increase of the cables angle of inclination (θ).

2.2.4 Numerical results for design *Objective-1* considering dead load and lane live load

The structural optimization for design *Objective-1* considering dead load and lane live load is conducted for cases with tower height below deck (H_b) equal to 30m, resulting in 15 case analyses (5 different values for H_a and 3 different values for tower cross-section). These analyses are performed and the optimal solution results for deck mass, stay-cable mass, and steel I-girder inertia, are displayed in Figure 2. 8.

The case of analysis for $H_a=40\text{m}$, $TL_1=6.0\text{m}$, and $TL_2=3.0\text{m}$, with $N=12$ and $I=0.007\text{m}^4$ presents the lightest deck mass (4880 tons) and the lowest mass of stay-cables (123 tons). For the equivalent case of analysis that considers truck loads, the optimized values are: $N = 7$, $I = 0.036\text{m}^2$, deck mass = 5311, and stay-cables mass = 128 tons. The considerable difference of deck steel I-girder inertia demonstrates the importance of considering truck loads in the optimization analysis. In terms of deck mass, by considering the truck loads, there is an increase of mass that varies from 8 to 12% (Table 2. 4).

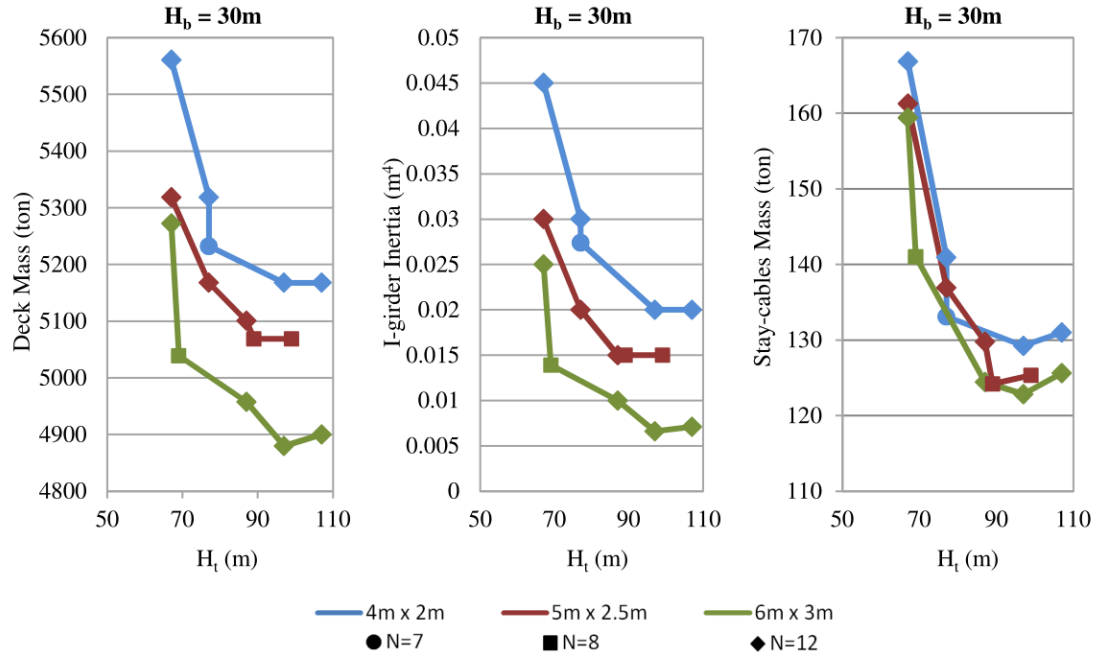


Figure 2. 8: Deck mass, stay-cables mass, and steel I-girder inertia due to dead and lane live loads as a function of tower dimensions TL1 x TL2.

Table 2. 4: Deck mass ratio (DL + lane LL)/(DL + truck and lane LL) obtained for *Objective-1*.

TL ₁ x TL ₂	H _a =10m	H _a =20m	H _a =30m	H _a =40m	H _a =50m
4m x 2m	0.88	0.88	0.90	0.91	0.92
5 x 2.5m	0.88	0.89	0.91	0.92	0.92
6 x 3m	0.92	0.91	0.92	0.92	0.92

2.2.5 Numerical results for design *Objective-1* considering dead load only

The structural optimization for design *Objective-1* considering dead load only is-evaluated for cases with tower height below deck $H_b=30m$. It is observed in Figure 2. 9 that for $H_a=30m$, $H_a=40m$, and $H_a=50m$, the I-girder inertia is equal to the lower bound ($I=0.005m^4$). The case of analysis for $H_a=50m$, $TL_1=5.0m$, and $TL_2=2.5m$, with $N=7$ and

$I=0.005\text{m}^4$ presents the lightest deck mass (4786 tons) and one of the lowest mass of stay-cables (120 tons). Comparison of the optimal solutions for dead load only, and for dead and truck plus lane live loads, reveals that considering live loads leads to an increase of deck mass that varies from 10 to 19% (Table 2. 5).

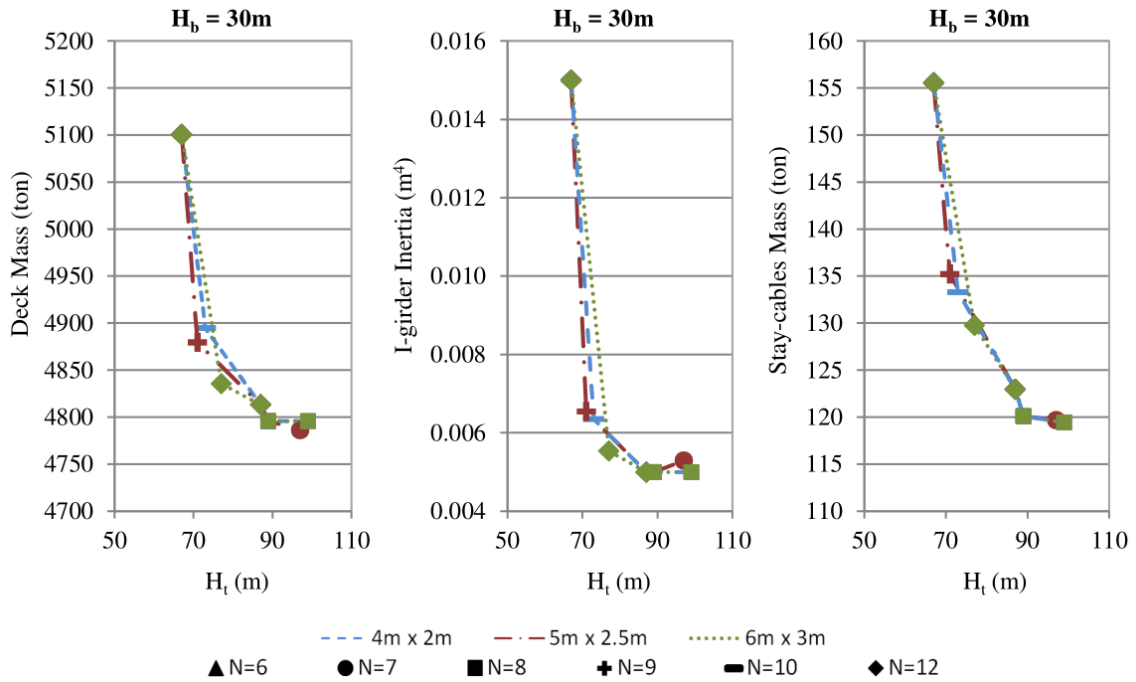


Figure 2. 9: Deck mass, stay-cables mass, and steel I-girder inertia due to dead load as a function of tower dimensions TL1 x TL2.

Table 2. 5: Deck mass ratio (DL)/(DL + truck and lane LL) obtained for *Objective-1*.

TL ₁ x TL ₂	H _a =10m	H _a =20m	H _a =30m	H _a =40m	H _a =50m
4m x 2m	0.81	0.81	0.83	0.84	0.85
5 x 2.5m	0.84	0.84	0.86	0.87	0.87
6 x 3m	0.89	0.87	0.89	0.90	0.90

2.2.6 Numerical results for design *Objective-2*

The optimal solutions for six cases of analysis – 2 cities (London, ON and North Bay, ON) and 3 values of tower height below the deck H_b (30m, 40m, 50m) - with the objective of obtaining the lowest cost of materials are evaluated. After comparing material costs (Figure 2. 10) and design variables obtained through optimization (Table 2. 6), one can observe that the lowest total material cost for both cities has been obtained for H_b equal to 30m.

Although cost factors for London-ON and North Bay-ON are about 15% difference for the steel (1.25 and 1.06, respectively), they are very similar for the concrete (1.45 and 1.50, respectively). As a result, the total material costs in London - ON are only 5%-9% more expensive than in North Bay – ON. With the increase of H_b , material total cost is also increased by 10% and 8% for London and North Bay, respectively. For both cities, the deck is responsible for 60% ($H_b = 50\text{m}$) to 65% ($H_b = 30\text{m}, 40\text{m}$) of the material cost.

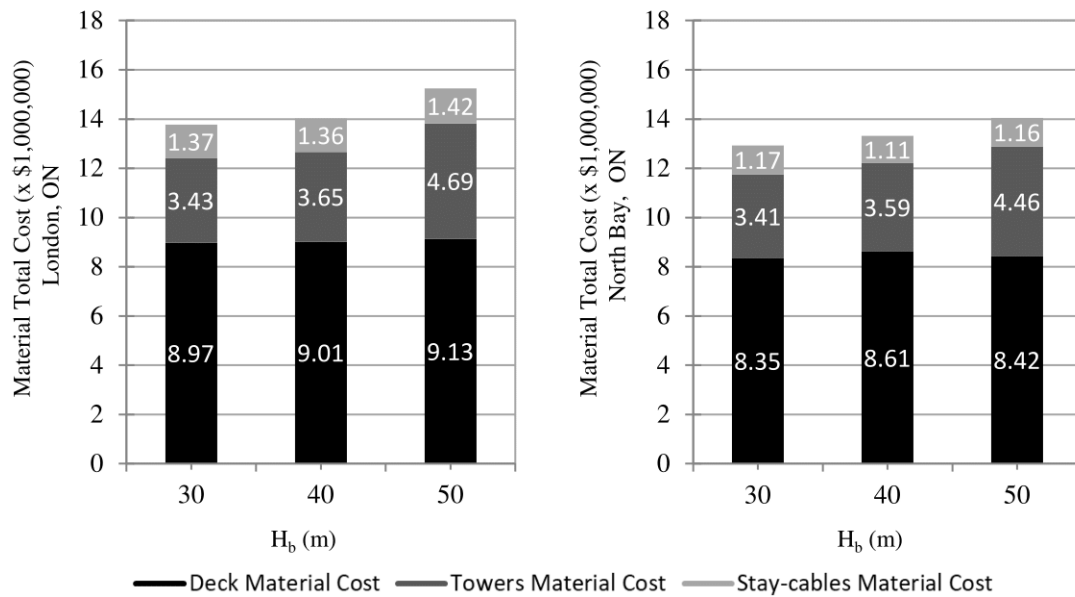


Figure 2. 10: Comparison of material costs for the considered case study.

Table 2. 6: Design variables obtained for the considered case study.

Elements	Variables	London, ON			North Bay, ON		
Towers	H _b (m)	30	40	50	30	40	50
	H _a (m)	46.0	47.3	45.3	42.0	47.4	46.0
	H _t (m)	93.0	104.3	112.3	89.0	104.4	113.0
	TL ₁ (m)	3.29	3.21	3.23	3.23	3.00	3.60
	TL ₂ (m)	1.14	1.14	1.59	1.24	1.27	1.24
Deck	I (m ⁴)	0.071	0.075	0.070	0.072	0.096	0.078
	t _c (m)	0.28	0.28	0.30	0.28	0.25	0.28
	D (m)	2.50	2.50	2.50	2.50	2.50	2.50
	b ₁ (m)	0.432	0.454	0.430	0.441	0.556	0.470
	t ₁ (m)	0.027	0.029	0.027	0.028	0.035	0.030
	b ₂ (m)	0.577	0.606	0.573	0.588	0.741	0.626
	t ₂ (m)	0.027	0.029	0.027	0.028	0.035	0.030
	w (m)	0.024	0.024	0.024	0.024	0.024	0.024
Cables	N	7	7	7	7	7	7
Material Cost (\$× 10 ⁶)		13,8	14,0	15,2	12,9	13,3	14,0

Table 2. 7 presents the constraint values for each case of analysis according to the constraint Equations 2.7 to 2.18. The constraint values confirm that the structures are properly optimized, once both the deck and the towers have their limiting constraint not smaller than -0.01 for the deck and -0.014 for the towers.

Table 2. 7: Constraint values (Equations 2.7 to 2.18) obtained for the considered case study.

Element	London, ON						North Bay, ON					
	H _b =30m		H _b =40m		H _b =50m		H _b =30m		H _b =40m		H _b =50m	
	g _i	Value	g _i	Value	g _i	Value	g _i	Value	g _i	Value	g _i	Value
Deck	g ₂	-0.008	g ₂	-0.001	g ₈	-0.008	g ₂	-0.004	g ₂	-0.01	g ₂	-0.001
	g ₈	-0.047	g ₈	-0.089	g ₂	-0.015	g ₈	-0.052	g ₈	-0.261	g ₈	-0.105
Tower	g ₁	-0.006	g ₄	-0.010	g ₄	-0.009	g ₁	-0.009	g ₄	-0.002	g ₄	-0.014
	g ₄	-0.091	g ₁	-0.015	g ₁	-0.084	g ₄	-0.092	g ₁	-0.043	g ₁	-0.094

The displacements at SLS and internal forces at ULS for the optimal cable-stayed bridge solutions for $H_b=30\text{m}$ in both cities are presented below. The two bridges have the same number of stay-cables ($N=7$), similar steel I-girder inertia ($I=0.071\text{m}^4$ and $I=0.072\text{m}^4$) and slight difference in H_a (less than 10%). The distribution of displacements and forces of the deck (Figures 2.11 and 2.12) and towers (Figures 2.13 and 2.14) are also similar for both bridges.

Small displacements at the towers (Table 2. 8) and deck (Figure 2. 11) show that the pre-tensioning forces (Figure 2. 15) are well distributed. Ratios between axial forces acting on the stay-cables and breaking loads have an average of 0.37 with maximum value equal to 0.47 for both bridges.

Table 2. 8: Maximum longitudinal displacements at the top of towers (SLS).

City	DL (cm)	LL (cm)
London, ON	3.1	16.9
North Bay, ON	2.7	16.1

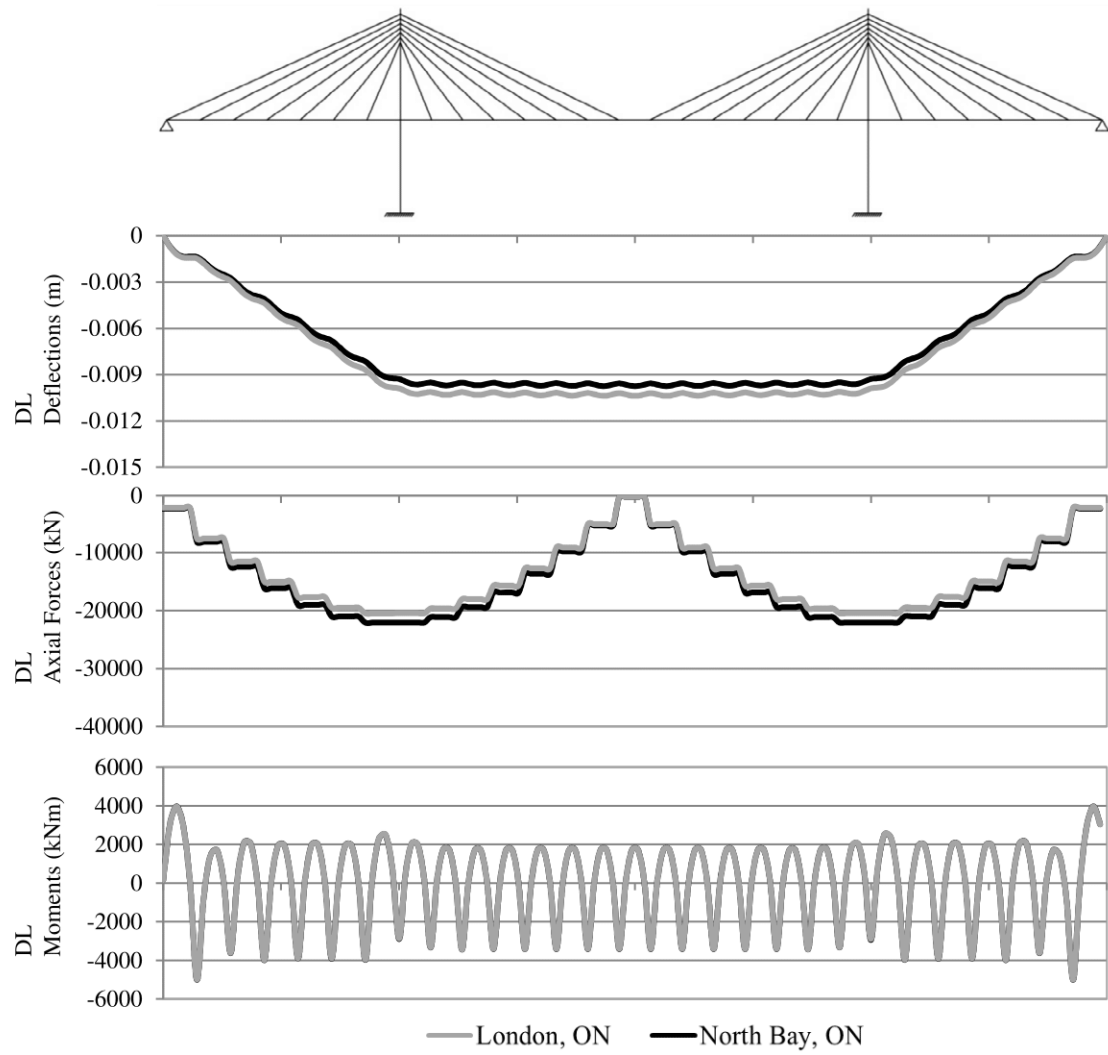


Figure 2. 11: Deflections, axial forces, and vertical bending moments at the deck spine due to dead loads for the considered case study.

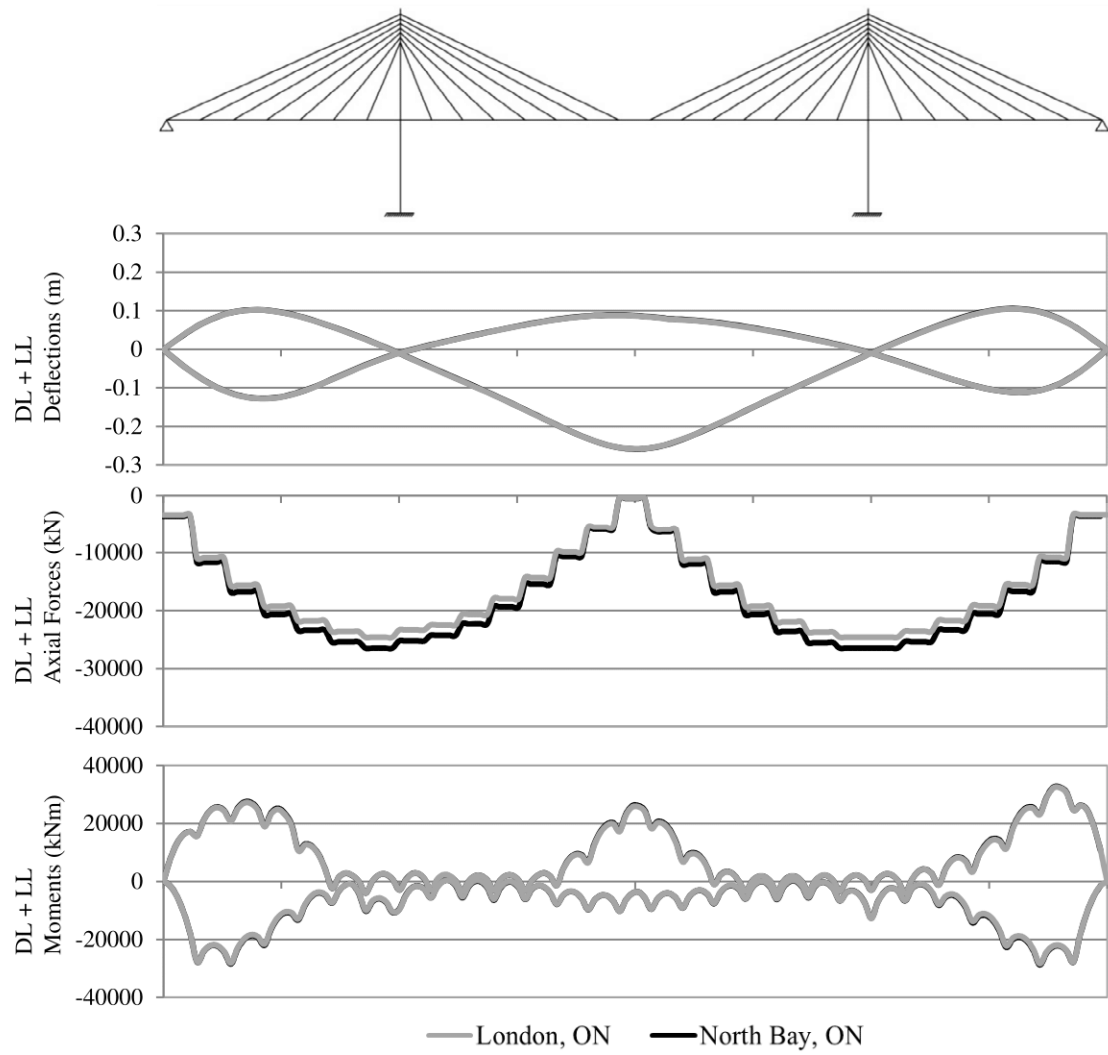


Figure 2. 12: Deflections, axial forces and vertical bending moments at the deck spine due to dead and live loads for the considered case study.

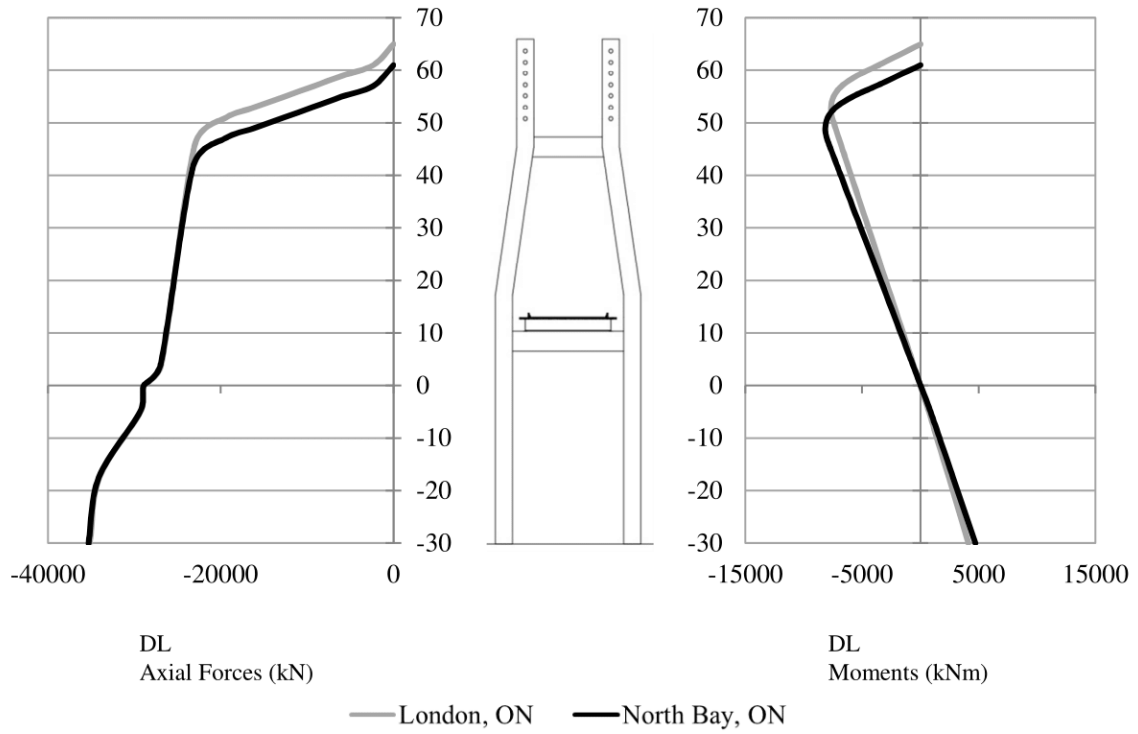


Figure 2.13: Axial forces and longitudinal bending moments in one of the tower's legs due to dead loads for the considered case study.

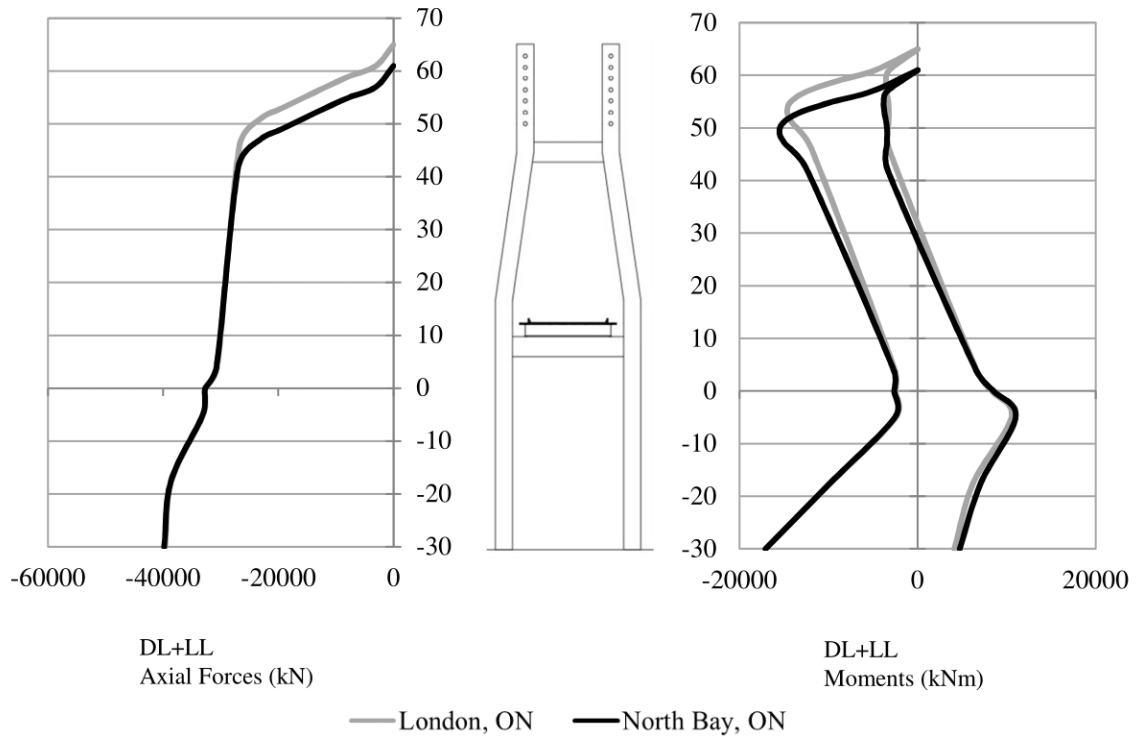


Figure 2.14: Axial forces and longitudinal bending moments in one of the tower's legs due to dead and live loads for the considered case study.

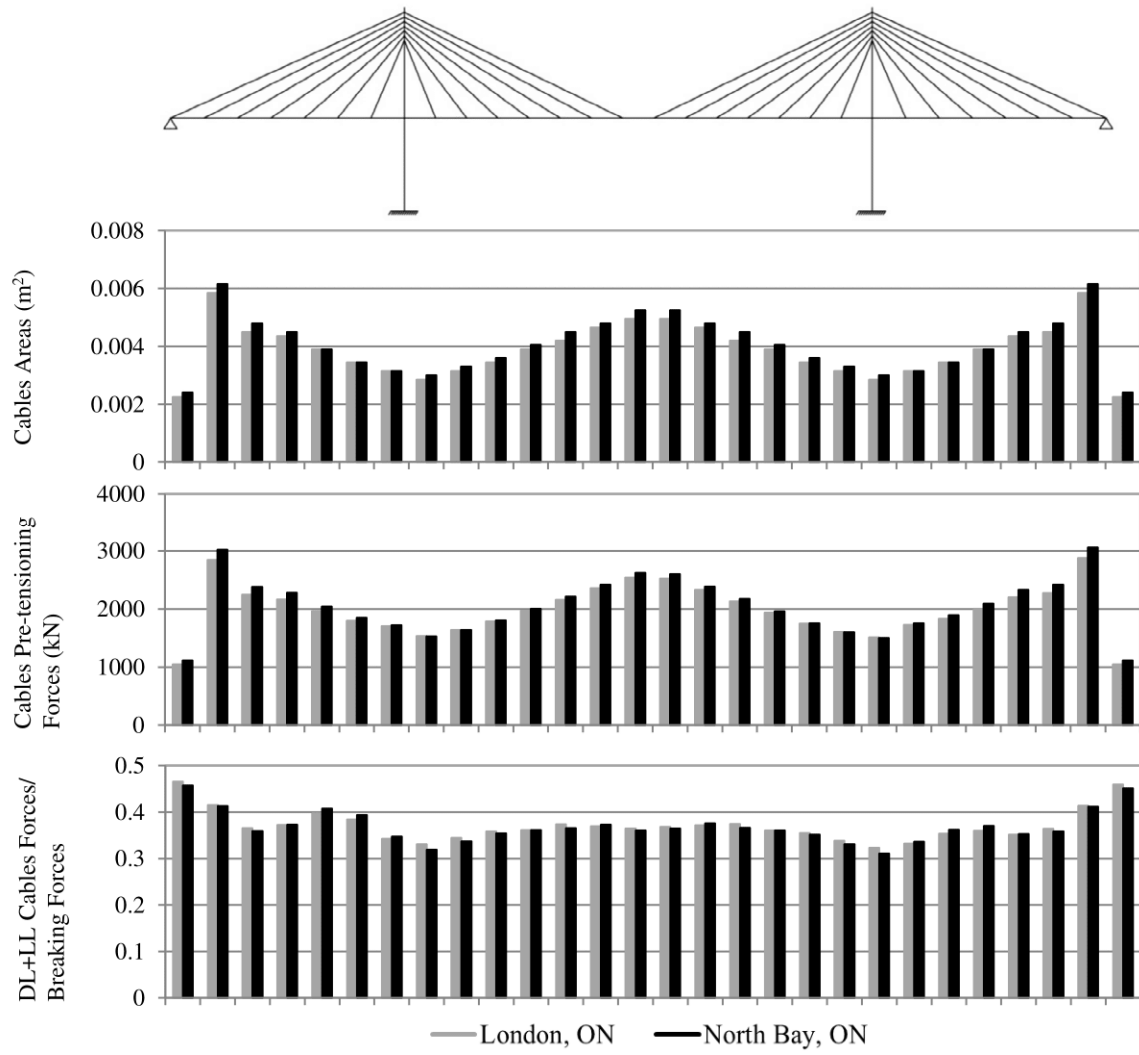


Figure 2. 15: Cables areas and pre-tensioning forces for the considered case study.

2.2.7 Comparison of costs from *Objective-1* and *Objective-2* considering dead load and truck plus lane live load

The solutions from *Objective-1* (i.e. minimum deck mass that attends all design constraints) illustrate that cases with tower cross-sections of 6m x 3m present the lowest value of deck mass for the various values of height below the deck (H_b). Table 2. 9 displays the optimal solutions from *Objective-1* with their location-specific cost of materials detailed by element for London-ON and North Bay-ON.

The costs of bridge configurations that are presented in Table 2. 9 for *Objective-1* are much higher than those that have been obtained for *Objective-2* (Table 2. 6), and vary between 32% and 34% for London-ON and 33% and 37% for North Bay-ON respectively. This considerable difference can be explained by the fact that *Objective-1* solutions have tower cross-sections 6m x 3m; while the *Objective-2* solutions have tower cross-sections of 3.29 x 1.14m, 3.21 x 1.14m, and 3.23 x 1.59m for London-ON, for example, with H_b equal to 30m, 40m, and 50m, respectively.

Table 2. 9: Material costs for the optimal solutions with minimum deck mass ($TL_1=6m$ and $TL_2=3m$).

H_b (m)	Elements	Mass (ton)	<i>Objective-1</i> Material Costs	
			London, ON	North Bay, ON
30	Deck	5304	\$ 7,216,643	\$ 6,717,297
	Towers	15326	\$ 11,946,922	\$ 12,090,223
	Cables	128	\$ 1,220,723	\$ 1,035,173
	Total	20757	\$ 20,384,288	\$ 19,842,693
40	Deck	5397	\$ 7,608,790	\$ 7,049,838
	Towers	15059	\$ 11,735,716	\$ 11,877,274
	Cables	132	\$ 1,261,088	\$ 1,069,403
	Total	20587	\$ 20,605,594	\$ 19,996,514
50	Deck	5417	\$ 7,687,953	\$ 7,116,968
	Towers	18281	\$ 14,264,714	\$ 14,432,545
	Cables	130	\$ 1,241,114	\$ 1,052,465
	Total	23828	\$ 23,193,781	\$ 22,601,978

To accurately compare the costs from *Objective-1* and *Objective-2*, it is necessary to consider solutions with similar tower cross-sections. In Tables 2.10 and 2.11, the optimal solution obtained with *Objective-1* for $H_b=30\text{m}$, $TL_1=3.0\text{m}$, and $TL_2=1.5\text{m}$ is compared with the optimal solution from *Objective-2* for $H_b=30\text{m}$ (Table 2. 6).

The difference in total material costs is only 0.4% for London-ON and 5% for North Bay-ON, demonstrating the efficacy of the approach for attending different design objectives.

Table 2. 10: Comparison of material costs for *Objective-1* ($H_b=30\text{m}$, $H_a=50\text{m}$, $TL_1=3.0\text{m}$, and $TL_2=1.5\text{m}$) and *Objective-2* ($H_b=30\text{m}$) optimal solutions in London-ON.

Elements	<i>Objective-1</i>		<i>Objective-2</i>	
	Mass (ton)	Cost	Mass (ton)	Cost
Deck	5733	\$ 8,897,196	6214	\$ 8,973,406
Towers	4528	\$ 3,632,440	4065	\$ 3,429,717
Cables	135	\$ 1,291,557	143	\$ 1,366,262
Total	10395	\$ 13,821,193	10422	\$ 13,769,385

Table 2. 11: Comparison of material costs for *Objective-1* ($H_b=30\text{m}$, $H_a=40\text{m}$, $TL_1=3.0\text{m}$, and $TL_2=1.5\text{m}$) and *Objective-2* ($H_b=30\text{m}$) optimal solutions in North Bay-ON.

Elements	<i>Objective-1</i>		<i>Objective-2</i>	
	Mass (ton)	Cost	Mass (ton)	Cost
Deck	5858	\$ 8,576,245	6242	\$ 8,345,242
Towers	4583	\$ 3,809,325	4088	\$ 3,408,941
Cables	144	\$ 1,166,617	144	\$ 1,169,575
Total	10585	\$ 13,552,187	10474	\$ 12,923,758

2.3 Validation of the discrete phases design approach

Comparisons between the optimized solutions provided by *Objective-1* (lightest deck weight) and *Objective-2* (lowest material cost for the entire structure) presented in Tables 2.10 and 2.11 indicate consistency of the approach proposed in this chapter. Additionally, the constraint values presented in Table 2. 7 are very close to the allowable limits to attend the SLS and ULS, demonstrating that an optimum solution is obtained. Finally, a case example presented by Hassan *et al.* (2014) is performed considering exactly the same: (i) cable-stayed bridge fixed dimensions (total length, deck width, etc.), (ii) material properties and cost, (iii) design constraints, (iv) design variables lower and upper bounds and (iv) load combinations in order to validate the Discrete Phases Design Approach.

The cable-stayed bridge considered in the validation is similar to the geometry presented in Figure 1, with two I-girder composite deck and hollow reinforced concrete box tower cross-section. The concrete slab deck is 14.20m (B_t) wide and includes 2 lanes. The bridge total length is $L=350\text{m}$ with a main span $L_1=171.70\text{m}$ and side span $L_2= 89.15\text{m}$. For the structural steel the material properties are: modulus of elasticity $E_s=200\text{GPa}$, specific weight $\gamma_s=77\text{kN/m}^3$, yield stress $F_y=350\text{MPa}$, and cost $C_s=12,000\text{\$/ton}$. For the concrete: modulus of elasticity $E_c=24.87\text{GPa}$, specific weight $\gamma_c=24\text{kN/m}^3$, compressive strength $f'_c=30\text{MPa}$, and cost $C_c=4,218\text{ \$/m}^3$. For the stay cables: modulus of elasticity $E_{sc}=205\text{GPa}$, specific weight $\gamma_{sc}=82.40\text{kN/m}^3$, breaking stress $T_{sc}=1.6\text{GPa}$, and cost $C_{sc}=60,000\text{ \$/ton}$.

The design constraints are equivalent to the ones presented in Item 2.2.1.5, but the constraint related to the displacements at the top of towers due to live loads (Equation 2.10) is not taken into account in order to have the same conditions as the case optimized by Hassan *et al.* (2014). The design variables and their bounds are as follows: number of cables N [4, 15], deck I-girder inertia I [0.005m^4 , 0.50 m^4], concrete thickness t_c [0.16m, 0.40m], tower cross-section dimensions TL_1 [1.0m, 6.0m] and TL_2 [1.0m, 5.0m], tower height above the deck H_a [10.5m, 42.0m]. The dominant ULS load combination is 1.1(DL) + 1.7(LL) and the SLS load combination is 1.0(DL) + 0.9(LL). For the live loads (LL), only the uniformly distributed load is considered in the analysis.

The optimized design variables and the costs obtained with the Discrete Phases Design Approach are compared to the results presented by Hassan *et al.* (2014) in Table 2. 12. The Discrete Phases Approach reduces the I-girder depth from 2.06m to 1.25m when comparing to Hassan *et al.* (2014). That might be explained by the fact that this girder depth reduction occurs together with an increase of number of stay-cables and tower longitudinal stiffness by almost 29.4%. Overall, the total cost is reduced by 2.0%, allowing the validation of the approach presented in this chapter.

Table 2. 12: Comparison of material costs and design variables for validation of the Discrete Phases Design Approach.

Elements	Variables	Hassan <i>et al.</i> (2014)	Discrete Phases Design Approach
Tower	H _a (m)	32.5	31.3
	TL ₁ (m)	2.75	3.12
	TL ₂ (m)	1.00	1.00
	Cost (\$)	1,219,385	1,355,493
Deck	t _c (m)	0.16	0.16
	D (m)	2.06	1.25
	b ₁ (m)	0.357	0.363
	t ₁ (m)	0.019	0.023
	b ₂ (m)	0.438	0.484
	t ₂ (m)	0.023	0.023
	w (m)	0.012	0.012
	Cost (\$)	6,661,027	5,563,805
Cables	N	6	7
	Cost (\$)	3,076,943	3,819,542
Total Cost (\$)		10,957,355	10,738,840

2.4 Conclusions

In this study, the structural optimization of composite steel-concrete two I-girder cable-stayed bridges is accomplished by adopting a *5-Phases* approach. This approach is based on three-dimensional finite element models and the Real Code Genetic Algorithm (RCGA). One of the advantages of this approach is that by using the concept of primary and secondary variables, the total number of variables to be optimized with the RCGA procedure is significantly reduced. Two independent objective functions are considered in the optimization process of a cable-stayed bridge with total length $L=400\text{m}$, main span $L_1=200\text{m}$, and side spans $L_2=100\text{m}$.

The first design objective, *Objective-1*, aims to obtain the lightest deck mass that attends to all design criteria. It is observed that robust tower cross-sections with greater area and inertias provide lower values of deck mass. It is also noted that the stay-cables mass tends to increase/decrease proportionally with an increase/decrease in deck mass because the stay-cable areas are selected to achieve a deck continuous beam type of behaviour. Additionally it is noted that for different tower cross-sections, the minimum deck masses are obtained for height above the deck H_a equal to 40m or 50m.

When comparing the optimal solutions of dead load only versus that from dead and truck plus lane live loads, the former led to 10% (6mx3m tower cross-section) to 19% (4mx2m tower cross-section), increase in the deck mass values. Besides that, when comparing the optimal solutions of dead and lane live loads versus dead and truck plus lane live loads, the former provides 8% (6mx3m tower cross-section) to 12% (4mx2m tower cross-section) higher deck mass values. These results show the importance of not only considering the live loads, but also of considering both the truck and the lane loads.

The data from *Objective-1* provides curves that relate deck rigidity, towers stiffness and stay-cable mass for cases where the deck steel I-girder and the number of cables are optimized for obtaining the lightest deck possible. These curves can be used for any type of cable-stayed bridge deck and towers cross-section, once the limiting constraint is the displacement at the deck due to truck plus lane live loads.

The second design objective, *Objective-2*, aims to obtain the lowest total material cost that attends to all design criteria. The material cost for two cities is considered and shows that despite difference in cost, the design variables have similar values for the same construction site conditions. As the *Objective-1* optimal solution tends to have a more slender deck and robust tower cross-sections, the cost of its solutions cannot be directly compared to *Objective-2* optimal material costs. When *Objective-1* and *Objective-2* solutions have analogous tower cross-sections dimensions, their total material cost differs by less than 5%.

Overall, the results from the *5-Phases* approach provides small displacement values for the deck and towers, and well distributed internal forces. Therefore, the discrete phases approach can be successfully used for structural optimization of cable-stayed bridges under dead and moving live loads, and for two distinct design objectives – minimum deck weight or minimum material cost.

References

- AASHTO. 2012. LRFD Bridge Design Specifications, 6th edition, Washington, D.C., USA.
- Adeli, H., Zhang, J., 1995. Fully nonlinear analysis of composite girder cable-stayed bridges. *Computers & structures*, 54(2): 267-277.
- CAN/CSA-S6-14, 2014, Canadian Highway Bridge Design Code.
- Chen, D.W., Au, F.T.K., Tham, L.G., and Lee, P.K.K. 2000. Determination of initial cable forces in prestressed concrete cable-stayed bridges for given design deck profiles using the force equilibrium method. *Computers and Structures*, 74(1): 1–9.
- Deb, K. 2000. An efficient constraint handling method for genetic algorithms. *Computer methods in applied mechanics and engineering*, 186: 311-338.
- Ernst, J.H. 1965. Der E-Modul von Seilen unter berucksichtigung des Durch- hanges. *Der Bauingenieur*, 40(2): 52–55 (In German).
- Hassan, M.M., Nassef, A.O., and El Damatty, A.A. 2012. Determination of optimum post-tensioning cable forces of cable-stayed bridges. *Engineering Structures*, 44: 248–259.
- Hassan, M.M., Nassef, A.O., and Damatty, A.A. El. 2013a. Surrogate Function of Post-Tensioning Cable Forces for Cable-Stayed Bridges. *Advances in Structural Engineering*, 16(3): 559–578.
- Hassan, M.M., Nassef, A.O., and Damatty, A.A. El. 2013b. Optimal design of semi-fan cable-stayed bridges. *Canadian Journal of Civil Engineering*, 40(3): 285–297.
- Hassan, M.M., El Damatty, A.A., and Nassef, A.O. 2014. Database for the optimum design of semi-fan composite cable-stayed bridges based on genetic algorithms. *Structure and Infrastructure Engineering*, 11(8): 1054–1068.
- Janjic, D., Pircher, M., and Pircher, H. 2003. Optimization of Cable Tensioning in Cable-Stayed Bridges. *Journal of Bridge Engineering*, 8(3): 131–137.
- Lee, T.Y., Kim, Y.H., and Kang, S.W. 2008. Optimization of tensioning strategy for asymmetric cable-stayed bridge and its effect on construction process. *Structural and Multidisciplinary Optimization*, 35(6): 623–629.
- Michalewicz, Z., Fogel, D.B. 2000. *How to solve it: modern heuristics*. Springer-Verlag Berlin Heidelberg.
- Negrão, J.H.O., and Simões, L.M.C. 1997. Optimization of cable-stayed bridges with three-dimensional modelling. *Computers & Structures*, 64(1–4): 741–758.

- Pedro, J.J., and Reis, A.J. 2016. Composite cable-stayed bridges: state of the art. *Proceedings of the Institution of Civil Engineers - Bridge Engineering*, 169(1): 13–38.
- Podolny JR, W., SCALZI, J.B. 1976. *Construction and Design of Cable-Stayed Bridges*. John Wiley & Sons, Inc. USA.
- Simões, L.M.C., and Negrão, J.H.O. 1994. Sizing and geometry optimization of cable-stayed bridges. *Computers & Structures*, 52(2): 309-321.
- Sivanandam, S.N., Deepa, S.N. 2008. *Introduction to Genetic Algorithms*. Springer.
- Svensson, H. 2012. *Cable-Stayed Bridges. 40 Years of Experience Worldwide*. 1 ed. Ernst & Sohn GmbH & Co.KG.
- Troitsky, M. S. 1988. *Cable-Stayed Bridges: Theory and Design*. 2 ed. BSP Professional Books, Oxford.
- Wang, P H; Tseng, T C; Yang, C.G. 1993. Initial shape of cable-stayed bridges. *Computers & Structures* , 47(I): 111–123.
- Wilson, J.C, and Gravelle, W. 1991. Modelling of a cable-stayed bridge for dynamic analysis. *Earthquake Engineering and Structural Dynamics*, 20(8): 707–721.

Chapter 3

3 Comparison between the theoretical and experimental wind responses of a full aeroelastic model test of a cable-stayed bridge

3.1 Introduction

Long-span bridges are susceptible to dynamic responses due to buffeting wind loads, even if the structure is considered stable in flutter and vortex shedding phenomena. Additionally, the action of atmospheric turbulence on bridges significantly contributes to the envelopes of internal forces. In other words, the size of the structural elements may be governed by the fluctuating wind forces (Davenport, 1966; Holmes, 2015).

Two of the most usual wind tunnel techniques are exploited on the buffeting analyses: (1) the sectional model test, and (2) the full aeroelastic model test of the completed bridge. The first test determines the static aerodynamic force and moment coefficients, which are measured in both smooth and turbulent flows from a range of angles of wind attack. The second test provides information on the accelerations, displacements and moments in the sections of the deck and towers.

While only the external shape of the deck is modelled in the first model test, in the second model test all structural members – deck, towers, cables and connections – are modelled. Moreover, the geometric properties, masses, and stiffnesses must be scaled to respect the mode shapes and the frequencies of the prototype bridge. Thus, the full aeroelastic model test is relatively expensive, due to the need of manufacturing a complex scaled model, as well as it is time-consuming because even the surrounding topography needs to be considered.

Considering all that, two approaches to evaluate bridge responses under turbulent wind action are examined and compared for the case example of the Prospect Verona Bridge, Maine (USA). The first approach is theoretical while being fed by experimental data from sectional wind tunnel test and is based on: (i) the general procedure of equivalent static buffeting wind loads developed by Davenport and King (1984); and (ii) the Finite Element

Method (FEM). The equivalent static wind loads equate to an effective load distribution that is applied to the bridge deck and should produce the same effects—such as the displacements and moments—that are expected from the fluctuating wind loads (Holmes, 2015). These effective wind loads are a function of: (1) the static aerodynamic force and the moment coefficients, which are obtained from the sectional model test; (2) the spectrums of the longitudinal and vertical velocities that describe the distribution of the turbulence with frequency (ESDU 74031; Holmes, 2015); (3) the aerodynamic admittances that reflect the influence of the gust size in relation to the size of the structure (Davenport, 1966; Davenport, 1977; Matsuda *et al.*, 1999); (4) the joint acceptance function, which specifies the capacity of the turbulence to excite each mode of vibration (Davenport, 1966; Davenport, 1977; Davenport and King, 1982). Additionally, gust factors are considered with respect to the towers in order to reflect the effect of the buffeting loads on these elements. Mean and peak wind loads are applied to the finite element model and displacements obtained from the theoretical approach are examined.

The second approach is experimental and is based on testing the full aeroelastic model of the cited bridge tested at The Boundary Layer Wind Tunnel Laboratory at Western University (King *et al.*, 2005). The displacements at the deck and top of the towers are correlated to determine how accurately the first approach (theoretical) can predict results compared to the second approach (experimental).

3.2 Wind loads and bridge responses

The formulation to estimate the equivalent static buffeting loads on the bridge deck follows the general approach developed for the study of wind action on the Sunshine Skyway Bridge, Florida (Davenport and King, 1984). This approach takes into consideration the fact that persistent movement of a long-span bridge in a strong wind is due to its various mode shapes, and that this behavior can be simulated by utilizing mode shapes of the first symmetric and the first antisymmetric in each of the following movements of the deck: lateral bending, vertical bending, and torsional rotation, totalizing mode shapes. In this way, other than mean wind loads, peak wind loads that reflect the background and the

resonant components of the response are applied to the bridge deck. While the background component introduces the influence of the load frequency range that is too low to excite the structure, the resonant components reflect the influence of each mode shape of the structure that is considered in the response estimation.

The quasi-steady equations for motion of deck in gusty wind can be expressed according to the following equations (Davenport, 1966):

$$F'_X(\eta, t) = \rho \bar{U} B C_{F_X} u(t) + \frac{1}{2} \rho \bar{U} B \frac{dC_{F_X}}{d\alpha} w(t) \quad (3.1.a)$$

$$F'_Z(\eta, t) = \rho \bar{U} B C_{F_Z} u(t) + \frac{1}{2} \rho \bar{U} B \frac{dC_{F_Z}}{d\alpha} w(t) \quad (3.1.b)$$

$$M'_\theta(\eta, t) = \rho \bar{U} B^2 C_{M_\theta} u(t) + \frac{1}{2} \rho \bar{U} B^2 \frac{dC_{M_\theta}}{d\alpha} w(t) \quad (3.1.c)$$

where η, X, Z are the deck longitudinal, transversal, and vertical directions respectively (see Figure 3. 1); $F'_X(\eta, t)$, $F'_Z(\eta, t)$ and $M'_\theta(\eta, t)$ are the quasi-steady horizontal force (wind direction), vertical force and pitching moment to be applied to the bridge deck due to the turbulent wind flow; C_{F_X} , C_{F_Z} and C_{M_θ} are the force coefficients obtained from the static sectional model test; $\frac{dC_{F_X}}{d\alpha}$, $\frac{dC_{F_Z}}{d\alpha}$ and $\frac{dC_{M_\theta}}{d\alpha}$ are the slopes of force coefficients at a specific angle of attack α ; ρ is the air mass density; \bar{U} is the mean wind speed at the deck height; B is the deck width; $u(t)$ and $w(t)$ are the horizontal and vertical velocity fluctuations.

The mean-square fluctuating generalized horizontal and vertical forces, and pitching moment for the j th mode of vibration are given by:

$$\overline{Q'^2_{X,j}} = \int_0^L \int_0^L \overline{F'_X(\eta_1, t) F'_X(\eta_2, t)} \phi_j(\eta_1) \phi_j(\eta_2) d\eta_1 d\eta_2 \quad (3.2.a)$$

$$\overline{Q'^2_{Z,j}} = \int_0^L \int_0^L \overline{F'_Z(\eta_1, t) F'_Z(\eta_2, t)} \phi_j(\eta_1) \phi_j(\eta_2) d\eta_1 d\eta_2 \quad (3.2.b)$$

$$\overline{Q'^2_{\theta,j}} = \int_0^L \int_0^L \overline{F'_\theta(\eta_1, t) F'_\theta(\eta_2, t)} \phi_j(\eta_1) \phi_j(\eta_2) d\eta_1 d\eta_2 \quad (3.2.c)$$

where $\phi_j(\eta)$ is the j th mode shape function.

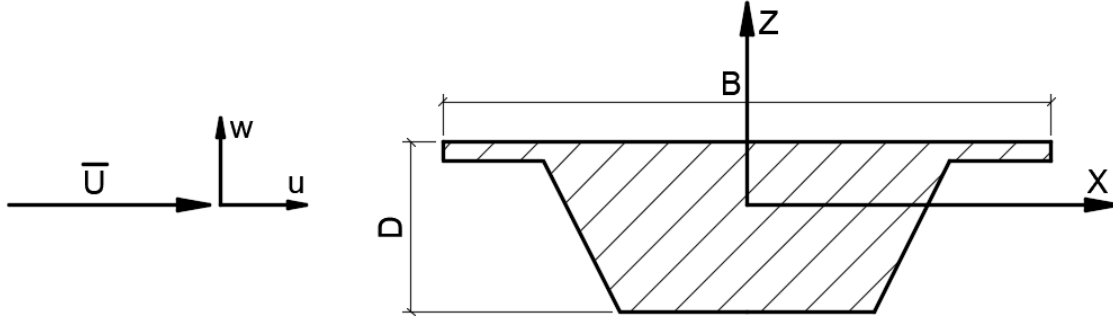


Figure 3. 1: Scheme of deck cross-section dimensions, mean and turbulent wind speeds, and axis representation.

The power spectral density of the fluctuating generalized forces in the direction X, Z and θ as a function of the reduced frequency f^* can be expressed by the equations below (adapted from Davenport and King, 1984):

$$S_{Q'_{x,j}}(f^*) = \left[(qBC_{F_x})^2 4 \left(\frac{\sigma_u}{\bar{U}} \right)^2 \frac{S_{uu}(f^*)}{\sigma_u^2} + \left(qB \frac{dC_{F_x}}{d\alpha} \right)^2 \left(\frac{\sigma_w}{\bar{U}} \right)^2 \frac{S_{ww}(f^*)}{\sigma_w^2} \right] |J_j(f^*, \eta_1, \eta_2)|^2 \quad (3.3.a)$$

$$S_{Q'_{z,j}}(f^*) = \left[(qBC_{F_z})^2 4 \left(\frac{\sigma_u}{\bar{U}} \right)^2 \frac{S_{uu}(f^*)}{\sigma_u^2} + \left(qB \frac{dC_{F_z}}{d\alpha} \right)^2 \left(\frac{\sigma_w}{\bar{U}} \right)^2 \frac{S_{ww}(f^*)}{\sigma_w^2} \right] |J_j(f^*, \eta_1, \eta_2)|^2 \quad (3.3.b)$$

$$S_{Q'_{\theta,j}}(f^*) = \left[(qB^2 C_{F_\theta})^2 4 \left(\frac{\sigma_u}{\bar{U}} \right)^2 \frac{S_{uu}(f^*)}{\sigma_u^2} + \left(qB^2 \frac{dC_{F_\theta}}{d\alpha} \right)^2 \left(\frac{\sigma_w}{\bar{U}} \right)^2 \frac{S_{ww}(f^*)}{\sigma_w^2} \right] |J_j(f^*, \eta_1, \eta_2)|^2 \quad (3.3.c)$$

$$f^* = \frac{fB}{\bar{U}} \quad (3.4)$$

where σ_u and σ_w are the standard deviation of longitudinal and vertical wind velocity fluctuations; $I_u = \frac{\sigma_u}{\bar{U}}$ and $I_w = \frac{\sigma_w}{\bar{U}}$ are the wind longitudinal and vertical turbulence intensity; $S_{uu}(f^*)$ and $S_{ww}(f^*)$ are the power spectral density for longitudinal and vertical wind velocity, respectively; $|J(f^*, \eta_1, \eta_2)|^2$ is the joint acceptance function.

To calculate the power spectral density of the fluctuating generalized forces $S_{Q'}$ (Eq. 3.3), the following parameters are used to describe the wind action:

1. the variation of the mean wind speed according to the height above the ground is calculated using the logarithm profile, which is considered to be the most precise expression to simulate the wind speed profile;

2. the spectral density function for the longitudinal turbulence S_{uu} was estimated using the von Karman spectral equation, which is generally accepted as the best analytical representation of isotropic turbulence (ESDU 74031):

$$\frac{f S_{uu}(f)}{\sigma_u^2} = \frac{4\left(\frac{f l_u}{U}\right)}{\left[1 + 70.8\left(\frac{f l_u}{U}\right)^2\right]^{5/6}} \quad (3.5)$$

$$l_u = \frac{25\bar{z}^{0.35}}{z_0^{0.063}} \quad (3.6)$$

where σ_u^2 is the variance of longitudinal velocity fluctuation; l_u is the turbulence length scale; and \bar{z} is the effective height.

3. the vertical velocity component has different characteristics, and its power spectral density function S_{ww} is estimated by adopting the Busch and Panofsky spectral equation (Holmes, 2015):

$$\frac{f S_{ww}(f)}{\sigma_w^2} = \frac{2.15\left(\frac{f \bar{z}}{U}\right)}{1 + 11.16\left(\frac{f \bar{z}}{U}\right)^{5/3}} \quad (3.7)$$

where σ_w^2 is the variance of vertical velocity fluctuation.

In order to estimate the interaction between the gust and the structure, the joint acceptance function is employed to consider the ability of the turbulence to excite each one of the modes of vibration that are being considered in the analysis (Davenport, 1966; Davenport, 1977; Davenport and King, 1982). The equation for the joint acceptance function $|J(f^*, \eta_1, \eta_2)|^2$ is given by Davenport and King (1984).

$$|J(f^*, \eta_1, \eta_2)|^2 = \frac{1}{\bar{N}^2} \int_0^L \int_0^L R_{F'1F'2}(\eta_1, \eta_2, f^*) \phi(\eta_1) \phi(\eta_2) d\eta_1 d\eta_2 \quad (3.8)$$

$$\bar{N} = \int_0^L \phi(\eta)^2 d\eta \quad (3.9)$$

$$R_{F'1F'2}(\eta_1, \eta_2, f^*) = e^{\frac{-Y(\eta_1 - \eta_2)f^*}{B}} \quad (3.10)$$

where $R_{F'_1 F'_2}(\eta_1, \eta_2, f^*)$ is the cross spectrum of forces F'_1 and F'_2 at cross sections η_1 and η_2 for the frequency f^* , and Y is a constant with values ranging between 5 and 8 that defines the effective width of the correlation.

The power spectral density of displacements in the three considered directions X, Z and θ can be expressed as follow; (adapted from Davenport and King, 1984):

$$S_{X',j}(f^*) = \frac{1}{K_j^2} |H_j(f^*)|^2 |\chi_X(f^*)|^2 S_{Q'_{X,j}}(f^*) \quad (3.11.a)$$

$$S_{Z',j}(f^*) = \frac{1}{K_j^2} |H_j(f^*)|^2 |\chi_Z(f^*)|^2 S_{Q'_{Z,j}}(f^*) \quad (3.11.b)$$

$$S_{\theta',j}(f^*) = \frac{1}{K_j^2} |H_j(f^*)|^2 |\chi_\theta(f^*)|^2 S_{Q'_{\theta,j}}(f^*) \quad (3.11.c)$$

where K_j is the structure stiffness; $|H_j(f^*)|^2$ is the mechanical admittance; $|\chi_X(f^*)|^2$, $|\chi_Z(f^*)|^2$ and $|\chi_\theta(f^*)|^2$ are the aerodynamic admittances, which reflect the influence of the sizes of both, the gust and the structure (Davenport, 1966; Davenport, 1977) on the capacity of the gust to affect the structure. According to Matsuda *et al.* (1999), aerodynamic admittance are difficult parameters to be measured in wind tunnel test and are often adopted as the Davenport function (Eq. 3.12; Davenport, 1962 *apud* Matsuda *et al.*, 1999) for longitudinal buffeting forces and as Holmes function (Eq. 3.13; Holmes, 1975 *apud* Matsuda *et al.*, 1999) for vertical buffeting forces and pitching buffeting moments.

$$|\chi_X^u(f')|^2 = \frac{2}{(kf')^2} (kf' - 1 + e^{-kf'}) \quad (3.12)$$

$$|\chi_{Z,\theta}^w(f^*)|^2 = \frac{1}{1+4f^*} \quad (3.13)$$

where $f' = fD/\bar{U}$ is the reduced frequency as a function of the deck height D ; $f^* = fB/\bar{U}$ is the reduced frequency in function of the deck width B ; k is the decay factor.

The mean-square value of fluctuating generalized deflections ($\sigma_{X',j}^2$, $\sigma_{Z',j}^2$ and $\sigma_{\theta',j}^2$) are obtained by integrating the power spectral density of displacements over all frequencies:

$$\sigma_{X',j}^2 = \int_0^\infty \frac{1}{K_j^2} |H_j(f^*)|^2 |\chi_X(f^*)|^2 S_{Q'_{X,j}}(f^*) \frac{\bar{U}}{B} df^* \quad (3.14.a)$$

$$\sigma_{z',j}^2 = \int_0^\infty \frac{1}{K_j^2} |H_j(f^*)|^2 |\chi_z(f^*)|^2 S_{Q',z,j}(f^*) \frac{\bar{U}}{B} df^* \quad (3.14.b)$$

$$\sigma_{\theta',j}^2 = \int_0^\infty \frac{1}{K_j^2} |H_j(f^*)|^2 |\chi_\theta(f^*)|^2 S_{Q',\theta,j}(f^*) \frac{\bar{U}}{B} df^* \quad (3.14.c)$$

The mean-square value of the equivalent static forces ($\sigma_{\bar{F}',x,j}^2$, $\sigma_{\bar{F}',z,j}^2$ and $\sigma_{\bar{F}',\theta,j}^2$) are then obtained from the mean-square deflections as showed below.

$$\sigma_{\bar{F}',x,j}^2 = \int_0^\infty |H_j(f^*)|^2 |\chi_x(f^*)|^2 S_{Q',x,j}(f^*) \frac{\bar{U}}{B} df^* \quad (3.15.a)$$

$$\sigma_{\bar{F}',z,j}^2 = \int_0^\infty |H_j(f^*)|^2 |\chi_z(f^*)|^2 S_{Q',z,j}(f^*) \frac{\bar{U}}{B} df^* \quad (3.15.b)$$

$$\sigma_{\bar{F}',\theta,j}^2 = \int_0^\infty |H_j(f^*)|^2 |\chi_\theta(f^*)|^2 S_{Q',\theta,j}(f^*) \frac{\bar{U}}{B} df^* \quad (3.15.c)$$

Davenport (1977) divided the area underneath the integrand from Equations 3.15 into two parts: the background component and the resonant component. For background part which the frequencies are too low to excite the structure, the mechanical admittance $|H(f^*)|^2 = 1$. For the resonant part, each frequency mode of vibration evaluated is represented by the reduced frequency f_0^* . The terms $|\chi_z(f_0^*)|^2$ and $S_{Q',z,j}(f_0^*)$ are constant, while the integral of the mechanical admittance is found to be equal to $\frac{\pi f_0^*}{4\xi}$ by using the method of poles (Crandall and Mark, 1963 *apud* Holmes, 2015).

The background mean-square equivalent static forces in X, Z and θ directions are then written as:

$$\sigma_{\bar{F}',B,x}^2(f^*) = \int_0^\infty |\chi_x(f^*)|^2 S_{Q',x,j}(f^*) \frac{\bar{U}}{B} df^* \quad (3.16.a)$$

$$\sigma_{\bar{F}',B,z}^2(f^*) = \int_0^\infty |\chi_z(f^*)|^2 S_{Q',z,j}(f^*) \frac{\bar{U}}{B} df^* \quad (3.16.b)$$

$$\sigma_{\bar{F}',B,\theta}^2(f^*) = \int_0^\infty |\chi_\theta(f^*)|^2 S_{Q',\theta,j}(f^*) \frac{\bar{U}}{B} df^* \quad (3.16.c)$$

And the resonant mean-square equivalent static forces are given by:

$$\sigma_{\bar{F}'_{R,X,j}}^2(f_0^*) = |\chi_X(f^*)|^2 S_{Q'_{X,j}}(f_0^*) \frac{\pi f_0^* \bar{U}}{4\xi B} \quad (3.17.a)$$

$$\sigma_{\bar{F}'_{R,Z,j}}^2(f_0^*) = |\chi_Z(f^*)|^2 S_{Q'_{Z,j}}(f_0^*) \frac{\pi f_0^* \bar{U}}{4\xi B} \quad (3.17.a)$$

$$\sigma_{\bar{F}'_{R,\theta,j}}^2(f_0^*) = |\chi_\theta(f^*)|^2 S_{Q'_{\theta,j}}(f_0^*) \frac{\pi f_0^* \bar{U}}{4\xi B} \quad (3.17.a)$$

where; ξ is the total (structural + aerodynamic) damping.

The equivalent static buffeting forces ($\bar{F}'_{k,j}$) per unit length for each mode of vibration considering the background and resonant components are calculated as follows by g:

$$\sigma_{\bar{F}'_{k,j}} = \sqrt{(g_B \times \sigma_{\bar{F}'_{B,k}})^2 + (g_{R_j} \times \sigma_{\bar{F}'_{R,k,j}})^2} \quad (3.18)$$

$$\bar{F}'_{k,j} = \sigma_{\bar{F}'_{k,j}} \times \Phi_j(\eta) \quad (3.19)$$

$$g = \sqrt{2\ln(vT)} + 0.577/\sqrt{2\ln(vT)} \quad (3.20)$$

where $k = X, Z$ or θ ; $\sigma_{\bar{F}'_{k,j}}$ is the standard deviation of the equivalent static buffeting force (longitudinal, vertical or pitching moment) of the j th mode due to the background and resonant components; $\sigma_{\bar{F}'_{B,k}}$ and $\sigma_{\bar{F}'_{R,k,j}}$ are the standard deviation of the forces due to the background (Eq. 3.16) and resonant (Eq. 3.17) contributions, respectively; g_B and g_{R_j} are the background and resonant peak factors. The peak factor expression (Eq. 3.20) was developed by Davenport (1964).

Besides mean wind loads at deck, towers and cables, and the deck buffeting peak wind loads as described above, tower peak wind loads are also considered in this study. Peak wind loads for the towers are calculated only for alongwind direction, by calculating a gust factor according to Solari (1987, 1993a, 1993b).

3.3 Methodology

The displacements at the deck and towers of a bridge estimated through a full aeroelastic model tested in wind tunnel (experimental approach) are predicted by applying mean and peak wind loads due to buffeting in a Finite Element Model (theoretical approach) of the same bridge. The methodology for comparing the two approaches is described in Figure 3.2.

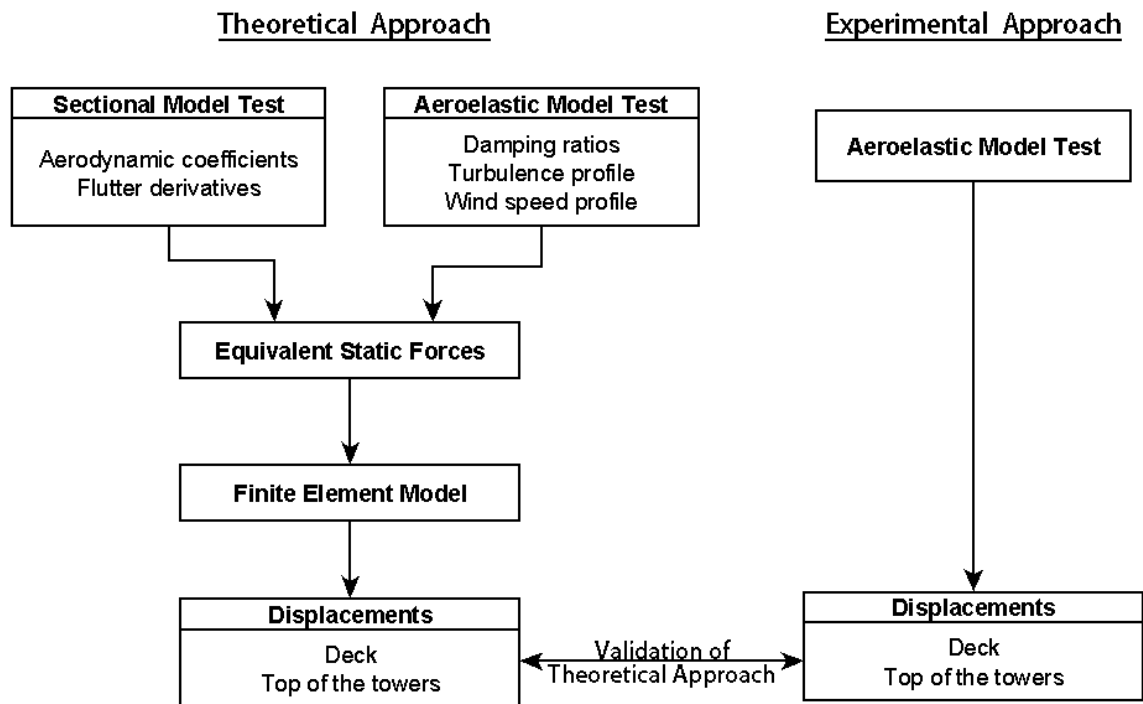


Figure 3. 2: Flowchart of the comparison between theoretical and experimental approaches.

The theoretical approach utilizes the following parameters from sectional model tests: (i) aerodynamic force coefficients; (ii) slopes of force coefficients from the static sectional model test; and (iii) flutter derivatives from the dynamic sectional model test to calculate the aerodynamic damping. In order to be consistent with the comparisons between the two approaches, structural damping ratios, turbulence profile, and wind speed profile used to calculate the equivalent static forces due to buffeting wind should be the same as those

registered in the wind tunnel tests of the full aeroelastic model. Once all six parameters are defined, the equivalent static forces due to buffeting wind loads are calculated according to the Equations presented in Section 2.

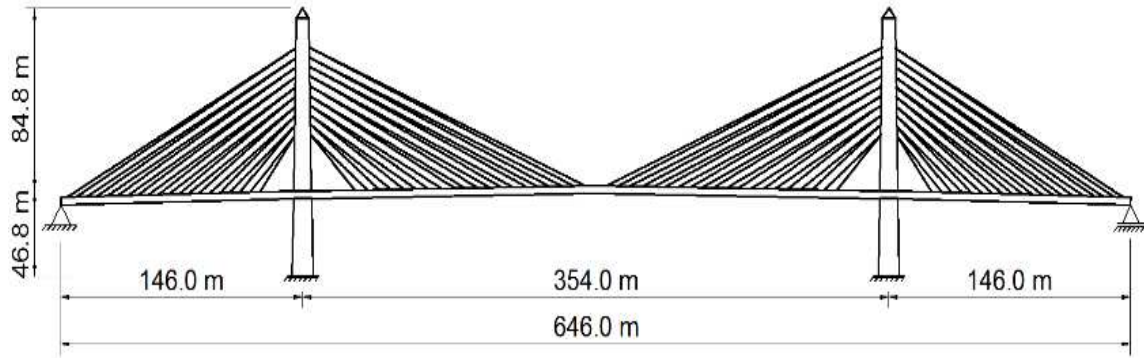
A finite element model is constructed to achieve the same frequencies and mode shapes as the full aeroelastic model. Mean wind loads at the deck, towers, and cables as well as peak wind loads at the deck and towers are applied to the finite element model. Geometric non-linear analysis of the bridge before the free vibration analysis to determine natural frequencies and mode shapes is performed and the displacements provided at the deck and top of towers for mean and peak wind loads are compared to those provided by the experimental approach.

3.4 Case study

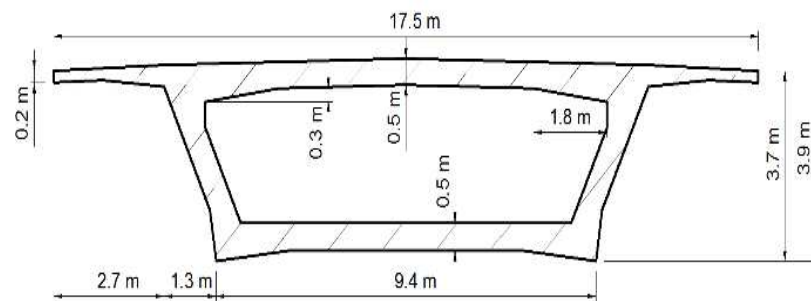
The Prospect Verona Bridge Maine, USA (King et al, 2005) has been chosen as the case study. The cable-stayed bridge has a main span length of 354 m and two side spans of 146 m each. Therefore, the total length of the bridge is 646 m as shown in Figure 3. 3.a. One of the side spans has the first 34.7 m in a curve, for which the horizontal radius is equal to 121.8 m. The typical cross-section of the bridge deck consists of a concrete box-girder with a width of 17.5 m and a depth of 3.9 m (Figure 3. 3.b).

Since the box-girder cross-section provides considerable torsional rigidity, the deck superstructure is supported by only one plan of stay cables. Forty cables support the main span and twenty cables support each side span, totalizing eighty cables in a semi-harp arrangement. The two towers are 84.8 m above the deck level and consist of a concrete tubular section of variable heights.

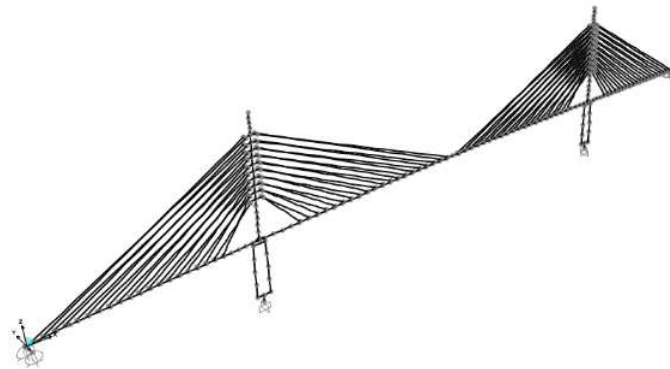
The concrete have a modulus of elasticity $E_c = 30.442\text{GPa}$, while the steel of the stay cables, have a modulus of elasticity $E_s = 193\text{GPa}$. The geometric properties of the bridge elements are presented in Table 3. 1.



(a) Geometry of the bridge (adapted from King *et al.*, 2005).



(b) Cross-section of the side span.



(c) Finite element model.

Figure 3. 3: Bridge geometry, cross-section of the side span, and finite element model of the cable-stayed bridge.

Table 3. 1: Geometric properties of the structural elements.

Element	Area (m ²)	Minor inertia (m ⁴)	Major inertia (m ⁴)	Torsional Constant (m ⁴)
Deck – main span	10.65	22.39	226.46	49.69
Deck – side span	17.11	34.18	296.37	81.35
Upper tower	17.39 - 32.80	44.77 – 67.25	110.78 – 379.93	91.10 – 218.71
Lower tower	16.25	3.63	61.35	6.38
Cables	0.006 – 0.0108	(2.87 – 9.28)10 ⁻⁶	(2.87 – 9.28)10 ⁻⁶	(0.57 – 1.86)10 ⁻⁵

3.4.1 Theoretical approach

The finite element model was developed using three-dimensional frame elements to simulate the deck and towers, and three-dimensional nonlinear truss elements to simulate the stay cables, as shown in Figure 3. 1.c. The deck was modelled using a single spine that passes through its centre of gravity. The cable anchorages and deck spine were connected by massless rigid links to achieve the proper offset of the cables from the centre line of the deck.

In order to conduct a nonlinear analysis under dead loads and pre-tensioning forces, the P- Δ and the large displacements effects were taken into account by using the following equation for the local tangent stiffness matrix:

$$[K_T]_b = [K_E]_b + [K_G]_b \quad (3.21)$$

where $[K_E]_b$ and $[K_G]_b$ are the elastic (Weaver and Gere, 1980) and the geometric (Nazmy and Ghaffar, 1990) stiffness matrices for the three-dimensional frame elements, respectively. The sag effect on the cables was dealt with by replacing each cable with a truss element of an equivalent cable stiffness. The equivalent tangent modulus of elasticity (E_{eq}) is given by (Ernst, 1965):

$$E_{eq} = \frac{E_{cs}}{1 + \frac{(w_{cs}H)^2 A_c E_{cs}}{12T^3}} \quad (3.22)$$

where E_{cs} is the cable material effective modulus of elasticity; A_c is the cross-sectional area of the cable; H is the horizontal projection of the cable; w_{cs} is the weight per unit length of the cable; and T is the tension in the cable.

The frequencies and mode shapes, which are also inputs for the equivalent static forces calculation, are determined using the deformed configuration obtained in the static nonlinear analysis of the bridge under dead loads and pre-tensioning forces. Table 3. 2 presents the obtained frequencies associated to the six mode shapes considered in the analysis and the corresponding values from the full aeroelastic model (in the prototype scale). It can be seen that the theoretical values are well correlated with the experimental ones, demonstrating that the finite element model has the proper stiffness and mass simulation of the structure.

The static sectional model test and the full aeroelastic model test of the cable-stayed bridge were performed in The Boundary Layer Wind Tunnel Laboratory at Western University (King et al., 2005). The aerodynamic force coefficients and their slopes obtained from the sectional model test are listed in Table 3. 3 for angle of attack equal to zero.

Table 3. 2: Frequencies and mode shapes.

Mode Shape		Frequency (Hz)	
		Wind Tunnel	FEM
Drag	Symmetric	0.242	0.248
	Anti-symmetric	0.782	0.778
Lift	Symmetric	0.327	0.340
	Anti-symmetric	0.500	0.510
Torsion	Symmetric	1.104	1.238
	Anti-symmetric	2.198	2.490

Table 3. 3: Aerodynamic coefficients and theirs slopes for a wind attack of 0°.

Direction	Coefficients	Slopes
Drag	0.261	-0.382
Lift	0.161	0.867
Torsion	0.129	0.013

According to King *et al.* (2005), the aeroelastic model was tested with roughness length equal to 0.030m (≈ 0.1 ft).

Despite this fact, the roughness length applied in the theoretical approach has to be adjusted to 0.183m (≈ 0.6 ft) in order to achieve matching longitudinal turbulence intensity profile and wind speed profile from the full aeroelastic model test at the deck height (46.9m). Figure 3. 4 presents the theoretical and experimental profiles describing the wind velocity.

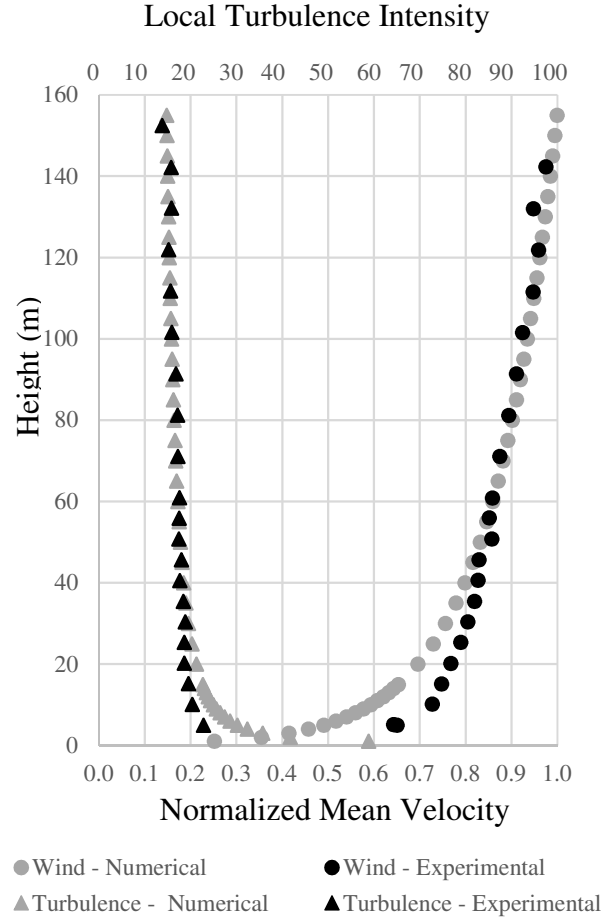


Figure 3. 4: Longitudinal turbulence intensity profile and mean wind speed profile obtained experimentally from the full aeroelastic model test and the ones used in the theoretical approach.

As the vertical turbulence intensity profile was not provided by King *et al.* (2005), it is adopted according to Holmes (2015):

$$\sigma_w = 1.375u_* \quad (3.23)$$

where σ_w is the standard deviation of vertical wind speed, and u_* is the friction velocity. This means that σ_w is taken as $0.55\sigma_u$.

The structural damping ratios for vertical movements (0.16%), lateral movements (0.5%) and torsion (1.3%) are adopted in accordance with the full aeroelastic model test. The alongwind aerodynamic damping is calculated according to Eurocode 1 (Part 1-4, 2005):

$$\xi_{ax}(f_0) = \frac{\rho C_D B \bar{U}}{2 \bar{m} \omega_0} \quad (3.24)$$

where $\xi_{ax}(f_0)$ is the alongwind aerodynamic damping of the lateral mode of vibration with frequency f_0 ; C_D is the drag coefficient; \bar{m} is the deck mass per unit of length; and $\omega_0 = 2\pi f_0$, the angular frequency.

The crosswind and torsional aerodynamic damping ratios are calculated according to Davenport (1982). As a dynamic sectional model test was not performed by King *et al.* (2005) in order to provide the flutter derivatives, the flutter derivative H_1^* is estimated by Equation 3.26 (Davenport, 1982).

$$\xi_{az}(f_0^*) = \frac{-\rho B^2}{\bar{m}} \frac{H_1^*(f_0^*)}{2} \quad (3.25)$$

$$H_1^*(f_0^*) = \frac{-1}{4\pi} \frac{C_z'}{f_0^*} \quad (3.26)$$

$$\xi_{a\theta}(f_0^*) = \frac{-\rho B^4}{I_0} \frac{A_2^*(f_0^*)}{2} \quad (3.27)$$

where $\xi_{az}(f_0^*)$ and $\xi_{a\theta}(f_0^*)$ are the crosswind and torsional aerodynamic damping of the vertical and torsional mode of vibrations with reduced frequency f_0^* , respectively; I_0 is the polar moment of inertia; $H_1^*(f_0^*)$ and $A_2^*(f_0^*)$ are flutter derivatives. In the lack of an approximated equation to estimate $A_2^*(f_0^*)$, the torsional aerodynamic damping is neglected in this case study.

The mean and buffeting equivalent static forces of each deck mode of vibration are applied separately to the FEM model of the cable-stayed bridge. The total deck peak displacements

obtained after linear analyses are combined by taking the root-mean-square of displacement of the six modes of vibration that are being evaluated.

3.4.2 Experimental Approach

The 1:200 scaled aeroelastic model was tested in an open country exposure with roughness length equal to 0.03048m (1ft). A detailed topographic model of the hills in the surrounding of the prototype was constructed to simulate the features of the terrain. The wind speed profile and longitudinal turbulence intensity profile used for the testing are presented in Figure 3. 4.

The results, in terms of displacements, of the full aeroelastic model test were obtained by measuring and recording the time histories of non-contacting laser displacement transducers located at different positions of the deck, such as at $\frac{1}{4}$ and at $\frac{1}{2}$ of the main span, and at the top of the towers. The mean and the peak values of the displacements were recorded for a range of wind speeds. The mean values were obtained by taking the arithmetic average of time history over the time of 15 minutes, and corrected to the time of 60 minutes. While the peak values were obtained by taking the root-mean-square (RMS), of the time history, and multiplying it by a statistically-based peak factor of 3.5. The total response is equal to the mean value plus or minus the peak value.

3.4.3 Results

The comparison between the theoretical and experimental approaches are presented for displacements at the middle of main span, one-fourth of main span, and top of one tower.

The comparisons of mean displacement values are presented in Figure 3. 5 to Figure 3. 8 as a function of the deck height wind speed. A good correlation for the mean drag displacements for the deck for wind speeds up to 40m/s is observed (see Figure 3. 5). For wind speeds greater than 40m/s, the theoretical approach tends to predict slightly smaller values than the experimental approach. The same good behavior is observed for the mean rotations on the deck for wind speeds up to 40m/s as shown in Figure 3. 7, although for wind speeds greater than that, the theoretical approach results are slightly greater than the experimental approach values. Overall, the mean drag displacements and the mean

rotations have a good agreement as well as the mean lateral displacements at the top of the first tower. On the other hand, the mean lift displacements comparisons do not show a good correlation at the main span. It can be observed that the experimental approach provides smooth curves for drag displacements and rotations. However the mean lift curve exhibits very small displacements with floating values for wind speed up to 40m/s, and after that a more stable increasing response. It is worth noting that the upstream topography simulated in the test may have affected the wind flow on the side spans and part of the main span imposing small deviation from the 0° angle of attack condition over the sea water (as considered in the theoretical approach).

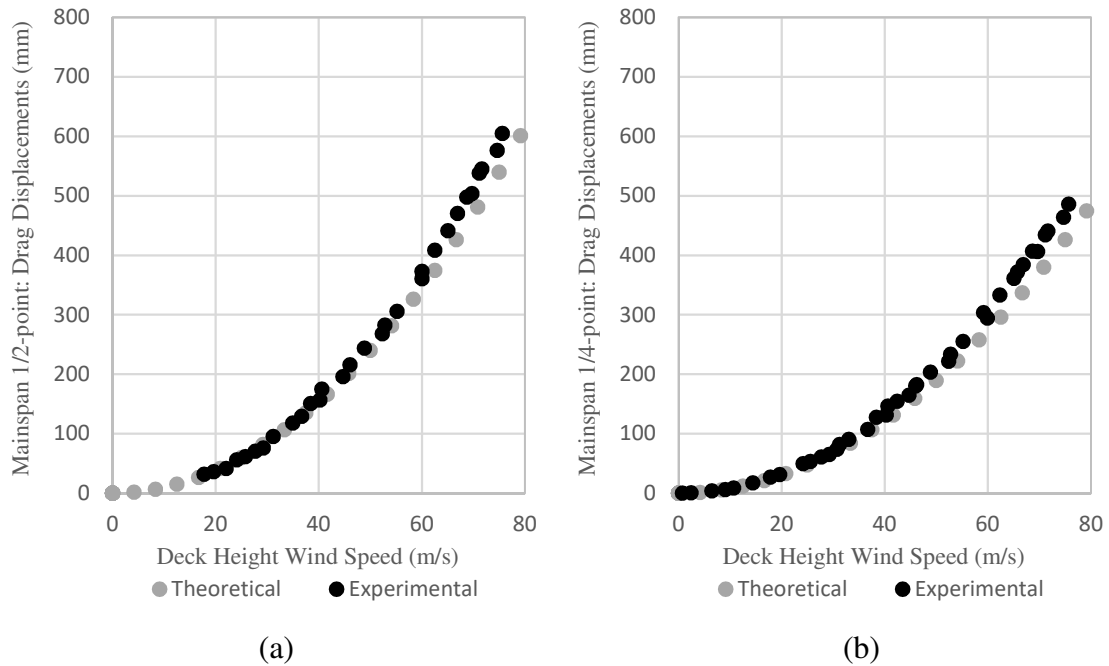


Figure 3. 5: Comparison of mean drag displacements: (a) at $\frac{1}{2}$ -point of main span; (b) at $\frac{1}{4}$ -point of main span.

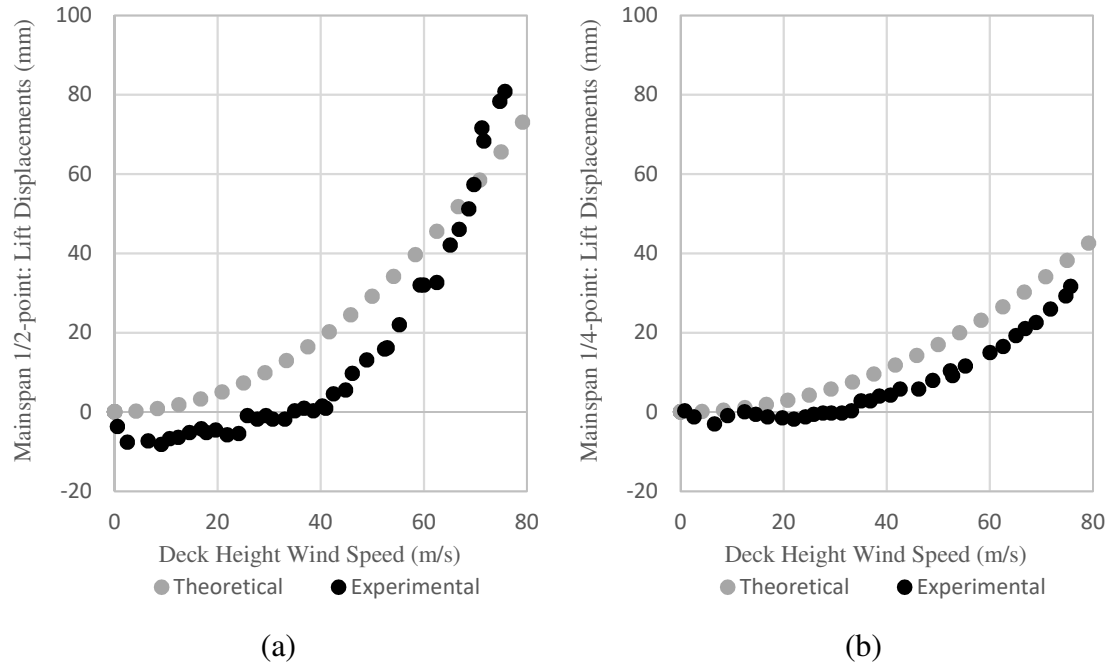


Figure 3. 6: Comparison of mean lift displacements: (a) at $\frac{1}{2}$ -point of main span; (b) at $\frac{1}{4}$ -point of main span.

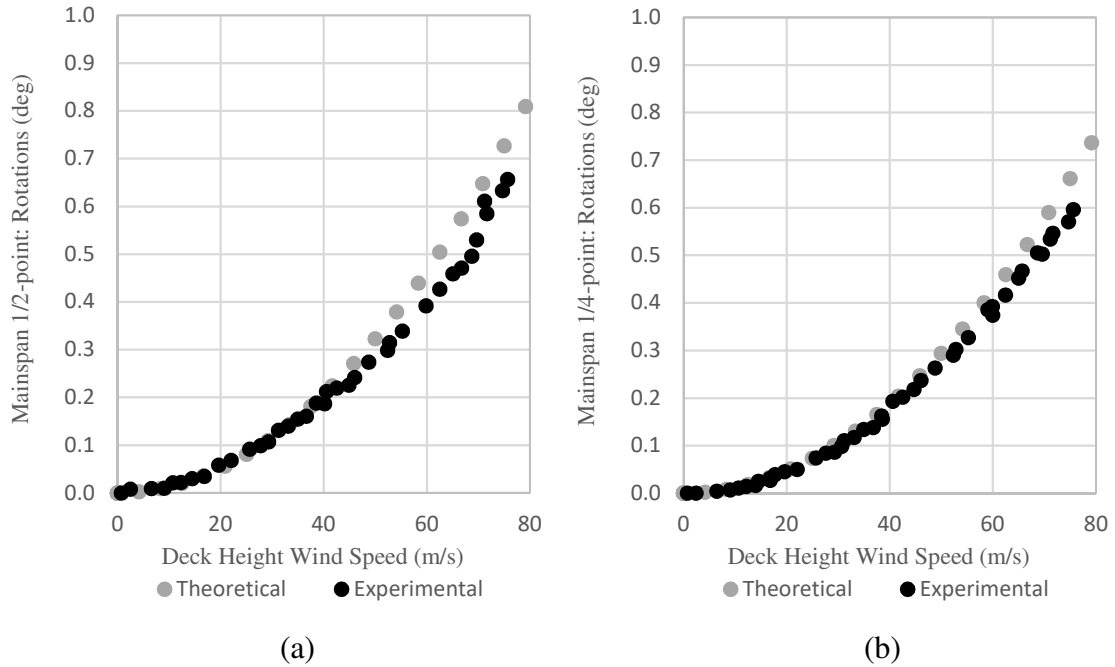


Figure 3. 7: Comparison of mean rotations: (a) at $\frac{1}{2}$ -point of main span; (b) at $\frac{1}{4}$ -point of main span.

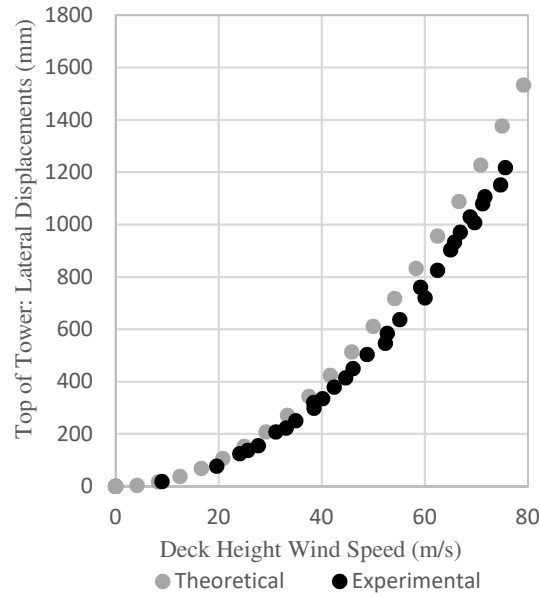


Figure 3. 8: Comparison of mean lateral displacements at the top of the 1st tower.

The comparisons of peak values between the two approaches are presented in Figure 3. 9 to Figure 3. 12. A good agreement of peak drag displacements is observed for wind speeds up to 40m/s, same behavior that is noticed for the mean drag displacements. The peak lift displacements of the deck from the theoretical approach, contrary to the mean lift displacements behavior, tend to be smaller than those obtained from the experimental approach. The lift displacements at 1/4-point at the main span have very good correlation for wind speeds above 60m/s. It is necessary to emphasize that the vertical turbulence intensity profile applied to the full aeroelastic model was not provided; this way, in the theoretical approach the vertical turbulence was adopted from the literature and could not be checked experimentally.

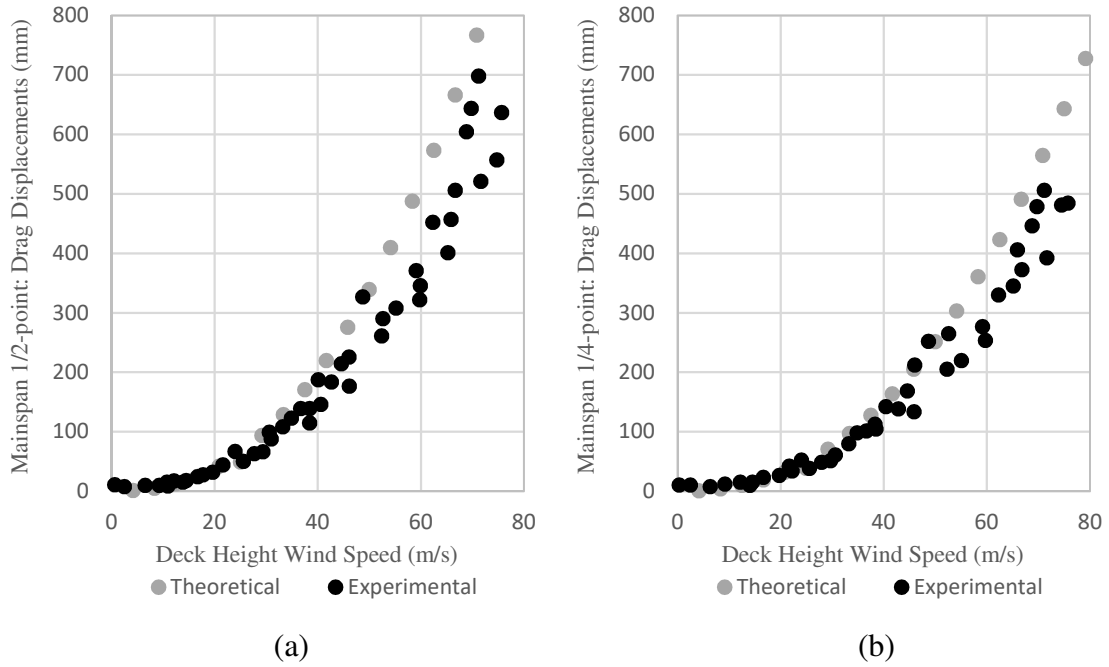


Figure 3. 9: Comparison of peak drag displacements: (a) at $\frac{1}{2}$ -point of main span; (b) at $\frac{1}{4}$ -point of main span.

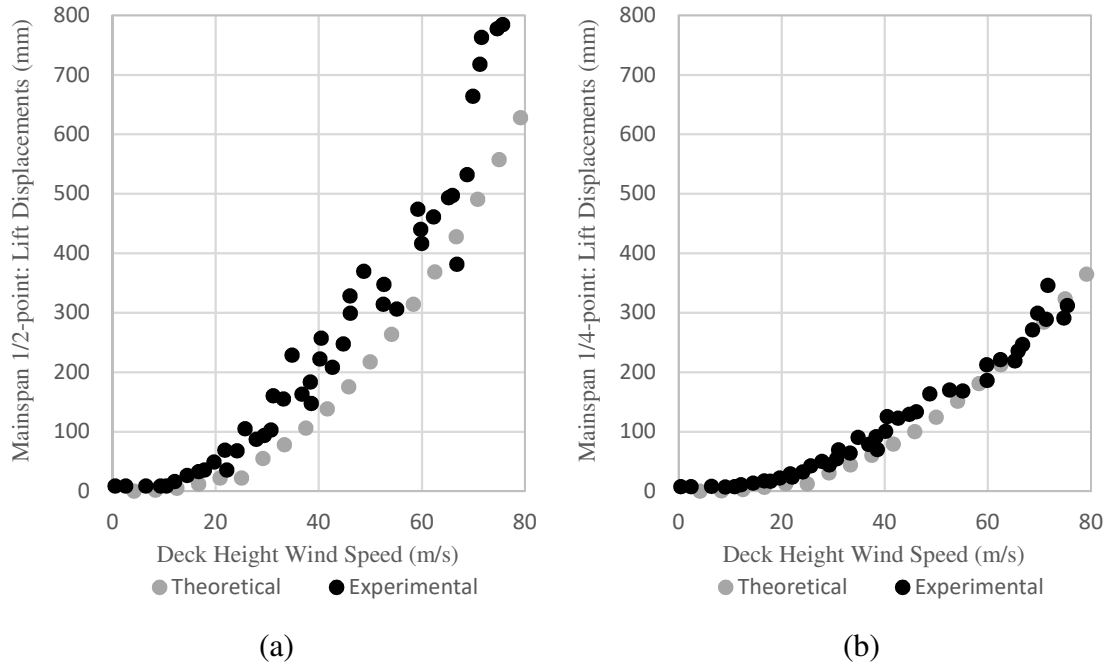


Figure 3. 10: Comparison of peak lift displacements: (a) at $\frac{1}{2}$ -point of main span; (b) at $\frac{1}{4}$ -point of main span.

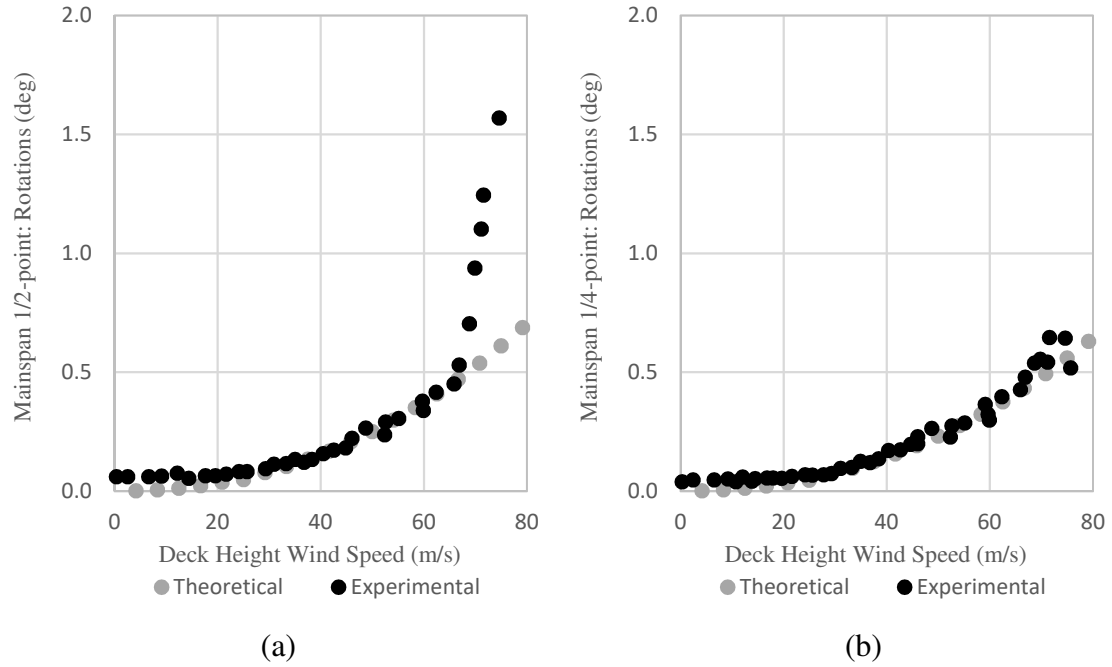


Figure 3. 11: Comparison of peak rotations: (a) at $\frac{1}{2}$ -point of main span; (b) at $\frac{1}{4}$ -point of main span.

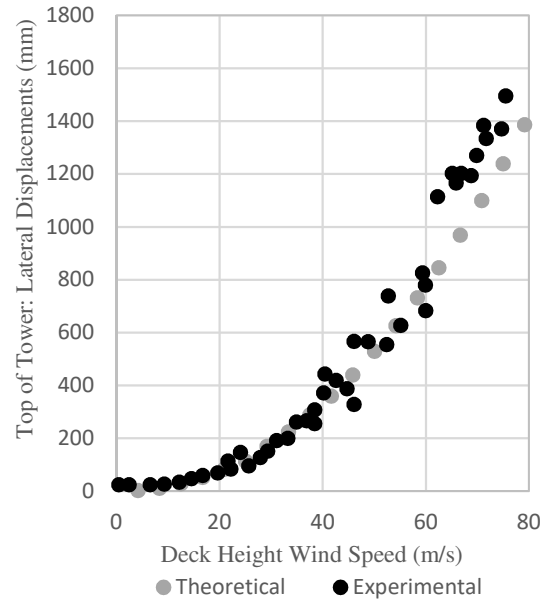


Figure 3. 12: Comparison of peak lateral displacements at the top of the 1st tower.

The peak rotations shown in Figure 3. 11.(a) for the midpoint of the main span obtained through the experimental approach shows a change of slope at the wind speed of 65.9m/s that can be explained by the detection of flutter phenomenon. The same behavior cannot be perceived in the theoretical approach, once the equivalent static forces applied to the finite element model take into account only the buffeting phenomenon. The peak rotations at ¼-point of main span present excellent correlation for the whole range of wind speed. For the peak lateral displacements at the top of the 1st tower, the experimental approach provides greater rotations values for wind speeds above 60m/s. Other than that, the top of the tower has a good correlation as shown in Figure 3. 12.

3.5 Conclusions

A theoretical-experimental comparison has been carried out to estimate how accurately the theoretical approach, constituted by a FEM model under equivalent static aerodynamic loading that considers the results from the sectional model test can estimate the results provided by the experimental approach, established solely by the full aeroelastic model test. The comparisons indicate that the theoretical approach overall can successfully estimate the displacements of the experimental approach.

It is observed an excellent correlation for drag displacements and rotations on the deck for wind speeds up to 40m/s, for both peak and mean values. For higher wind speeds the numerical results tend to be slightly greater or less than the experimental ones. The lateral displacements at the top of the first tower present a very good correlation for the peak values for wind speeds up to 60m/s.

The mean and peak rotations have an overall excellent correlation for the whole range of wind speeds. On the other hand, the lift displacements do not present a very good correlation between the approaches. Nevertheless, the correlation can be considered satisfactory once the lift peak displacements from the experimental approach are able to follow the same trends as the ones from the theoretical approach. While at the ½ -point,

the numerical peak lift displacements are smaller than the experimental values, at the $\frac{1}{4}$ -point the displacements have a great correlation for wind speeds above 60m/s.

The differences between the theoretical and experimental approaches analyses can be attributed to uncertainties encountered during the process of obtaining the displacements for both approaches. Some of the main uncertainties are:

1. The experimental approach takes into account the general features of the prototype terrain, while the static sectional model test from theoretical approach does not consider the influence of the topography. Small deviations of the angle of attack from the 0° condition adopted in the theoretical analysis may have influenced the responses;
2. The experimental approach can detect other phenomena like vortex shedding and flutter, while the theoretical approach considers only the buffeting phenomenon;
3. The theoretical approach considers approximated aerodynamic damping ratios, once they are function of the flutter derivatives. Dynamic sectional tests were not realized for the bridge in study, so the flutter derivatives were estimated according to Davenport et al. (1982);
4. The theoretical approach considers approximated aerodynamic admittance functions to describe the effect of the relation between the sizes of the gust and structure, which are naturally and more accurately taken into account during the experimental approach;
5. The theoretical approach considers a vertical turbulence intensity profile that could not be checked or corrected to attend the one utilized in the experimental approach.

Considering the magnitude of the differences between the theoretical and experimental approaches results as well as the source of uncertainties that cause these differences, one can conclude that the theoretical approach provides a satisfactory way of performing buffeting wind loads analysis.

References

- AASHTO. 2012. LRFD Bridge Design Specifications, 6th edition, Washington, D.C., USA.
- Crandall, S.H., Mark, W.D. 1963. Random vibration in mechanical systems. Academic Press, New York, apud Holmes, J.D. 2015. Wind loading of structures. 3 ed. Taylor & Francis Group.
- Davenport, A.G. 1962. Buffeting of a suspension bridge by storm winds, J. Struct. Div. ASCE, 88: 233-268 apud Matsuda, K., Hikami, Y., Fujiwara, T., Moriyama, A. 1990. Aerodynamic admittance and the 'strip theory' for horizontal buffeting forces on a bridge deck. Journal of Wind Engineering and Industrial Aerodynamics, 83: 337-346.
- Davenport, A.G. 1964. Note on the distribution of the largest value of a random function with application to gust loading. Proceedings, Institution of Civil Engineering, 28: 187-196.
- Davenport, A.G. 1966. The action of wind on suspension bridges. Keynote Paper. Intl. Symp. Suspension Bridges.
- Davenport, A.G. 1977. The prediction of the response of structures to gusty wind. International Research Seminar on Safety of Structures under Dynamic Loading, Trondheim, Norway, v. 1, pp.257-284.
- Davenport, A.G., King, J.P.C. 1982. Technical report. A Study of Wind Effects for the Sunshine Skyway Bridge, Tampa, Florida – Concrete Alternate. The Boundary Layer Wind Tunnel Laboratory – The University of Western Ontario, London, Ontario, Canada.
- Davenport, A.G., King, J.P.C. 1984. Dynamic wind forces on long span bridges using equivalent static loads. IABSE, 12th Congress, Vancouver, BC, Canada, pp. 705-712.
- Ernst, J.H. 1965. Der E-Modul von Seilen unter berucksichtigung des Durch- hanges. Der Bauingenieur, 40(2): 52–55 (In German).
- ESDU 74031. 1974. Characteristics of atmospheric turbulence near the ground, Part II: Single point data for strong winds (neutral atmosphere). Engineering Sciences Data Unit.
- Holmes, J.D. 1975. Prediction of the response of a cable stayed bridge to turbulence. Proceedings of the Fourth International Conference on Wind Effects on Buildings and Structures, Heathrow, 187-197, apud Matsuda, K., Hikami, Y., Fujiwara, T., Moriyama, A. 1990. Aerodynamic admittance and the 'strip theory' for horizontal buffeting forces on a bridge deck. Journal of Wind Engineering and Industrial Aerodynamics, 83: 337-346.

- Holmes, J.D. 2015. Wind loading of structures. 3 ed. Taylor & Francis Group.
- King, J.P.C., Kopp, G., Vickery, P.J., Mikitiuk, M., Kong, L. 1999. Technical report. A structure of wind effects for Prospect Verona Bridge Maine, USA. The Boundary Layer Wind Tunnel Laboratory – The University of Western Ontario, London, Ontario, Canada.
- Matsuda, K., Hikami, Y., Fujiwara, T., Moriyama, A. 1990. Aerodynamic admittance and the 'strip theory' for horizontal buffeting forces on a bridge deck. *Journal of Wind Engineering and Industrial Aerodynamics*, 83: 337-346.
- Nazmy, A.S., Abdel-Ghaffar, A.M. 1990. Three-dimensional nonlinear static analysis of cable-stayed bridge. *Computers & Structures*, 34(2): 257-271.
- Solari, G. 1987. Turbulence modeling for gust loading. *Journal of Structural Engineering*, 113(7): 1550-1569.
- Solari, G. 1993b. Gust buffeting. I: peak wind velocity and equivalent pressure. *Journal of Structural Engineering*, 119(2): 365-382.
- Solari, G. 1993b. Gust buffeting. II: dynamic alongwind response. *Journal of Structural Engineering*, 119(2): 383-398.
- Weaver, W., Gere, J. 1980. *Matrix Analysis of Framed Structures*. Van Nostrand Reinhold, New York, NY, USA.

Chapter 4

4 Structural optimization of two I-girder composite cable-stayed bridges under the action of dead, live and wind loads

4.1 Introduction

Cable-stayed bridges are efficient structures due to their several advantages, and at the same time they are challenging structures due to the integrated behaviour of their structural components (Podolny, 1976; Troitsky, 1988; Svensson, 2012).

According to Svensson (2012), the number of cable-stayed bridges has been increasing since the 1970s, given the numerous benefits when compared to other type of bridges. As span lengths have recently increased significantly, cable-stayed bridges are becoming more flexible and consequently more susceptible to dynamic actions, specially from wind loads.

To simplify and improve the design process of cable-stayed bridges, many studies were dedicated to their structural automatization and optimization. In some studies, optimization is restricted to the stay cable pre-tensioning forces (Wang *et al.*, 1993; Chen *et al.*, 2000; Janjic *et al.*, 2003; Hassan *et al.*, 2012 and 2013a; Martins *et al.*, 2015) in which only dead and superimposed loads are considered. While in other studies, the optimization is more encompassing by considering the optimization of deck, tower, and stay-cables dimensions in addition to stay-cable pre-tensioning forces.

Long *et al.* (1999) studied the optimization of a composite box girder cable-stayed bridge. Deck, tower and cable dimensions were optimized under dead and live loads using Powell's direct search method with the objective of obtaining minimum cost of the superstructure.

Simões & Negrão (1994, 2000) and Negrão & Simões (1997) have optimized different cable-stayed bridges with box-girder decks. Dimensions and geometry were optimized under the action of dead and live loads, and erection configurations, with goals related to minimum cost and stresses. Entropy based technique and Pareto solution were used for

solving the multi-objective problem. Ferreira & Simões (2011) also considered seismic loading during the optimization process with the objective of obtaining reduced stresses.

Hassan *et al.* (2013b, 2015) optimized main span length, tower height, number of cables, deck and tower cross-section dimensions considering the action of dead, lane live loads and lateral mean wind loads. The optimization aimed obtaining the minimum design cost by using Real Coded Genetic Algorithm (RCGA) and Finite Element Method (FEM). The stay-cables pre-tensioning forces were obtained through surrogate functions previously developed by Hassan *et al.* (2013a).

Considering that engineers are adopting thinner and lighter decks while considering longer spans, dynamic analysis becomes an important matter during the design and optimization of cable-stayed bridges. The main objective of this study is to evaluate how buffeting wind loads affect structural optimization procedures. Primary focus is given to buffeting wind loads because they are an inevitable phenomenon (Zhu *et al.*, 2007), and depending on the wind magnitude, fluctuating forces may govern the selection of structural component dimensions (Davenport, 1966; Holmes, 2015). The critical wind velocity for vortex shedding, classical flutter, single mode torsional flutter, torsional divergence and galloping are also checked during the optimization process to guarantee that structures are aerodynamically stable. This task is accomplished by using a numerical tool developed in-house that integrates: (i) the Finite Element Method (FEM) for modelling and analyzing the structure; (ii) the Real Coded Genetic Algorithm (RCGA) for determining optimum design variables that achieve minimum material cost of the structure; and (iii) the Discrete Phase Design Approach. The FEM and RCGA were adapted from Hassan's work (2013b, 2015), while the Discrete-Phase Design Approach was developed in this study.

The variables to be optimized are divided into two categories: main and secondary variables. The main variables are the independent design variables and consist of the following: number of stay-cables, deck I-girder inertia, concrete slab thickness, tower height above the deck, and tower cross-section longitudinal and transverse external dimensions. The secondary variables are dependent on the main variables values and are determined in Phases 1 to 3 of the Discrete-Phase Design Approach. Phase 1 determines

the I-girder dimensions as a function of the I-girder inertia that minimize the girder cross-sectional area. Phases 2 and 3 determine the stay-cables area and pre-tensioning forces, respectively. Phases 4 to 7 involve determining natural frequencies and mode shapes, calculating displacements and internal forces due to live loads and buffeting wind loads based on the approach described and validated in Chapter 3, and checking the critical wind velocity of aerodynamic excitations. The Serviceability Limit State (SLS) and Ultimate Limit State (ULS) criteria are checked during Phase 8.

In this chapter, the structural optimization of cable-stayed bridges described in Chapter 2 and based on the Discrete-Phase Design Approach, FEM and RCGA methods is extended. Three more discrete phases are added to the algorithm in order to: (i) perform free vibration analysis; (ii) evaluate critical wind velocities of aerodynamic effects; (iii) determine displacements and internal forces due to mean and buffeting wind loads.

The chapter starts by introducing the design variables, the objective function to be minimized and the design constraints to be satisfied. In sequence, the design methodology is presented focusing on the three discrete phases that are added for considering the wind loads. In order to illustrate the procedure, a case study for the design optimization of a cable-stayed bridge is considered under different SLS parameters.

The research significance of this study is described below:

1. As described in Chapter 2, one of the main advantages of the Discrete-Phase Design Approach is the practicality of adding new phases for considering additional effects in the optimization of cable-stayed bridges. This is applied in this chapter by adding three new discrete phases to the approach for considering the wind effect.
2. Three different basic wind velocities are considered in the study in order to assess the structure geometry and material cost behavior with the increase of the wind speeds.
3. Comparisons between four load combinations is assessed for estimating the significance of considering the wind loads during the optimization process of cable-

stayed bridges. The most dominant load combination for different basic wind velocities are also assessed. The load combinations considered in these comparisons are: (i) dead and live loads; (ii) dead and wind loads; (iii) dead, live and wind loads; (iv) the load combinations (i), (ii) and (iii) are simultaneously considered.

4. A correlation between the results considering different SLS parameters is performed in order to evaluate the influence of these parameters in deck rigidity and tower longitudinal stiffness relation as well as in the structure material cost.
5. Structural optimization of cable-stayed bridges are completed with and without the consideration of critical wind velocities of aerodynamic effects to estimate the influence of these constraints in the optimization process.

4.2 Description of numerical tool

4.2.1 Design variables

The vector of design variables \vec{x} includes the main variables:

$$\vec{x} = \{x_1 \quad x_2 \quad x_3 \quad x_4 \quad x_5 \quad x_6\}^{-1} \quad (4.1)$$

where x_1 is the total number of cables ($2 \times 4 \times N$), N is the number of cables in half of the main span in one plan of cables; x_2 is the deck I-girder inertia (I); x_3 is the concrete slab thickness (t_c); x_4 is the tower height above the deck (H_a); x_5 and x_6 are the longitudinal (TL_1) and the transversal (TL_2) external dimensions of the towers cross-section, respectively.

The secondary design variables are dependent on the main variables values. This way, instead of being considered as design variables to be optimized directly using RCGA, they are optimized by the Discrete Phase Design Approach. This leads to a large reduction in computational cost. The secondary variables are:

1. I-girder deck dimensions: I-girder depth (D), top flange (b_1 , t_1), bottom flange (b_2 , t_2) and web (w) dimensions are calculated as a function of the main variable x_2 (I);
2. Stay-cable areas (A_i ; $i=1,4 \times N$) which are calculated as a function of the design variables x_1 (N), x_2 (I) and x_3 (tc);
3. Stay-cable pre-tensioning forces (T_i ; $i=1,4 \times N$) which are calculated as a function of the design variables x_1 (N), x_2 (I) and x_3 (tc), and the secondary variables A_i .

The total length of the bridge (L), the main span (L_1), the side spans (L_2), the tower height below the deck (H_b) and the deck width (B) are determined by the topography and traffic conditions, and thereby are considered as constants during the optimization process. Some of the main and secondary variables are presented in Figure 4. 1.

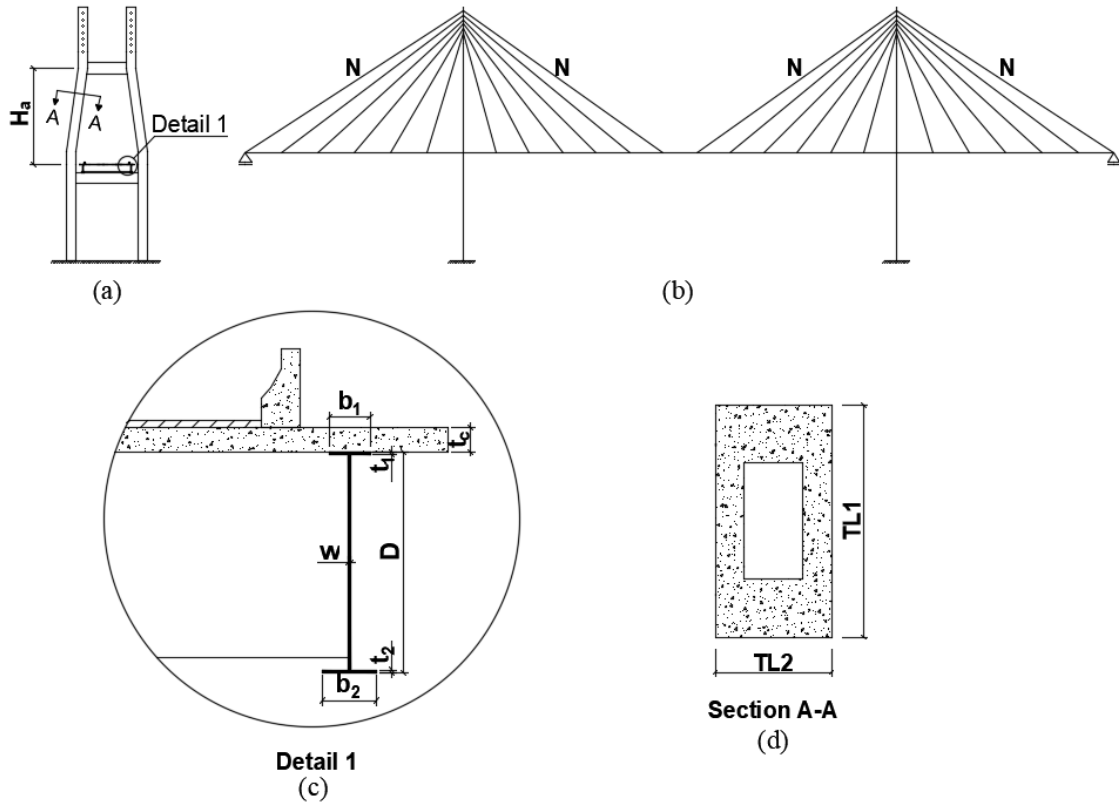


Figure 4. 1: Main and secondary variables.

4.2.2 Design constraints

The constraints are defined to satisfy the Serviceability Limit State (SLS) and Ultimate Limit State (ULS) based on the Canadian Highway Bridge Design Code (CAN/CSA-S6-14). Some of the SLS that are not covered by CAN/CSA-S6-14 are specified according to the AASHTO (2012) or the designer specifications. The design constraint functions (g_j , $j=1,10$) at the Serviceability Limit State (SLS) are as follow:

- Displacements at the deck due to dead and superimposed loads (δ_{DL+SL}) as a function of the maximum displacement C_1 specified by the designer:

$$g_1 = \frac{C_1 \times \delta_{DL+SL}}{\text{span length}} - 1.0 \leq 0 \quad (4.2)$$

- Displacements at the deck due to live loads (δ_{LL}) according to the AASHTO (2012):

$$g_2 = \frac{800 \times \delta_{LL}}{\text{span length}} - 1.0 \leq 0 \quad (4.3)$$

- Displacements at the deck due to wind loads (δ_{WL}) as a function of the maximum displacement C_3 specified by the designer:

$$g_3 = \frac{C_3 \times \delta_{WL}}{\text{span length}} - 1.0 \leq 0 \quad (4.4)$$

- Displacements at the deck due to live (δ_{LL}) and wind (δ_{WL}) loads as a function of the maximum displacement C_4 specified by the designer:

$$g_4 = \frac{C_4 \times (\delta_{LL} + \delta_{WL})}{\text{span length}} - 1.0 \leq 0 \quad (4.5)$$

- Control of permanent deflections at the deck according to CAN/CSA-S6-14:

$$g_5 = \frac{M_{DL}}{S} + \frac{M_{SL}}{S_{3n}} + \frac{M_{LL}}{S_n} - 0.90F_y \leq 0 \quad (\text{positive moment regions}) \quad (4.6)$$

$$g_6 = \frac{M_{DL}}{S} + \frac{M_{SL} + M_{LL}}{S'} - 0.90F_y \leq 0 \quad (\text{negative moment regions}) \quad (4.7)$$

where M_{DL} , M_{SL} and M_{LL} are the bending moments at SLS due to dead load, superimposed load, and live load; S , S' , S_n , S_{3n} are the elastic section modulus of the steel section only, the steel section and reinforcement within the effective width of the slab, the steel girder and the concrete slab using a modular ratio n and $3n$, respectively.

- Displacements at the towers due to dead and superimposed loads (Δ_{DL+SL}) as a function of the maximum displacement C_7 specified by the designer:

$$g_7 = \frac{C_7 \times \Delta_{DL+SL}}{H_t} - 1.0 \leq 0 \quad (4.8)$$

where H_t is the total length of tower.

- Displacements at the towers due to dead and superimposed loads (Δ_{DL+SL}), and live loads (Δ_{LL}) as a function of the maximum displacement C_8 specified by the designer:

$$g_8 = \frac{C_8 \times (\Delta_{DL+SL} + \Delta_{LL})}{H_t} - 1.0 \leq 0 \quad (4.9)$$

- Displacements at the towers due to dead and superimposed loads (Δ_{DL+SL}), and wind loads (Δ_{WL}) as a function of the maximum displacement C_9 specified by the designer:

$$g_9 = \frac{C_9 \times (\Delta_{DL+SL} + \Delta_{WL})}{H_t} - 1.0 \leq 0 \quad (4.10)$$

- Displacements at the towers due to dead and superimposed loads (Δ_{DL+SL}), live (Δ_{LL}) and wind (Δ_{WL}) loads as a function of the maximum displacement C_{10} specified by the designer:

$$g_{10} = \frac{C_{10} \times (\Delta_{DL} + \Delta_{LL} + \Delta_{WL})}{H_t} - 1.0 \leq 0 \quad (4.11)$$

The design constraint functions (g_j ; $j=11,18$) at the Ultimate Limit State (ULS) are as follow:

- Combined shear and moment at the deck according to CAN/CSA-S6-14:

$$g_{11} = \frac{V_f}{V_r} - 1.0 \leq 0 \quad (4.12)$$

$$g_{12} = \frac{M_f}{M_r} - 1.0 \leq 0 \quad (4.13)$$

$$g_{13} = 0.727 \frac{M_f}{M_r} + 0.455 \frac{V_f}{V_r} < 0 \quad (4.14)$$

where V_f is the factored shear force at ULS; M_f is the factored bending moment at ULS; V_r is the factored shear resistance; M_r is the factored bending moment resistance.

- Axial compression and bending at the deck according to CAN/CSA-S6-14:

$$g_{14} = \frac{C_f}{C_r} + \frac{U_{1x}M_{fx}}{M_{rx}} + \frac{U_{1y}M_{fy}}{M_{ry}} - 1.0 \leq 0 \quad (4.15)$$

where C_f is the factored compressive force at ULS; M_{fx} and M_{fy} are the factored bending moment at ULS about x-axis and y-axis; C_r is the factored compressive resistance; M_{rx} and M_{ry} are the factored bending moment resistance about x-axis and y-axis; U_{1x} and U_{1y} are factors to account for moment gradient and second order effects.

The combined axial force and bending moment are also verified for both deck and towers by considering interaction diagrams, providing the constraints g_{15} and g_{16} , respectively. More details about the interaction diagram can be obtained in WIGHT & MacGREGOR (2009).

- Biaxial loading at the towers according to CAN/CSA-S6-14:

$$\frac{1}{P_{rxy,tower}} = \frac{1}{P_{rx,tower}} + \frac{1}{P_{ry,tower}} - \frac{1}{P_{0,tower}} \quad (4.16)$$

$$g_{17} = \frac{M_{fx,tower}}{M_{rx,tower}} + \frac{M_{fy,tower}}{M_{ry,tower}} - 1.0 \leq 0 \quad (4.17)$$

where $P_{rxy,tower}$ is the factored axial resistance in compression with biaxial loading; $P_{rx,tower}$ and $P_{ry,tower}$ are the factored axial resistance in compression

corresponding to $M_{rx,tower}$ and $M_{ry,tower}$, respectively; $P_{0,tower}$ is the factored axial resistance in pure compression; $M_{fx,tower}$ and $M_{fy,tower}$ are the factored bending moment at ULS about x-axis and y-axis; and, $M_{rx,tower}$ and $M_{ry,tower}$ are the factored bending moment resistance about x-axis and y-axis.

- Stay-cables axial forces:

$$g_{18} = \frac{T_f}{F_B} - 0.50 \leq 0 \quad (4.18)$$

where T_f is the factored axial forces at ULS, and F_B is the breaking force.

The design constraints (g_j ; $j=19,23$) related to wind limited amplitudes and instability phenomena are as follow:

- Vortex shedding excitation critical velocity $U_{cr,vortex}$ (CNR-DT 207/2008):

$$g_{19} = U_{cr,vortex} - U_{m,k} < 0 \quad (4.19)$$

$$U_{cr,vortex} = \frac{f_i B}{S_t} \quad (4.20)$$

where $U_{m,k}$ is the mean wind velocity for return period $T_R=k$ years; $U_{cr,vortex}$ is the critical velocity for the i -th mode of vibration with frequency f_i ; and S_t is the Strouhal number.

- Single mode torsional flutter limitation:

$$g_{20} = A_2^*(f_{\theta,i}) - \frac{4I_m \xi_{s,\theta,i}}{\rho B^4} < 0 \quad (4.21)$$

where $A_2^*(f_{\theta,i})$ is a function of the torsional frequency mode and of the wind velocity; I_m is the mass moment of inertia; $\xi_{s,\theta,i}$ is the structural damping of the i -th torsional mode; ρ is the air mass density.

- Classical flutter critical velocity $U_{cr,flutter}$ given by Selberg equation (Svensson, 2012):

$$g_{21} = U_{cr,flutter} - U_{m,k} < 0 \quad (4.22)$$

$$U_{cr,flutter} = 2\pi B \eta' f_B \left[1 + \left(\frac{f_T}{f_B} - 0.5 \right) \sqrt{\frac{0.72mr}{\pi \rho B^3}} \right] \quad (4.23)$$

where f_B and f_T are the first bending and the first torsional bending frequencies; η' is a reduction factor function of the ratios f_T/f_B and $(D+t_c)/B$ (Klöppel, 1967 apud Svensson, 2012); m is the mass per length; and r is the mass of gyration.

- Galloping critical velocity $U_{cr,galloping}$:

$$g_{22} = U_{cr,galloping} - U_{m,k} < 0 \quad (4.24)$$

$$U_{cr,galloping} = \frac{2f_B B}{\left| \frac{dC_z}{d\alpha} \right|} S_c \quad (4.25)$$

where $\frac{dC_z}{d\alpha}$ is the first derivative of vertical force coefficient; and S_c is the Scruton number.

- Torsional divergence critical velocity $U_{cr,divergence}$:

$$g_{23} = U_{cr,divergence} - U_{m,k} < 0 \quad (4.26)$$

$$U_{cr,divergence} = \sqrt{\frac{-2GJ_t}{\rho B^2 \frac{dC_\theta}{d\alpha}}} \quad (4.27)$$

where $\frac{dC_\theta}{d\alpha}$ is the first derivative of torsion force coefficient; G is the shear modulus of the material; and J_t is the torsional moment of inertia of the cross-section.

4.2.3 Objective function

The objective of this optimization is to obtain the minimum material cost of deck, towers and stay-cables that attend all the ULS and SLS requirements. The objective function $F(\vec{x})$ is defined as follow:

$$F(\vec{x}) = C(\vec{x})_{deck} + C(\vec{x})_{towers} + C(\vec{x})_{cables} \quad (4.28)$$

where \vec{x} is the design variables vector, $C(\vec{x})_{deck}$, $C(\vec{x})_{towers}$ and $C(\vec{x})_{cables}$ are the material cost of deck, towers and cables for the design variables vector \vec{x} . The material costs are obtained from construction companies and RSMeans (2013). The deck costs are: \$3,125/t of steel; \$1,300/m³ of concrete; \$2,400/t of reinforcement. For the towers the costs are: \$1,200/m³ of concrete and \$2,400/t of steel. The stay-cables cost is \$7,650/t of strands. Coefficients obtained from RSMeans (2013) are also applied to the costs in order to reflect the specific costs of the city in which the cable-stayed bridge is located .

4.2.4 Finite element model

The finite element model uses three-dimensional frame elements to represent the deck and towers, and three-dimensional truss elements to represent the stay-cables. The deck is modelled using a single spine simulating the concrete slab and I-girders, similar to the approach adopted by Wilson *et al.*(1991), and later used by Hassan *et al.* (2012, 2013a, 2013b). The stay-cable anchorages and deck spine are connected by massless rigid links to achieve the proper offset of cables from the centre line of the deck.

The only source of non-linearity contemplated in this study is the sag effect, which is considered substituting the modulus of elasticity of stay-cables by an equivalent tangent modulus (Eq. 4.29) established by Ernst (1965). This is justified by: (i) the limited effect that was observed by Wilson *et al.* (1991), Adeli & Zhang (1995) and Hassan *et al.* (2012) when considering fully nonlinear analysis of cable stayed bridges; (ii) the large number of analysis to perform the optimization of cable-stayed bridges considering the action of dead, live and wind loads; (iii) the fact that this study reproduces the initial design stage.

$$E_{eq} = \frac{E_{cs}}{1 + \frac{(w_{cs}H)^2 AE_{cs}}{12T^3}} \quad (4.29)$$

where E_{cs} is the cable material effective modulus of elasticity; A is the cross-sectional area; H is the horizontal projection of the cable; w_{cs} is the weight per unit length of the cable; and T is the tension in the cable.

4.2.5 Design methodology

The design methodology is based on the Discrete Phases Design Approach which is responsible for: (i) determining the value of the secondary variables; (ii) calculating the loads due to dead, superimposed, live and buffeting wind loads; (iii) checking the ULS and SLS requirements, and calculating the objective function values.

When only dead, superimposed and live loads are evaluated during the optimization process, the Discrete Phases Design Approach is composed by five design phases. By assessing buffeting wind loads as well, other three design phases are activated as described below.

4.2.5.1 Phases 1 to 4

Phases 1 to 4 are described in detail in Chapter 2.

4.2.5.2 Phase 5

Phase 5 involves solving an eigenvalue/eigenvector problem to obtain the frequencies and mode shapes of the bridge. When the live loads are part of the load combination analysis, the uniformly distributed live load is converted to linear mass, which is taken into account in the mass matrix; otherwise this matrix is formed considering only the mass of deck, towers and cables.

4.2.5.3 Phase 6

In this work emphasis is given to bridge buffeting excitation and before proceeding to the calculation of wind loads due to atmospheric turbulence (see Phase 7) some other mechanisms which can generate dynamic response and instability are addressed in this phase. Although vortex shedding can induce vibration classified as limited amplitude response it can generate sharp resonances causing intolerable stresses or fatigue problems on structures if submitted to prolonged time to this type of event. On the other hand, galloping and flutter (single mode torsional and classical) are classified as divergent amplitude response, in which the self-excited forces lead very rapidly to large amplitude values. The torsional divergence is classified as a non-oscillatory divergence that is

characterized by a negative aerodynamic torsional stiffness (Simiu & Scanlan, 1996; BD 49/01-Part 3, 2001). These latter three phenomena cause instability and must be avoided.

Critical wind speeds related to each of these phenomena are calculated and compared to the mean wind velocity at the deck height for return period of TR years (for example, TR=500 as prescribed by CNR-DT 207/2008) to guarantee that the structure is aerodynamically stable. In the case of vortex shedding this would be a condition to avoid the need to further investigate the induced vibration and check for cross wind amplitudes but is adopted here as a simplified criterion for aerodynamic stability.

4.2.5.4 Phase 7

In Phase 7, equivalent static buffeting wind loads at the deck are calculated according to the theoretical equations developed by Davenport & King (1984). Equivalent static wind loads are those that provide the same values of peak load effects as the dynamic fluctuating wind loads. Mean wind loads at deck, towers and stay-cables; and peak wind loads at deck and towers are applied to the complete FEM model in order to obtain the results in terms of displacements and internal forces. The peak wind loads at the towers are determined by calculating a gust factor (Solari 1987, 1993a, 1993b).

The cable-stayed bridge behavior due to turbulence induced excitation can be simulated by 6 modes of vibration Davenport & King (1984): the first symmetric and the first antisymmetric lateral, vertical and torsional mode shapes (see Figure 4. 2). Peak wind loads, with background and resonant components, are calculated as a function of:

1. static aerodynamic forces and moment coefficient obtained from a sectional model test;
2. flutter derivatives obtained from a dynamic sectional model test for calculating the aerodynamic damping ratios;
3. spectrums of longitudinal and vertical turbulence velocities;
4. aerodynamic admittance to relate the size of the gust and the structure;
5. joint acceptance function to reproduce the capacity of the turbulent flow to excite the modes of vibration.

The static coefficients and flutter derivatives used in the numerical tool are obtained from Lin *et al.* (2005) in which they provided static force coefficients for four plate girder cross-sections, with deck width and I-girder depth (B/D) ratios equal to 4.0, 6.7, 10.0, and 13.3. Flutter derivatives were also provided as a function of B/D ratio and reduced frequency of the mode shape being analyzed. The aerodynamic coefficients and flutter derivatives obtained from Lin *et al.* (2005) are provided in Appendix E.

The spectrums of longitudinal and vertical velocities are evaluated considering the spectrum of Harris (ESDU 74031, 1974) and the spectrum of Busch and Panofsky (Holmes, 2015), respectively. The aerodynamic admittances are calculated according to Davenport (1982) and Matsuda *et al.* (1999). The joint acceptance is estimated according to Davenport (1977 and 1982).

To validate the equivalent static buffeting loads at the deck implemented in the numerical tool, a numerical-experimental correlation has been previously performed for the Prospect Verona Bridge in Maine, USA. The results from the cable-stayed bridge full aeroelastic model tested in The Boundary Layer Wind Tunnel Laboratory at Western University and provided by King *et al.* (2005) were successfully compared to the results from the numerical procedure calculated using the numerical tool, as presented in Chapter 3.

The background ($\sigma_{\bar{F}'_{B,X}}^2(f^*)$, $\sigma_{\bar{F}'_{B,Z}}^2(f^*)$ and $\sigma_{\bar{F}'_{B,\theta}}^2(f^*)$) and resonant ($\sigma_{\bar{F}'_{R,X}}^2(f^*)$, $\sigma_{\bar{F}'_{R,Z}}^2(f^*)$ and $\sigma_{\bar{F}'_{R,\theta}}^2(f^*)$) mean-square equivalent static forces adapted from Davenport & King (1984) and Holmes (2015) are presented as follow:

$$\sigma_{\bar{F}'_{B,X}}^2(f^*) = \int_0^\infty |\chi_X(f^*)|^2 S_{Q'_{X,j}}(f^*) \frac{\bar{U}}{B} df^* \quad (4.30.a)$$

$$\sigma_{\bar{F}'_{B,Z}}^2(f^*) = \int_0^\infty |\chi_Z(f^*)|^2 S_{Q'_{Z,j}}(f^*) \frac{\bar{U}}{B} df^* \quad (4.30.b)$$

$$\sigma_{\bar{F}'_{B,\theta}}^2(f^*) = \int_0^\infty |\chi_\theta(f^*)|^2 S_{Q'_{\theta,j}}(f^*) \frac{\bar{U}}{B} df^* \quad (4.30.c)$$

$$\sigma_{\bar{F}'_{R,X,j}}^2(f_0^*) = |\chi_X(f^*)|^2 S_{Q'_{X,j}}(f_0^*) \frac{\pi f_0^* \bar{U}}{4\xi B} \quad (4.31.a)$$

$$\sigma_{\bar{F}'_{R,Z,j}}^2(f_0^*) = |\chi_Z(f^*)|^2 S_{Q'_{Z,j}}(f_0^*) \frac{\pi f_0^* \bar{U}}{4\xi B} \quad (4.31.b)$$

$$\sigma_{\bar{F}'_{R,\theta,j}}^2(f_0^*) = |\chi_\theta(f^*)|^2 S_{Q'_{\theta,j}}(f_0^*) \frac{\pi f_0^* \bar{U}}{4\xi B} \quad (4.31.c)$$

$$S_{Q'_{x,j}}(f^*) = \left[(qB C_{F_X})^2 4 \left(\frac{\sigma_u}{\bar{U}} \right)^2 \frac{S_{uu}(f^*)}{\sigma_u^2} + \left(qB \frac{dC_{F_X}}{d\alpha} \right)^2 \left(\frac{\sigma_w}{\bar{U}} \right)^2 \frac{S_{ww}(f^*)}{\sigma_w^2} \right] |J_j(f^*, \eta_1, \eta_2)|^2 \quad (4.32.a)$$

$$S_{Q'_{z,j}}(f^*) = \left[(qB C_{F_Z})^2 4 \left(\frac{\sigma_u}{\bar{U}} \right)^2 \frac{S_{uu}(f^*)}{\sigma_u^2} + \left(qB \frac{dC_{F_Z}}{d\alpha} \right)^2 \left(\frac{\sigma_w}{\bar{U}} \right)^2 \frac{S_{ww}(f^*)}{\sigma_w^2} \right] |J_j(f^*, \eta_1, \eta_2)|^2 \quad (4.32.b)$$

$$S_{Q'_{\theta,j}}(f^*) = \left[(qB^2 C_{F_\theta})^2 4 \left(\frac{\sigma_u}{\bar{U}} \right)^2 \frac{S_{uu}(f^*)}{\sigma_u^2} + \left(qB^2 \frac{dC_{F_\theta}}{d\alpha} \right)^2 \left(\frac{\sigma_w}{\bar{U}} \right)^2 \frac{S_{ww}(f^*)}{\sigma_w^2} \right] |J_j(f^*, \eta_1, \eta_2)|^2 \quad (4.32.c)$$

where X is the along-wind direction; Z is the cross-wind direction; θ represents the torsional movements; $f^* = fB/\bar{U}$ is the reduced frequency; \bar{U} is the mean wind velocity at the deck height; $S_{Q'_{x,j}}(f^*)$, $S_{Q'_{z,j}}(f^*)$ and $S_{Q'_{\theta,j}}(f^*)$ are the power spectral density of the mean square fluctuating generalized forces; $|\chi_X(f^*)|^2$, $|\chi_Z(f^*)|^2$ and $|\chi_\theta(f^*)|^2$ are the aerodynamic admittances; and ξ is the total (structural + aerodynamic) damping; q is the dynamic wind pressure; C_{F_X} , C_{F_Z} , C_{F_θ} , $\frac{dC_{F_X}}{d\alpha}$, $\frac{dC_{F_Z}}{d\alpha}$, $\frac{dC_{F_\theta}}{d\alpha}$ are the aerodynamic coefficients and their first derivatives; $S_{uu}(f^*)$ and $S_{ww}(f^*)$ are the spectrums of longitudinal and vertical turbulence velocities, respectively; σ_u e σ_w are the standard deviation of longitudinal and vertical fluctuations, respectively; $|J_j(f^*, \eta_1, \eta_2)|^2$ is the joint acceptance function. A detailed presentation of the equations used for calculating the peak wind loads due buffeting wind loads is found in Chapter 3.

4.2.5.5 Phase 8

Finally, displacements and internal forces due to dead and superimposed loads, live loads, mean and buffeting wind loads (obtained from Phases 3, 4 and 7, respectively), are checked against the design constraints presented in Equations 4.2 to 4.27. The objective function for minimum material cost is calculated, and penalties are applied if one or more requirements from SLS or ULS are not attended.

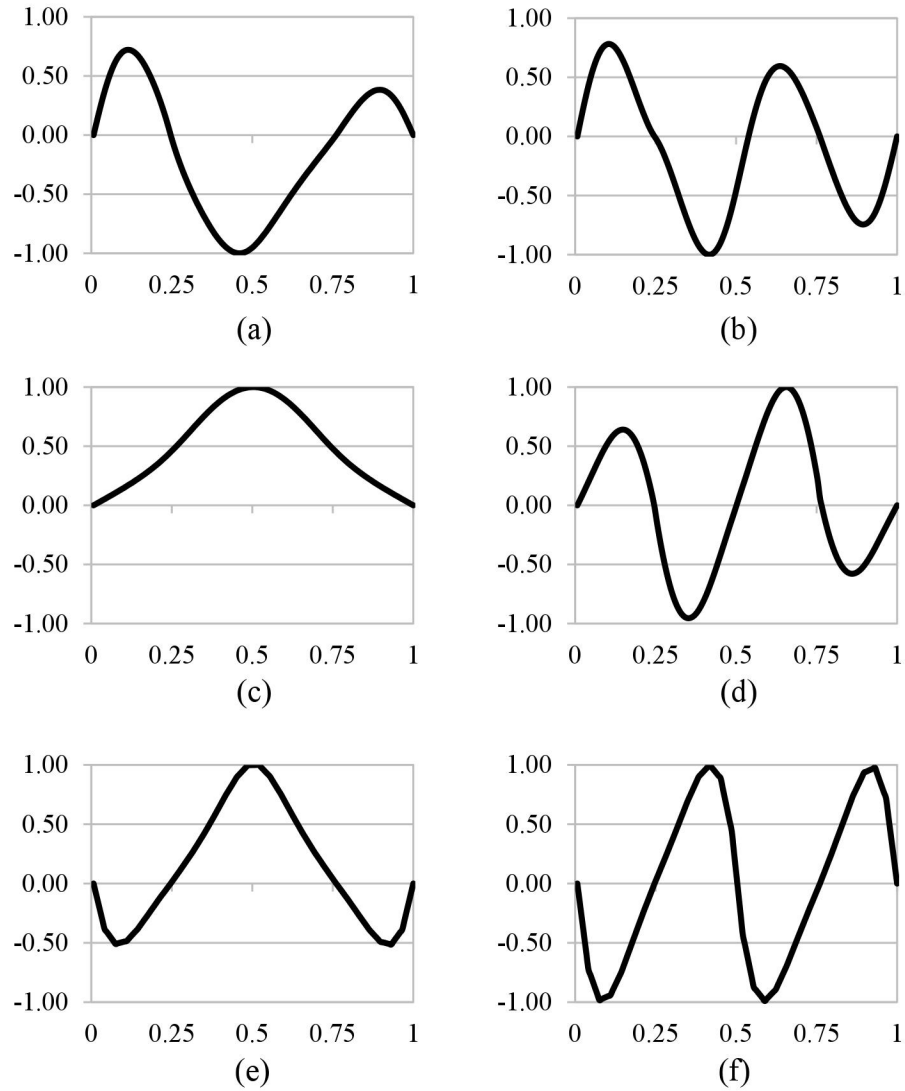


Figure 4. 2: Deck mode shapes: (a) 1st symmetric vertical mode; (b) 1st antisymmetric vertical mode; (c) 1st symmetric lateral mode; (d) 1st antisymmetric lateral mode; (e) 1st symmetric torsional mode; (f) 1st antisymmetric torsional mode.

4.2.6 Optimization technique

When the number of variables to be optimized are significantly large, the search space becomes substantial making it impossible to obtain the optimal solution through direct search. In these situations, evolutionary algorithms, like Real Coded Genetic Algorithm

(RCGA), are a good option because they are able to find a near optimum solution in a relatively short period of time (Rao, 2009; Michalewicz *et al.*, 2000; Jacobson *et al.*, 2015; Kramer, 2017). The RCGA is effective for avoiding local optimum if the population is large enough so that the algorithm can explore different areas of the search space.

The RCGA makes use of selection method to pick samples among all the population of solutions. Mutation and crossover operators are applied to these selected samples in order to generate new ones along the generations. In the end of each generation, the population is ordered according to their objective function values, with the best solution staying at the top of the list, while the worst ones are eliminated to keep the total number of samples constant. Elitism is also considered by saving a few best solutions to prevent them of being lost during the operations and to avoid extra computational time to recover previously eliminated solution. Throughout the generations and due to the operators applied, the samples start to convert to the same area of the search space where the global optimum is located.

The RCGA finds the design variable vector \vec{x} (Equation 4.1) which minimizes the objective function $F(\vec{x})$ (Equation 4.28) subjected to the design constraints g_j ($j=1,23$) presented in Equations 4.2 to 4.27.

Each sample, from the initial population or obtained throughout the generations, has a design variable vector \vec{x} that is evaluated by the eight phases of the Discrete Design Approach. In Phase 8 the objective function is calculated as follow:

1. If the sample solution is feasible, all the design constraints are respected, the objective function is equal to Equation 4.28;
2. If the sample solution is infeasible, at least one of the design constraint is violated, the objective function is given by the equation based on Deb (2000):

$$F(\vec{x}) = f_{max} + \sum_{j=1}^{23} g_j(\vec{x}) \quad (33)$$

where f_{max} is the fitness value of the worst feasible solution that has been observed.

4.2.7 Cable-stayed bridge optimum design algorithm

The RCGA procedure for the structural optimization of cable-stayed bridges considering dead, live and wind loads are described below:

Step 1: Define the constant geometry values: bridge total length (L), main span length (L_1), tower height below the deck (H_b), and deck width (B). Define the lower and upper bounds of the design variables.

Step 2: Define RCGA parameters: number of samples in the population (N_{POP}); number of generations (N_{GEN}); fitness value of the worst feasible solution (f_{max}); crossover and mutation operator parameters; number of samples to be saved for considering elitism ($N_{elitism}$).

Step 3: Define parameters for buffeting wind loads: basic wind velocity for SLS ($U_{0,SLS}$), ULS ($U_{0,ULS}$) and mean wind velocity at the deck height for aerodynamic stability checks ($U_{m,k}$); roughness length (z_0); and structural damping (ξ_s).

Step 4: Define the SLS and ULS load combination factors for dead, superimposed, live and wind loads.

GEN=0

Step 5: Initialize the population by generating randomly N_{POP} samples. For each one of the samples, the Discrete Phases Design Approach described in Section III.2.5 is performed, and its objective function value is calculated.

Step 6: Sort the population by ordering N_{POP} samples from the lowest to the highest objective function values.

Step 7: Save $N_{elitism}$ fittest candidates to be added to the population of the next generation.

GEN=GEN+1

Step 8: Apply crossover and mutation operators to samples from the previous generation to reproduce new samples that will compose the population of the current generation. For

each one of the new samples, the Discrete Phases Design Approach described in Section III.2.5 is performed, and its objective function value is calculated.

Step 9: Add the candidates from the previous generation to the new population starting by the fittest until this population achieve N_{POP} samples.

Step 10: Replace the samples with highest objective function values by the $N_{elitism}$ fittest candidates saved in Step 7, if they are no longer part of the new population provided by Step 9.

Step 11: Sort the population by ordering N_{POP} samples from the lowest to the highest objective function values. The lowest value is the fittest candidate to be the solution so far.

Step 12: If GEN is equal to N_{GEN} , deliver the solution. Go to Step 7, otherwise.

4.3 Case of study

4.3.1 Cable-stayed bridge optimum design algorithm

A composite two I-girders cable-stayed bridge is optimized using the design algorithm described step by step in Section III.2.7. The bridge has deck width $B=17\text{m}$, with 15m of distance between the two main girders. The total length $L=400\text{m}$, main span $L_1=200\text{m}$, and the two side spans $L_2=100\text{m}$ each. The tower height below the deck $H_b=30\text{m}$, and the distance between cable anchorages at the tower is 2m . The cross-section of the tower is a hollow reinforced concrete box, and the thickness of its cross-section is assumed to be equal to 20% of the external dimensions. Table 4. 1 presents the upper and lower bounds of the design variables.

In Phase 1 of design described in Section III.2.5.1, three parameters have to be chosen according to the designer. This case of study is based on the limit of Class 3 width-to-thickness ratio of cross-section elements (CAN/CSA-S6-14). A $b_1/b_2=0.75$ is assumed, which was observed in a number of real bridges; the maximum ratio b_2/D is assumed to be 0.20. The compressive strength of concrete, the yield strength of structural steel and the

breaking load of stay-cable strands are assumed to be equal to: $F_{sk} = 1.86GPa$ ($E_s = 195GPa$), $f'_{ck} = 30MPa$ ($E_c = 25.6GPa$), and $f_y = 350MPa$ ($E_s = 200GPa$), respectively.

Table 4. 1: Design variables: lower and upper bounds.

Design variable	Lower Bound	Upper Bound
N	6	12
I (m ⁴)	0.005	0.50
t _c (m)	0.25	0.30
TL ₁ (m)	3.00	7.00
TL ₂ / TL ₁	0.30	0.70
H _a /L ₁ (m)	0.05	0.25

The constants of the design constraints are defined by the user and in this case study are assumed as: $C_1 = 5,000$ (Eq. 4.2); $C_7 = 1,700$ (Eq. 4.8); $C_8 = C_9 = C_{10} = 500$ (Eq. 4.9 to 11). The constants C_3 (Eq. 4.4) and C_4 (Eq. 4.5) are tested for two different values: (i) 800 that is the constant value when only live load is evaluated (Eq. 4.3); (ii) and half of this value, 400, to assess the sensibility of the optimization to this parameter.

The hourly mean basic wind velocity adopted for the ULS analysis considers a return period of $T_R = 100$ years according to CAN/CSA-S6-14, once there is one span over 125m. The hourly mean basic wind velocity considered for calculating the critical velocities is equivalent to $T_R = 500$ years based on CNR-DT 207/2008. In the lack of a more specific guideline for the hourly mean basic wind velocity for SLS analyses, two different return periods were evaluated $T_R = 10$ years and $T_R = 2$ years. It should be mentioned that when the live loads are considered together with the wind loads, the recommended maximum wind velocity to be evaluated at SLS is 23m/s (EN 1991-1-4:2005+A1:2010). Above this wind velocity, the vehicles may become instable causing overturning incidents (Cook, 2007). Approximated values for logarithm decrement are obtained from EN 1991-1-4:2005+A1:2010.

The cable-stayed bridge is assumed to be constructed in London, ON. Based on the RSMeans (2013), the city-specific factors to be applied to the materials costs presented in Section III.2.3 are 1.45 and 1.25 for concrete and steel respectively. Although the hourly

mean basic wind velocity in London, ON for $T_R = 100$ is $U_{0,100} = 30.8\text{m/s}$, two other basic wind velocities are considered in the analyses: $U_{0,100} = 21.9\text{m/s}$ referent to the city Clapleau – ON; and $U_{0,100} = 42.2\text{m/s}$ referent to Cardston – AB. Only one set of material costs and three different basic wind velocities (see Table 4. 2) are considered to evaluate the effect of increasing wind velocity in the process of structural optimization of cable-stayed bridges. The effect of considering the critical wind velocity of aerodynamic stability checks is also evaluated in this case study. In light of all the considerations mentioned above, six main cases of analysis are taken into account as described in Table 4. 3. The load combinations factors at ULS (CAN/CSA-S6-14) and SLS used in this case study are specified in Table 4. 4.

Table 4. 2: Hourly mean basic wind velocities adapted from CAN/CSA-S6-14.

Basic Wind Velocity (m/s)	SLS		ULS	Aerodynamic Instabilities
	$T_R = 2$	$T_R = 10$	$T_R = 100$	$T_R = 500$
$V_{0,1}$	13.4	17.2	21.9	25.3
$V_{0,2}$	18.3	23.0	30.8	35.5
$V_{0,3}$	23.0	23.0	42.2	48.1

Table 4. 3: Main cases of analysis.

Case	SLS Return Period (years)	C_3 and C_4 (Eq. 4.4 and 4.5)	Aerodynamic Instabilities
A1	10	800	\times
A2			\checkmark
B1	02	800	\times
B2			\checkmark
C1	02	400	\times
C2			\checkmark

Table 4. 4: Load factor combinations.

Load Case	ULS Factors			SLS Factors		
	DL	LL	WL	DL	LL	WL
DL +LL	α	1.70	-	1.00	0.90	-
DL +WL	α	-	1.40	1.00	-	1.00
DL +LL+WL	α	1.40	0.45	1.00	0.90	1.00

Notes: DL=dead and superimposed loads; LL=live loads; WL=wind loads.

α : load factor provided by Table 3.3 of CAN/CSA-S6-14 depending on the type of material.

4.3.2 Results and Discussion

4.3.2.1 Importance of considering different load case configurations in the optimization process

Optimization of cable-stayed bridges are performed for case of analysis A1 ($T_{R,SLS} = 10$ years; $C_3 = C_4 = 800$) described in Table 4. 3. Three basic wind velocities $V_{0,1}$, $V_{0,2}$ and $V_{0,3}$ defined in Table 4. 2 are considered and four load combinations are assessed:

1. DL+LL case: dead, superimposed and live loads;
2. DL+WL case: dead, superimposed and wind loads;
3. DL+LL+WL case: dead, superimposed and live loads;
4. Three Cases: DL+LL, DL+WL, DL+LL+WL.

Figure 4. 3.a summarizes and presents the material cost of the ten optimization analyses described above versus the basic wind velocities. The optimization that considers only dead, superimposed and live loads (DL+LL) are not dependent on the wind velocities, so those results are shown as constant in the graph.

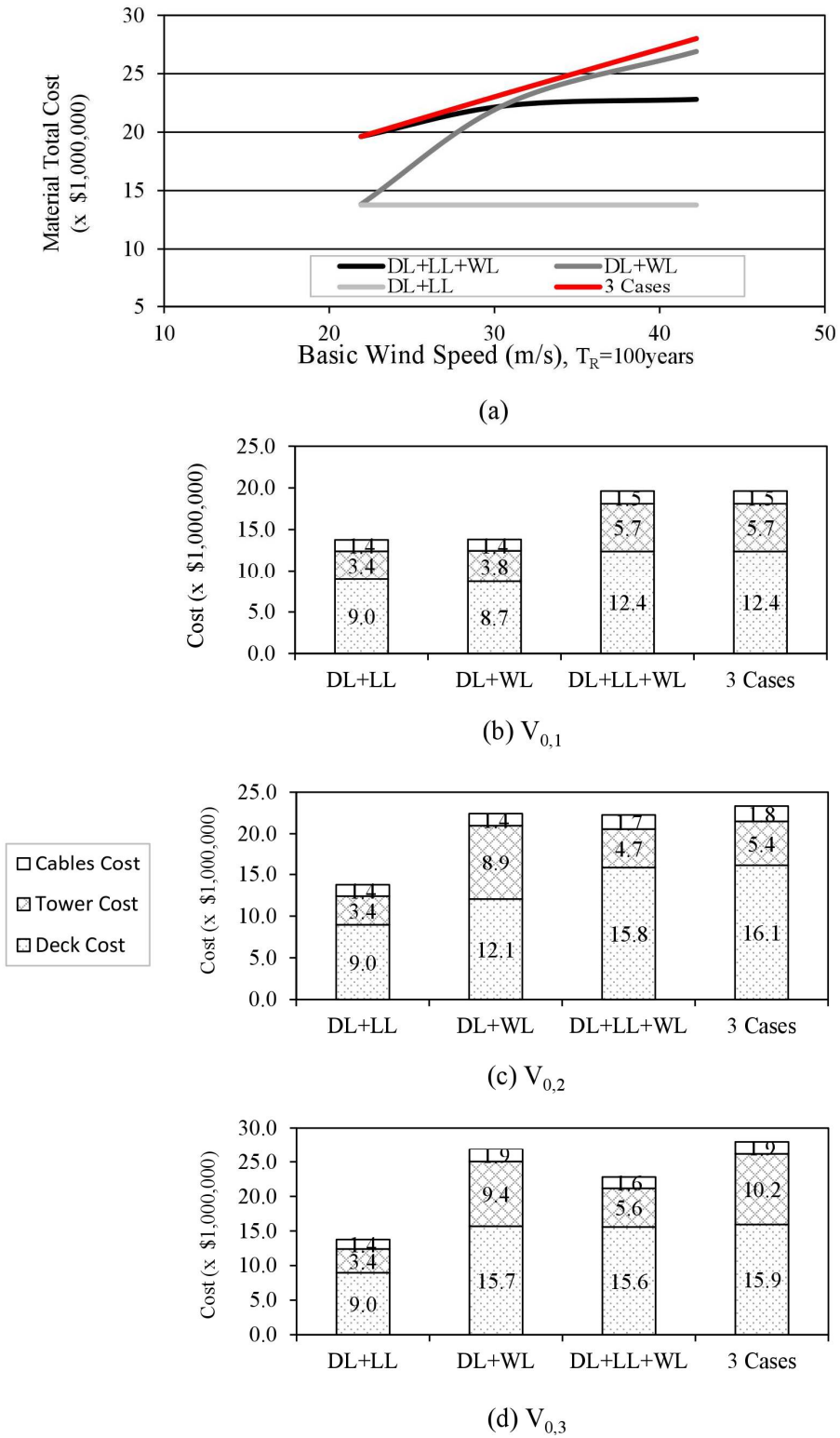


Figure 4. 3: Optimized material cost for distinct load combinations and different basic wind velocities.

Figure 4. 3.b-d shows that for the lowest wind velocity $V_{0,1}$, the Three Cases configuration presents the same material cost as DL+LL+WL case. For the wind velocity $V_{0,2}$, DL +WL case and DL+LL+WL case represent 96.1% and 95.3% of the Three Cases material cost, respectively. And for $V_{0,3}$, DL +WL case is equivalent to 96.4% of the Three Cases material cost. Results show that for lower wind speeds there is more influence of live and wind loads combined together (DL+LL+WL case), but the effect of wind loads (DL+WL case) on the structure become more pronounced as wind speed increases. For the intermediary wind velocity $V_{0,2}$, both DL+WL case and DL+LL+WL case are equally important for the final design.

Overall, these analyses demonstrate not only the importance of considering the mean and buffeting wind loads during the structural optimization process, but also of considering the Three Cases load combinations simultaneously.

4.3.2.2 Influence of evaluating different SLS parameters and deck rigidity and tower longitudinal stiffness behavior

All results from this section are obtained considering the three cases load combinations (DL+LL, DL+WL, DL+LL+WL) as it was previously determined in Section III.3.2.1. The influence of evaluating different SLS parameters is investigated by optimizing the cases A1 ($T_{R,SLS} = 10$ years; $C_3 = C_4 = 800$), B1 ($T_{R,SLS} = 2$ years; $C_3 = C_4 = 800$) and C1 ($T_{R,SLS} = 2$ years; $C_3 = C_4 = 400$), previously described in Table 4. 3.

Table 4. 5 presents the deck limiting constraints and the bridge material cost for nine cable-stayed bridges optimization analyses. The material cost from the most severe (A1) to the most bland (C1) case is reduced by 15.3%, 5.15% and 6.79% for the basic wind velocities $V_{0,1}$, $V_{0,2}$, and $V_{0,3}$, respectively. For the cases A1 and B1, the limiting design constraint of the deck is the vertical displacements due to dead, live and wind loads. For case C1, the limiting constraint at the deck is no longer displacements, but constraints related to resistance. This is explained by the value of constants C_3 and C_4 , which are equal to 800 for cases A1 and B1, and equal to 400 for case C1.

Table 4. 5: Deck limiting design constraint and material cost for cases A1, B1 and C1.

Wind (m/s)	A1		B1		C1	
	g_i	Cost (\$x10 ⁶)	g_i	Cost (\$x10 ⁶)	g_i	Cost (\$x10 ⁶)
V _{0,1}	0.029(g_4)	19.6	0.001(g_4)	17.4	0.226(g_{14})	16.6
V _{0,2}	0.023(g_4)	23.3	0.021(g_4)	22.1	0.328(g_{15})	22.1
V _{0,3}	0.013(g_4)	28.0	0.001(g_4)	27.9	0.034(g_{15})	26.1

Notes: V_{0,1}, V_{0,2} and V_{0,3} according to Table 4. 2

The relationship between deck rigidity and tower longitudinal stiffness for cases A1, B1 and C1 is presented in Figure 4. 4.(a). For all three cases, by increasing wind velocity from V_{0,1} to V_{0,2}, there is an accentuated augmentation of deck rigidity while a small increase of tower longitudinal stiffness is observed. When varying the wind velocity from V_{0,2} to V_{0,3} the opposite behavior is perceived, a considerable increase of tower stiffness accompanied by a small increase of deck stiffness.

In Figure 4. 4.(b-d), the inner circle corresponds to V_{0,1} while the exterior represents V_{0,3}. These graphs show that the optimized solutions for V_{0,2} present the greater proportion of deck cost ($\approx 70\%$ of the total material cost) when compared to the other basic wind velocities. These observations can be explained by the connected behavior of deck rigidity and tower stiffness displayed in Figure 4. 4.(a).

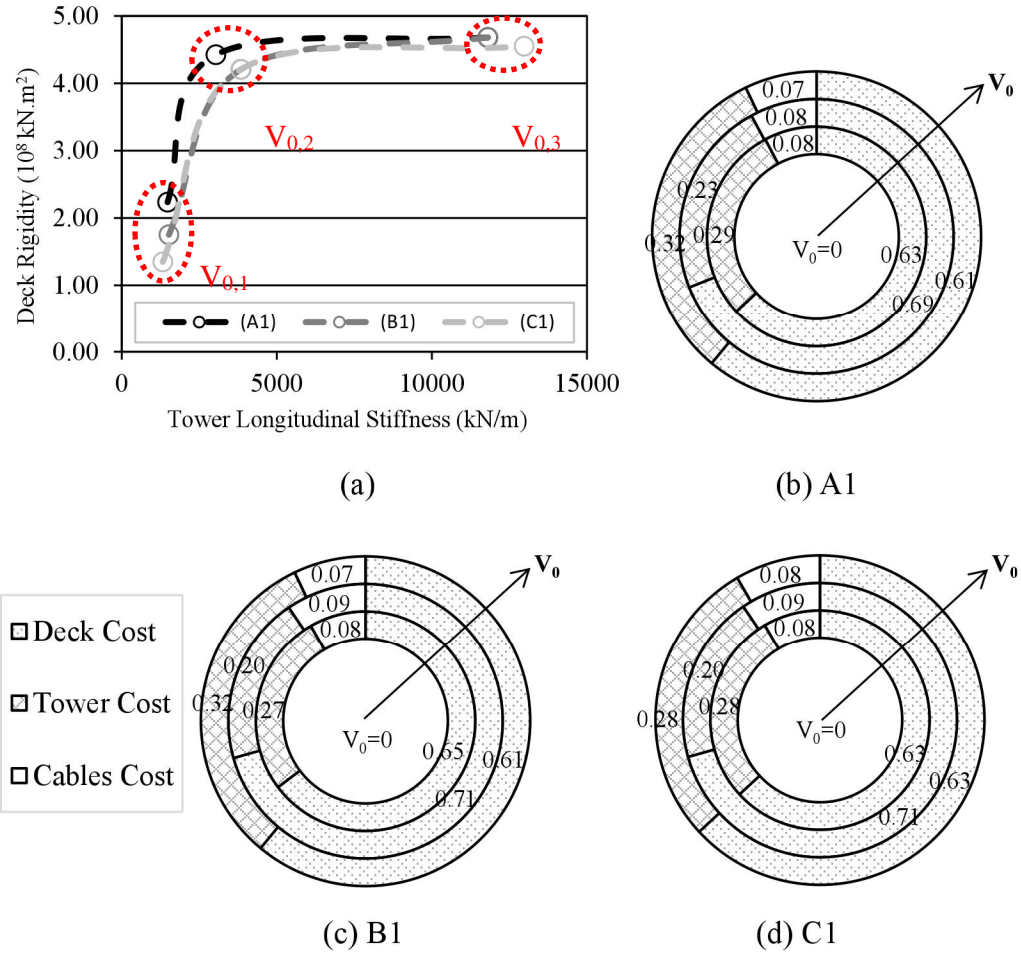


Figure 4. 4: (a) Relation between deck rigidity and tower longitudinal stiffness; (b), (c), (d) proportion of elements material cost for cases of analysis (A1), (B1), and (C1).

4.3.2.3 Influence of evaluating susceptibility to aerodynamic excitations

The results for six cases of analysis described in Table 4. 3, considering (A2, B2, and C2) or disregarding the susceptibility to aerodynamic excitations (A1, B1, and C1) are presented in Figure 4. 5. For basic wind velocity $V_{0,1}$, the same optimized structure is obtained with or without aerodynamic considerations, which infers that these wind speeds are too low to excite aerodynamic phenomena.

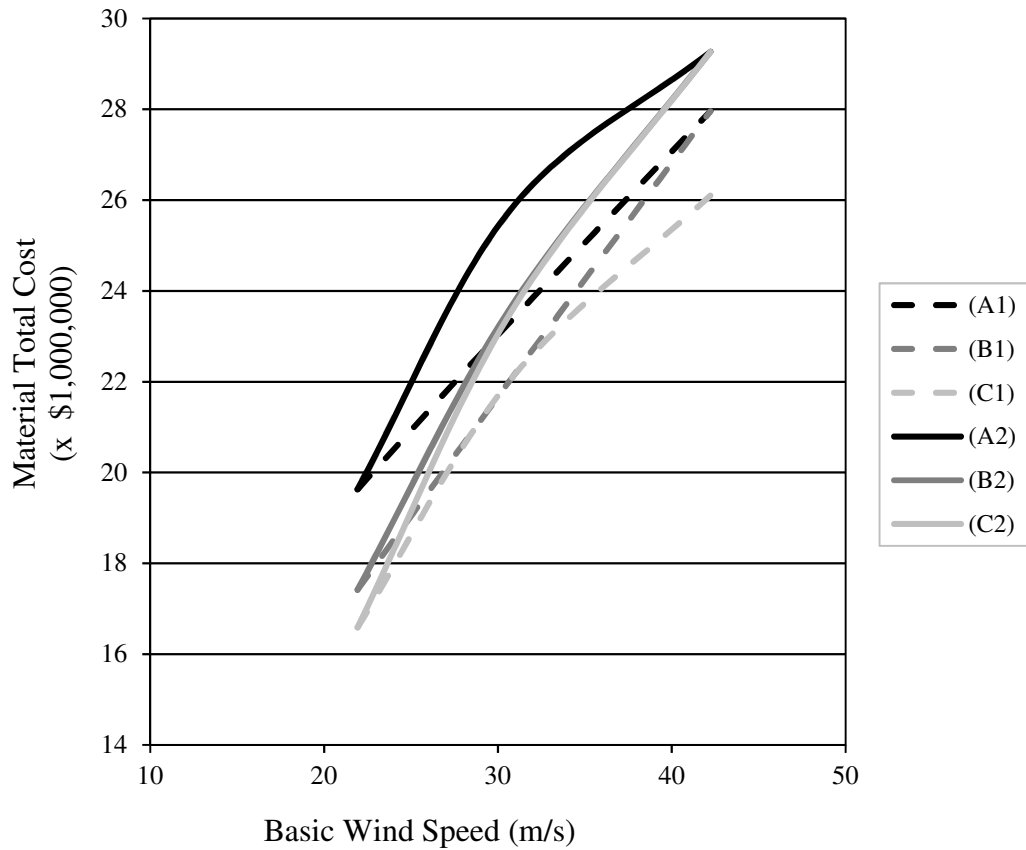


Figure 4. 5: Material total cost optimized for the six main cases of analysis: A1, B1, C1, A2, B2 and C2.

For basic wind velocity $V_{0,2}$, the optimized structures delivered for cases A1, B1 and C1 are susceptible to vortex shedding excitation. The optimized cable-stayed bridges provided by A2, B2 and C2 when compared to A1, B1 and C1 have a significant increase of tower longitudinal stiffness, varying between 40.4% and 56.7%, which reflects in the frequencies of vertical modes of vibration. The increase of material cost is equal to 9.6%, 6.7% and 6.3% for A2, B2 and C2, respectively. The geometry and dynamic properties of the optimized cable stayed bridges obtained for $V_{0,2}$ are presented in Table 4. 6.

For basic wind velocity $V_{0,3}$, the optimized structures provided by cases A1, B1 and C1 are susceptible to classical flutter. Cases A2, B2 and C2 give the same optimized cable stayed-bridge. This is explained by the fact that the limiting constraint is the critical velocity for classical flutter ($l_5 = 8.1 \times 10^{-4}$, Eq. 4.23), which does not depend on the parameters that differentiate

A2, B2 and C2. The increase in material cost varies between 4.30% (A1 to A2) and 10.8% (C1 to C2).

Table 4. 6: Design variables, frequencies and damping ratios for optimized cable-stayed bridges considering critical wind velocity $V_{0,2}$.

Element	Variables	Cases of Analysis for $V_{0,2}$					
		(A1)	(A2)	(B1)	(B2)	(C1)	(C2)
Towers	Ha (m)	23.8	32.2	13.4	13.9	13.4	20.6
	Ht (m)	70.8	77.2	60.4	60.9	60.4	67.6
	TL1 (m)	3.39	4.49	3.20	4.44	3.20	4.74
	TL2 (m)	2.30	2.16	2.15	1.92	2.15	2.15
Deck	tc (m)	0.28	0.29	0.25	0.25	0.25	0.25
	D (m)	4.00	4.00	4.00	4.00	4.00	3.75
	b1 (m)	0.691	0.699	0.680	0.710	0.680	0.696
	t1 (m)	0.044	0.044	0.043	0.045	0.043	0.044
	b2 (m)	0.922	0.932	0.906	0.946	0.906	0.928
	t2 (m)	0.044	0.044	0.043	0.045	0.043	0.044
	w (m)	0.039	0.039	0.039	0.038	0.039	0.036
Cables	N	7	6	7	7	7	7
1 st lateral bending mode	f (Hz)	0.65	0.60	0.62	0.61	0.62	0.67
	ξ_s (%)	0.64	0.64	0.64	0.64	0.64	0.64
	ξ_a (%)	0.11	0.11	0.12	0.12	0.12	0.11
	ξ_t (%)	0.75	0.75	0.76	0.76	0.76	0.75
1 st vertical bending mode	f (Hz)	0.39	0.42	0.38	0.42	0.38	0.42
	ξ_s (%)	0.64	0.64	0.64	0.64	0.64	0.64
	ξ_a (%)	3.03	1.92	3.33	2.16	3.33	2.09
	ξ_t (%)	3.67	2.56	3.97	2.80	3.97	2.73
1 st torsional mode	f (Hz)	0.89	0.92	0.84	0.91	0.84	0.95
	ξ_s (%)	0.64	0.64	0.64	0.64	0.64	0.64
	ξ_a (%)	0.42	0.69	0.10	0.64	0.10	0.68
	ξ_t (%)	1.06	1.33	0.74	1.28	0.74	1.32
Total Cost (x\$1,000,000)		23.337	25.802	22.058	23.644	22.058	23.531

Notes: ξ_s : structural damping; ξ_a : aerodynamic damping; $\xi_t = \xi_s + \xi_a$: total damping; $V_{0,1}$, $V_{0,2}$ and $V_{0,3}$ according to Table 4. 2.

4.4 Conclusions

In this study, the structural optimization of composite steel-concrete two I-girder cable-stayed bridges is performed by using a numerical tool that combines a Discrete Phases Design Approach, Finite Element Model (FEM) and Real Coded Genetic Algorithm (RCGA). Six main variables – number of stay-cables, deck I-girder inertia, thickness of concrete slab, tower height above the deck, and tower cross-section external dimension – are optimized via RCGA with the objective of obtaining the minimum material cost that attend all the design constraints. Secondary variables that are directly dependent on the main variables – deck I-girder dimensions, stay-cables areas and pre-tensioning forces – are determined throughout the phases that compose the Discrete Phases Design Approach.

The structural optimization considers dead and superimposed loads, live loads, mean and buffeting wind loads. The design constraints include SLS and ULS requirements, besides critical wind velocities of aerodynamic excitations. Three different hourly mean basic wind velocities are evaluated.

The significance of considering wind loads in the optimization process varies depending on many factors: basic wind speed and topography at the construction site; design code load factors; restrictions to the maximum displacements applied to the deck and towers specified by the designer; etc. Although there is a great number of possible configurations, comparing material cost as well as the main design variables for the different cases of analysis, it is observed that the wind loads have an important role in the structural optimization.

Contrasting results for three separated load combinations (DL+LL, DL+WL or DL+LL+WL) and for all the combinations simultaneously (Three Cases) shows the importance of considering the former during the optimization process. Among the three separated load combinations, DL+LL+WL tends to be the most important combination for lower basic wind velocities while DL+WL is more significant for higher wind speeds.

When comparing optimized cable-stayed bridge solutions for different SLS parameters, the cases with more severe restrictions provide higher values of material cost as expected. But most important, same relations between deck rigidity and tower longitudinal stiffness are observed with the increase of basic wind velocity, regardless of the SLS parameters adopted by the designer.

The results also show the importance of considering the critical wind velocities of aerodynamic stability, especially for higher values of basic wind velocity. A maximum increase in material cost of 10.8% is observed when taking into account the aerodynamic design constraints during the optimization.

Overall, the results show that when the structure is optimized without considering the wind loads, the structure tends to be more flexible and do not attend all the design requirements. In many cases of analyses, especially the ones with higher wind speeds, the final cable-stayed bridge optimized structure is obtained by considering not only dead, superimposed, live and wind loads, but also by considering restrictions to aerodynamic phenomena.

References

- AASHTO. 2012. LRFD Bridge Design Specifications, 6th edition, Washington, D.C., USA.
- Adeli, H., Zhang, J., 1995. Fully nonlinear analysis of composite girder cable-stayed bridges. *Computers & structures*, 54(2): 267-277.
- BD 49/01. 2001. Design Manual for Roads and Bridges, Volume 1. Highways Structures Approval Procedures and General Design, Section 3. General Design, Part 3 – Design Rules for Aerodynamic Effects on Bridges.
- CAN/CSA-S6-14, 2014, Canadian Highway Bridge Design Code.
- Chen, D.W., Au, F.T.K., Tham, L.G., and Lee, P.K.K. 2000. Determination of initial cable forces in prestressed concrete cable-stayed bridges for given design deck profiles using the force equilibrium method. *Computers and Structures*, 74(1): 1–9.
- Cook, N. 2007. Designer`s guide to EN1991-1-4 Eurocode 1: actions on structures, general actions, part 1-4: wind actions. Thomas Telford, UK.
- CNR-DT 207. 2008. Guide for the Assessment of Wind Actions and Effects on Structures. National Research Council of Italy.
- Davenport, A.G. 1966. The action of wind on suspension bridges. Keynote Paper. Intl. Symp. Suspension Bridges.
- Davenport, A.G. 1977. The prediction of the response of structures to gusty wind. International Research Seminar on Safety of Structures under Dynamic Loading, Trondheim, Norway, v. 1, pp.257-284.
- Davenport, A.G., King, J.P.C. 1982. Technical report. A Study of Wind Effects for the Sunshine Skyway Bridge, Tampa, Florida – Concrete Alternate. The Boundary Layer Wind Tunnel Laboratory – The University of Western Ontario, London, Ontario, Canada.
- Davenport, A.G., King, J.P.C. 1984. Dynamic wind forces on long span bridges using equivalent static loads. IABSE, 12th Congress, Vancouver, BC, Canada, pp. 705-712.
- Deb, K. 2000. An efficient constraint handling method for genetic algorithms. *Computer methods in applied mechanics and engineering*, 186: 311-338.
- EN 1991-1-4. 2005. Eurocode 1: Actions on structures - Part 1-4: General actions - Wind actions.
- Ernst, J.H. 1965. Der E-Modul von Seilen unter berucksichtigung des Durch- hanges. *Der Bauingenieur*, 40(2): 52–55 (In German).

- ESDU 74031. 1974. Characteristics of atmospheric turbulence near the ground, Part II: Single point data for strong winds (neutral atmosphere), Engineering Sciences Data Unit.
- Ferreira, F.L.S., Simoes, L.M.C. 2011. Optimum design of a controlled cable stayed bridge subject to earthquakes. *Structural and Multidisciplinary Optimization*, 44(4): 517–528.
- Hassan, M.M., Nassef, A.O., and El Damatty, A.A. 2012. Determination of optimum post-tensioning cable forces of cable-stayed bridges. *Engineering Structures*, 44: 248–259.
- Hassan, M.M., Nassef, A.O., and Damatty, A.A. El. 2013a. Surrogate Function of Post-Tensioning Cable Forces for Cable-Stayed Bridges. *Advances in Structural Engineering*, 16(3): 559–578.
- Hassan, M.M., Nassef, A.O., and Damatty, A.A. El. 2013b. Optimal design of semi-fan cable-stayed bridges. *Canadian Journal of Civil Engineering*, 40(3): 285–297.
- Hassan, M.M., El Damatty, A.A., and Nassef, A.O. 2014. Database for the optimum design of semi-fan composite cable-stayed bridges based on genetic algorithms. *Structure and Infrastructure Engineering*, 11(8): 1054–1068.
- Holmes, J.D. 2015. Wind loading of structures. 3 ed. Taylor & Francis Group.
- Jacobson L., Kanber, B. 2015. Genetic algorithms in Java basics. Apress.
- Janjic, D., Pircher, M., and Pircher, H. 2003. Optimization of Cable Tensioning in Cable-Stayed Bridges. *Journal of Bridge Engineering*, 8(3): 131–137.
- King, J.P.C., Kopp, G., Vickery, P.J., Mikitiuk, M., Kong, L. 2005. Technical report. A structure of wind effects for Prospect Verona Bridge Maine, USA. The Boundary Layer Wind Tunnel Laboratory – The University of Western Ontario, London, Ontario, Canada.
- Köppel, J., *Buchs and Bacchetta: Rheinbrücke Diepoldsau*. In: SchweizerIngenieur und Architekt, pp 1-6, 818-821, 1984 apud Svensson, H., 2012, Cable-Stayed Bridges, 40 Years of Experience Worldwide. 1 ed. Ernst & Sohn GmbH & Co.KG.
- Kramer O. 2017. Genetic algorithm essentials, *Studies in Computational Intelligence* 679. Springer.
- Lin, Y.Y., Cheng, C.M., Wu, J.C., Lan, T.L., Wu, K.T. 2005. Effects of deck shape and oncoming turbulence on bridge aerodynamics. *Tamkang Journal of Science and Engineering*, 8(1): 43–56.

- Long, W. 1999. Optimum design of cable-stayed bridges. *Structural Engineering and Mechanics*, 7(3): 241–257.
- Martins, A.M.B., Simões, L.M.C., Negrão, J.H.J.O. 2015. Cable stretching force optimization of concrete cable-stayed bridges including construction stages and time-dependent effects. *Structural and Multidisciplinary Optimization*, 51(3): 757–772.
- Matsuda, K., Hikami, Y., Fujiwara T., Moriyama, A. 1999. Aerodynamic admittance and the ‘strip theory’ for horizontal buffeting forces on a bridge deck. *Journal of Wind Engineering and Industrial Aerodynamics*, 83: 337-346.
- Michalewicz, Z., Fogel, D.B. 2000. *How to solve it: modern heuristics*. Springer-Verlag Berlin Heidelberg.
- Negrão, J.H.O., Simões, L.M.C. 1997. Optimization of Cable-Stayed Bridges with Three-Dimensional Modelling. *Computers & Structures*, 64: 741-758.
- Podolny JR, W., SCALZI, J.B. 1976. *Construction and Design of Cable-Stayed Bridges*. John Wiley & Sons, Inc. USA.
- Rao, S.S. 2009. *Engineering optimization: theory and practice*. 4 ed. John Wiley & Sons, Inc.
- RSMeans. 2013. *Heavy Construction Cost Data 2013*. RSMeans Engineering Department, 27th Edition.
- Simiu, E., Scanlan, R.H., 1996. *Wind Effects on Structures: Fundamentals and Applications to Design*. 3 ed. John Wiley & Sons, Inc.
- Simões, L.M.C., and Negrão, J.H.O. 1994. Sizing and geometry optimization of cable-stayed bridges. *Computers & Structures*, 52(2): 309-321.
- Simões, L.M.C., and Negrão, J.H.J.O. 2000. Optimization of cable-stayed bridges with box-girder decks. *Advances in engineering software*, 31(6): 417–423.
- Solari, G. 1987. Turbulence modeling for gust loading. *Journal of Structural Engineering*, 113(7): 1550-1569.
- Solari, G. 1993b. Gust buffeting. I: peak wind velocity and equivalent pressure. *Journal of Structural Engineering*, 119(2): 365-382.
- Solari, G. 1993b. Gust buffeting. II: dynamic alongwind response. *Journal of Structural Engineering*, 119(2): 383-398.
- Svensson, H. 2012. *Cable-Stayed Bridges. 40 Years of Experience Worldwide*. 1 ed. Ernst & Sohn GmbH & Co.KG.

- Troitsky, M. S. 1988. Cable-Stayed Bridges: Theory and Design. 2 ed. BSP Professional Books, Oxford.
- Wang, P H; Tseng, T C; Yang, C.G. 1993. Initial shape of cable-stayed bridges. Computers & Structures , 47(I): 111–123.
- Wight J.K., MacGregor, J.G. 2009. Reinforced concrete: mechanics and design. 6 ed. Pearson.
- Wilson, J.C, and Gravelle, W. 1991. Modelling of a cable-stayed bridge for dynamic analysis. Earthquake Engineering and Structural Dynamics, 20(8): 707–721.
- Zhu, L.D., Wang, M., Wang, D.L., Guo, Z.S., Cao, F.C. 2007. Flutter and Buffeting Performances of Third Nanjing Bridge over Yangtze River under Yaw Wind via Aeroelastic Model Test. Journal of Wind Engineering and Industrial Aerodynamics, 95: 1579-1606.

Chapter 5

5 Conclusions and Recommendations

The aim of this thesis is to perform structural optimization of two I-girder steel concrete composite cable-stayed bridges under permanent and transitory loads, with focus on evaluating the influence of considering moving live loads and buffeting wind loads. Chapter 1 provided an overview about stay-cable bridges configurations and behavior, and literature review related to the optimization of this type of structure. The optimization procedure based on FEM, RCGA and Discrete-Phase Design Approach was first introduced in Chapter 2, which consider permanent and moving live loads in the optimization process. In Chapter 3, a correlation between displacements of theoretical and experimental approaches due to mean and buffeting wind loads was performed to validate the former approach. The theoretical approach, validated in Chapter 3, was used in Chapter 4 for considering the structural optimization of cable-stayed bridges under the action of permanent loads, moving live loads, mean and buffeting wind loads. Items 5.1 to 5.3 summarize the main conclusions of each data chapter.

The structural optimization of cable-stayed bridges presented in this thesis provides a preliminary design. In order to perform the final design, some extra analysis and design cases, as described in Item 5.4, must be added to the numerical tool. Although the structural optimization delivers a preliminary design of cable-stayed bridge, the numerical tool has great contribution to the literature due to the inclusion of wind action. The comparisons presented in Chapter 4 demonstrate that by disregarding the wind action (mean and buffeting wind loads, as well as critical velocities of the aerodynamic phenomena), there is great possibility of having a preliminary design that will require significant modification when wind tunnel test is performed.

The material costs of optimum cable-stayed bridge solutions obtained in this thesis could not be compared to the material costs of cable-stayed bridges in service, once the former consists of a preliminary design as previously explained. Another fact that should be mentioned is that the conclusions presented for the structural optimization along the thesis

and summarized below depend on the lower and upper bounds adopted for the design variables and on the geometric values that were assumed constant.

5.1 Structural optimization of two I-girder composite cable-stayed bridges under the action of dead and live loads

Chapter 2 introduces the Discrete-Phases Approach that has two main characteristics. First, the variables are divided into two categories: (i) main variables: number of stay-cables, I-girder inertia, concrete slab thickness, tower cross-section external dimensions; (ii) secondary variables: I-girder dimensions, stay-cable areas and pre-tensioning forces. While the main variables are considered as design variables to be optimized via RCGA, the secondary variables are optimized indirectly by discrete phases. Secondly, the way the Discrete-Phases Approach was implemented simplifies the addition of new phases to account for other effects.

For considering the action of permanent and live loads, the Discrete-Phases Approach is composed of five phases: (i) Phase 1 determines I-girder dimensions to minimize the cross-section area; (ii) Phase 2 calculates stay-cables cross-sectional areas; (iii) Phase 3 determines stay-cables pre-tensioning forces, displacements and internal forces due to dead loads; (iv) Phase 4 estimates displacements and internal forces of the bridge under the action of live loads; and (v) Phase 5 combines the results from Phases 3 and 4 to check if they satisfy the ULS and SLS criteria.

Two design objectives were tested: (i) lightest deck mass; (ii) lowest material cost. Three load cases were considered: (i) dead and truck plus lane live loads; (ii) dead and lane live loads; (iii) dead load. The following conclusions can be drawn from this chapter:

- (i) The displacements obtained for the optimal solution in both deck and towers had very small values, demonstrating the efficiency of the design performed by the Discrete-Phases Design Approach together with RCGA and FEM.

- (ii) For the lightest deck mass as objective function, the tower cross-section dimensions tended to reach their upper bounds in order to provide a very rigid tower. The tower height above the deck also tended to reach its upper bound value to increase the angle of inclination of stay-cables, and consequently the capacity of supporting the deck.
- (iii) The displacements of both deck and towers approached the limiting constraints of all optimal solutions that considered deck mass as the objective function. This allowed the construction of curves that relate deck rigidity, towers stiffness and stay-cables mass and can be used for any type of deck and tower cross-sections.
- (iv) Stay-cables mass increase/decrease with an increase/decrease of deck mass, once the stay-cable cross-sectional areas were determined using a continuous beam FEM model of the deck.
- (v) By considering the truck in live load analysis, the deck mass value increased up to 12% when compared to optimum solutions that only consider uniformly distributed live load. These results demonstrate the importance of considering both truck and uniformly distributed live loads in the optimization process.
- (vi) When material cost was considered as the objective function, the optimal solutions could not be directly compared to the ones for the lightest deck mass. Despite this, when the solutions present analogous tower cross-section, their material cost differs by less than 5%.

5.2 Comparison between the theoretical and experimental wind responses of a full aeroelastic model test of a cable-stayed bridge

A comparison between the wind response of a cable-stayed bridge predicted by theoretical and experimental approaches was performed. In the theoretical approach, buffeting equivalent static forces due to turbulent wind flow were calculated taking into account static force coefficients provided by the static sectional model test, and other parameters such as gust spectral density, aerodynamic admittance, and joint acceptance function. Wind loads were then applied to the finite element model of a cable-stayed bridge case study to obtain mean and peak displacements of the deck and towers. These results were compared to the corresponding displacements obtained from the experimental approach, i.e. the full aeroelastic model test of the same bridge.

Some sources of uncertainties that can explain the differences in results between the two approaches were identified: (i) the theoretical vertical turbulence intensity profile could not be checked against the experimental one; (ii) in the lack of flutter derivatives values provided by dynamic sectional model tests, the theoretical approach considered approximated aerodynamic damping ratio equations; (iii) the theoretical approach also considered approximated aerodynamic admittance functions, which are naturally taken into account by the experimental approach; and (iv) unlike the theoretical approach, the experimental approach considered the features of the terrain and was able to identify other phenomena like vortex shedding and flutter. Despite the uncertainties summarized above, the theoretical-experimental correlations presented in Chapter 3 were very good for rotations, and more than satisfactory for drag and lift displacements at the deck. The correlations showed that the theoretical approach overall can successfully estimate the displacements of the experimental approach.

5.3 Structural optimization of two I-girder composite cable-stayed bridges under the action of dead, live and wind loads

As suggested by the bibliography presented in Chapter 1, the objective of Chapter 4 was to cover a gap in the literature, which is the consideration of buffeting wind loads during the optimization process of cable-stayed bridges. The structural optimization of steel-concrete composite I-girders cable-stayed bridges under the action of permanent loads, live loads, mean and peak buffeting wind loads was performed through the numerical tool used in Chapter 2 that is based on FEM, RCGA and Discrete-Phases Approach. In order to account for the wind effect, three new phases were added to the Discrete-Phases Approach: (i) for performing free vibration analysis; (ii) for determining displacements and internal forces due to mean and peak buffeting wind loads; and (iii) for estimating the critical wind velocities for aeroelastic phenomena.

A cable-stayed bridge case of study was optimized for obtaining the lowest material cost for the structure. Three basic wind velocities were evaluated, and different SLS parameters were assessed. Three load combinations were considered: (i) dead and live loads (DL+LL); (ii) dead, mean and buffeting wind loads (DL+WL); (iii) dead, live, mean and buffeting wind loads (DL+LL+WL). The conclusions that can be drawn from this chapter are:

- (i) Discrete-Phase Design Approach's advantage related to the practicality of incorporating new phases to account for other effects has been verified.
- (ii) The results showed that the load combinations DL+LL+WL and DL+WL tend to be the most critical case for lower and higher wind velocities, respectively. This demonstrates the importance of considering wind loads even for the lowest value of basic wind speed ($V_{0,1}$).
- (iii) The same relations between deck rigidity and tower longitudinal stiffness were observed with the increase of basic wind speed, independently of the SLS parameters adopted for the structural optimization process.

- (iv) The results demonstrated that by considering critical wind velocities of aerodynamic phenomena as constraints, the material cost increased up to 10.8%, demonstrating the relevance of these constraints in the optimization process.

Overall, this thesis contributes by providing a new procedure for structural optimization of cable stayed-bridges based on FEM, RCGA, and Discrete-Phases Design Approach. This procedure simultaneously reduces the number of design variables, and facilitates future implementation of additional load cases. Moreover, this thesis demonstrated the significance of considering truck live loads, the importance of evaluating buffeting wind loads and assessing critical wind velocities for aeroelastic phenomena.

5.4 Recommendations for future research

For future research, the following suggestions are made in order to complement this study:

- Add a new phase to the Discrete-Phase Design Approach to calculate the loads due to vortex shedding excitation, instead of considering its critical velocity as a design constraint.
- Add new phases to the Discrete-Phase Design Approach for considering seismic analysis and to evaluate construction stages.
- Add a new phase for performing fatigue analysis.
- Account for the dynamic interaction vehicle-structure.
- Account for the fluid-structure interaction.
- Account for creep and shrinkage of concrete.

Additionally, other parameters can be included to:

- Perform structural optimization for longer spans of cable stayed bridge, with different proportions of main and side spans.
- Consider different number of stay-cables per spans.
- Consider different tower cross-sections along the height and consider the thicknesses of the hollow concrete box cross-section as design variables.
- Consider different deck I-girder inertia of deck cross-section along the bridge length.

Appendices

Appendix A: Examples of cable-stayed bridges constructed in the last 40 years.

Table A. 1: Concrete cross-section cable-stayed bridges (Svensson, 2012).

Cross-section	Bridge Name	Country	Year	Main span (m)
Thin concrete beams	Diepoldsau Bridge	Switzerland	1985	97
	Evripos Bridge	Greece	1993	215
2 concrete girders	River Leven Bridge	Scotland	1995	115.2
	East Huntington Bridge	USA	1985	274
	Rosario-Victoria Bridge	Argentina	2000	330
	Helgeland Bridge	Norway	1991	425
Box girder	Brotonne Bridge	France	1977	320
	2 nd Panama Canal Bridge	Panama	2004	420
	Barrios de Luna Bridge	Spain	1983	440
	Skarnsundet Bridge	Norway	1991	530

Table A. 2: Steel cross-section cable-stayed bridges (Svensson, 2012).

Cross-section	Bridge Name	Country	Year	Main span (m)
Box girder	Alamillo Bridge	Spain	1992	200
	Rhine River at Ilverich Bridge	Germany	2002	287
	Rhine River Wesel Bridge	Germany	2009	335
	Sava at Ada Bridge	Serbia	2011	376
	St. Nazaire Bridge	France	1975	404
	Tatara Bridge	Japan	1999	890
	Sutong Bridge	China	2008	1088
	Russki Bridge	Russia	2012	1104
2 box girders	Stonecutters Bridge	China	2009	1018

Table A. 3: Composite steel-concrete cross-section cable-stayed bridges (Svensson, 2012; Pedro & Reis, 2016)

Cross-section	Bridge Name	Country	Year	Main span (m)
2 plate girders	Heinola Bridge	Finland	1994	165
	Elbe River Bridge	Germany	2008	192
	Burlington Bridge	USA	1993	201
	Quincy Bridge	USA	1987	274
	Cape-Girardeau Bridge	USA	2004	350
	Sunshine Skyway Bridge Composite alternative	USA	1982	366
	Industrial Ring Road Bridges	Thailand	2006	398
	Nanpu Bridge	China	1991	423
	Second Severn Crossing Bridge	South Wales	1996	456
	Alex Fraser Bridge	Canada	1986	465
	Arthur Ravenel Bridge	USA	2005	471
	John James Audubon Bridge	USA	2011	482.5
	Rion-Antirion Bridge	Greece	2005	560
	Erqi Yangtze River Bridge	China	2011	616
3 plate girders	Hooghly Bridge	India	1992	457
4 plate girders	Baytown Bridge	USA	1995	381
	Ting Kau Bridge	Hong Kong	1998	475
2 box girders	Xupu Bridge	China	1997	590
	Yangpu Bridge	China	1993	602
	Queensferry Crossing Bridge	Scotland	2017	650
Truss deck	Karnali Bridge	Nepal	1993	325
	Mercosur Bridge	Venezuela	-	360
	Oresund Bridge	Sweden- Denmark	2000	490
Hybrid	Baluarte Bridge	Mexico	2013	520

References

- Svensson, H. 2012. Cable-Stayed Bridges. 40 Years of Experience Worldwide. 1 ed. Ernst & Sohn GmbH & Co.KG.
- Pedro, J.J., and Reis, A.J. 2016. Composite cable-stayed bridges: state of the art. Proceedings of the Institution of Civil Engineers - Bridge Engineering, 169(1): 13–38.

Appendix B: I-girder dimensions for width-to-thickness limit ratio of Class 3 in order to minimize the cross-section area.

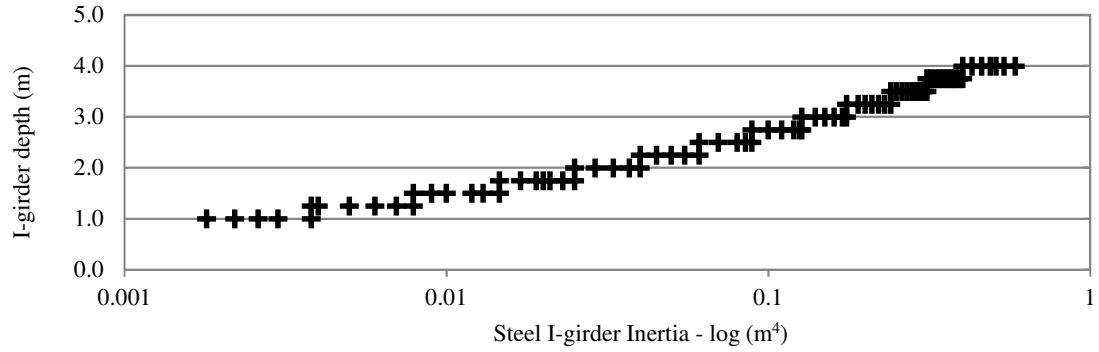


Figure B. 1: I-girder depth as a function of the Class 3 I-girder inertia.

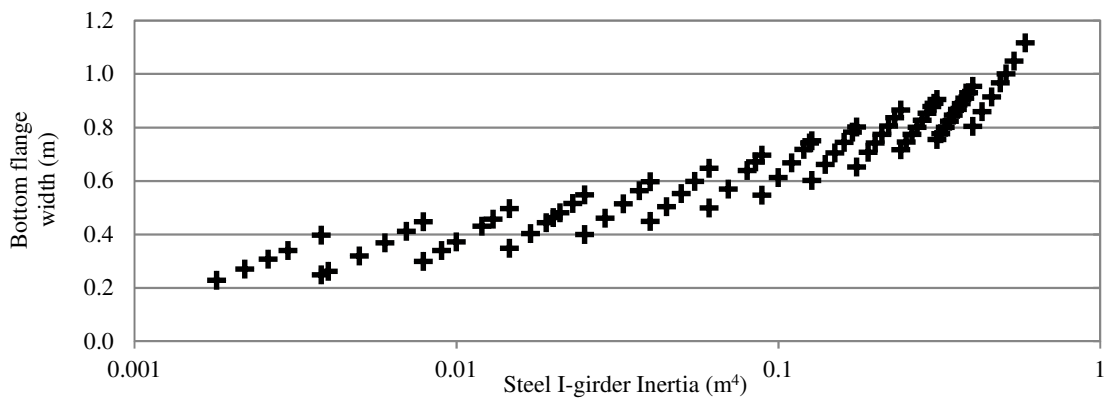


Figure B. 2: Bottom flange width as a function of the Class 3 I-girder inertia.

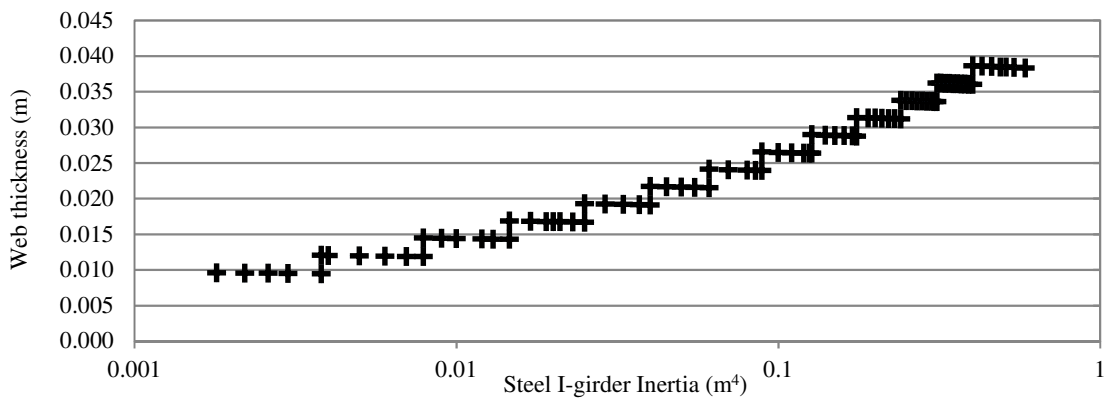


Figure B. 3: Web thickness as a function of the Class 3 I-girder inertia.

Appendix C: I-girder dimensions for width-to-thickness limit ratio of Class 2 in order to minimize the cross-section area.

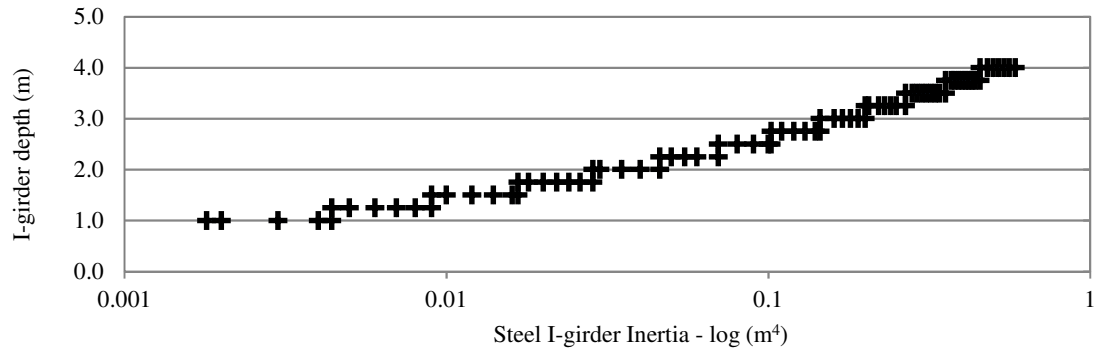


Figure C. 1: I-girder depth as a function of the Class 2 I-girder inertia.

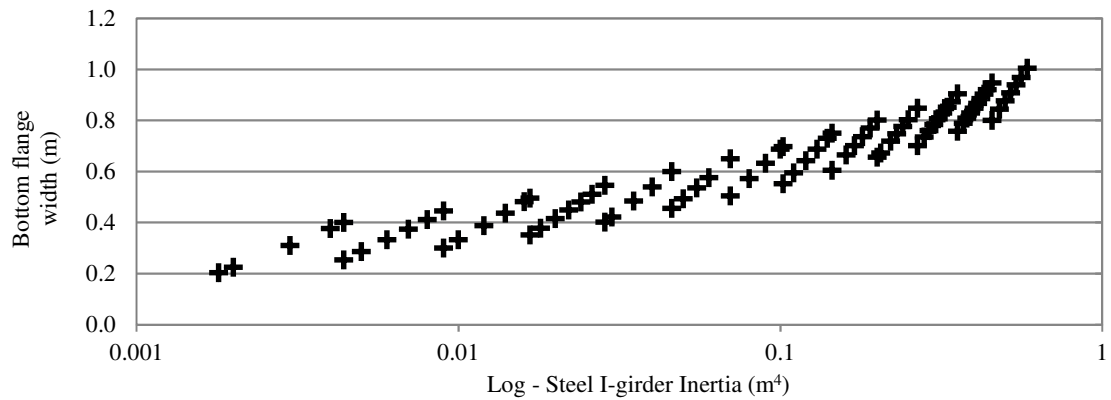


Figure C. 2: Bottom flange width as a function of the Class 2 I-girder inertia.

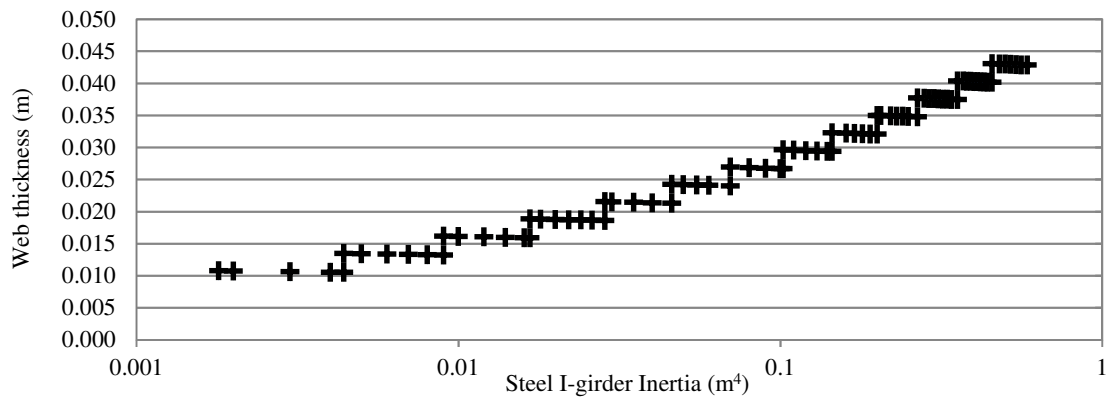


Figure C. 3: Web thickness as a function of the Class 2 I-girder inertia.

Appendix D: Finite element modelling of concrete-steel composite two I-girders deck

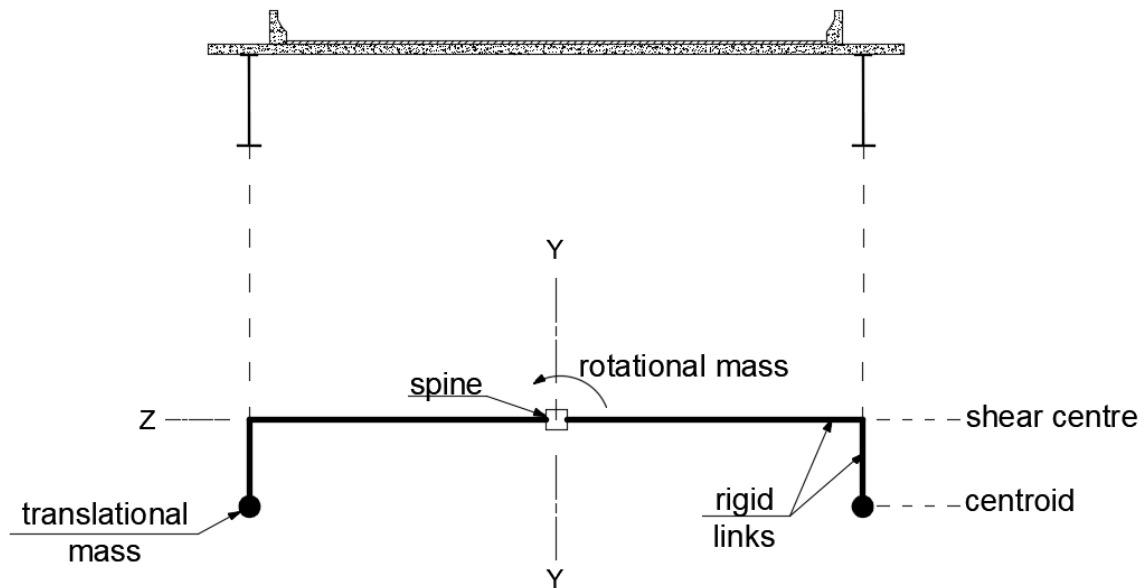


Figure D. 1: Finite element modelling of concrete-steel composite two I-girders deck according to Wilson *et al.* (1991).

The composite steel-concrete deck modelled as a spine is positioned at the concrete slab elevation to provide the correct geometry of the model. Two horizontal rigid links, both with length equal to the half distance between I-girders, are considered to give the correct offset of the stay-cables. In addition, two vertical links with length equal to the distance between the shear centre and the centroid are considered in order to provide the proper torsional and transversal behavior of the deck (WILSON *et al.*, 1991). The stay-cables anchorages at the deck are positioned at the connection of the horizontal and vertical rigid links. Translational masses and rotational masses are applied to the model in order to calculate the mass matrix to be used in the dynamic analysis.

Reference

Wilson, J.C, and Gravelle, W. 1991. Modelling of a cable-stayed bridge for dynamic analysis. *Earthquake Engineering and Structural Dynamics*, 20(8): 707–721.

Appendix E: Aerodynamic coefficients and flutter derivatives

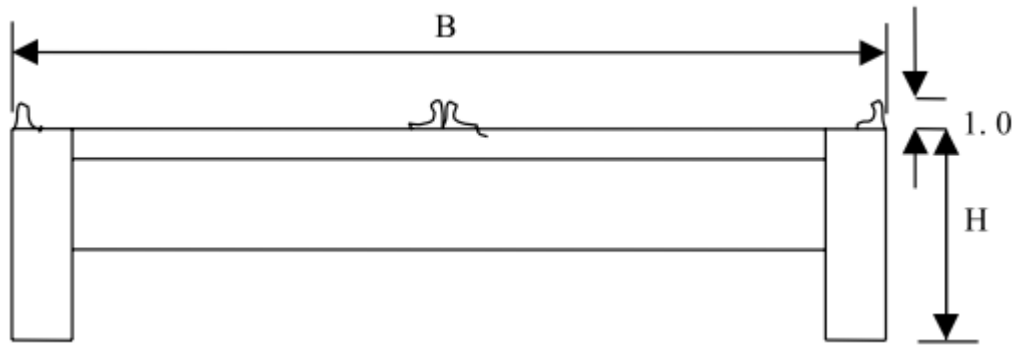


Figure E. 1: Geometry of plate girder section model evaluated by Lin *et al.* (2005).

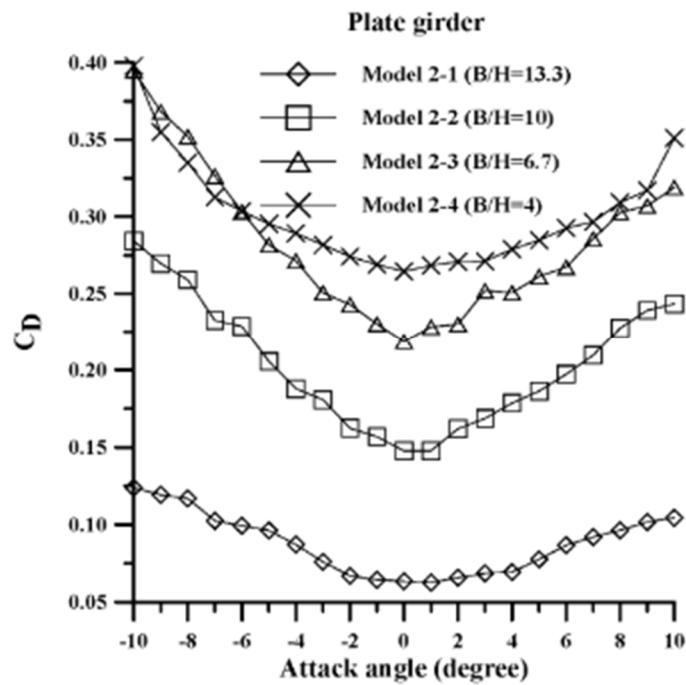


Figure E. 2: Drag coefficients (Lin *et al.*, 2005).

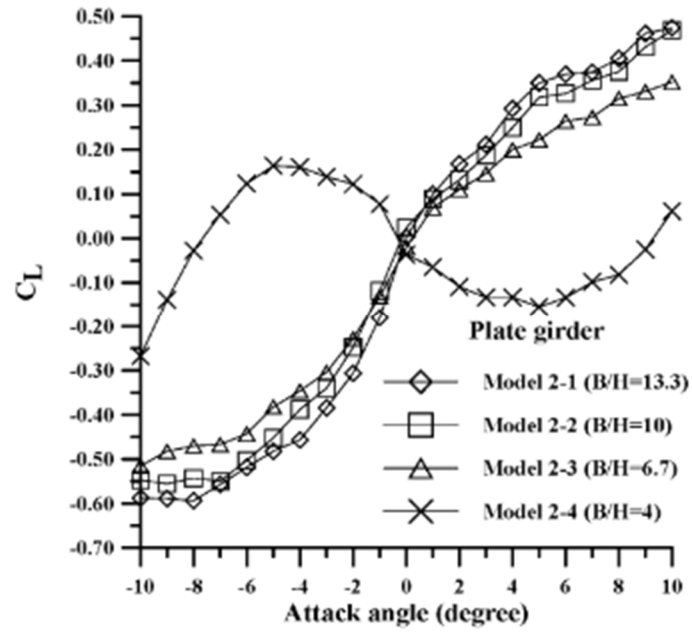


Figure E. 3: Lift coefficients (Lin *et al.*, 2005).

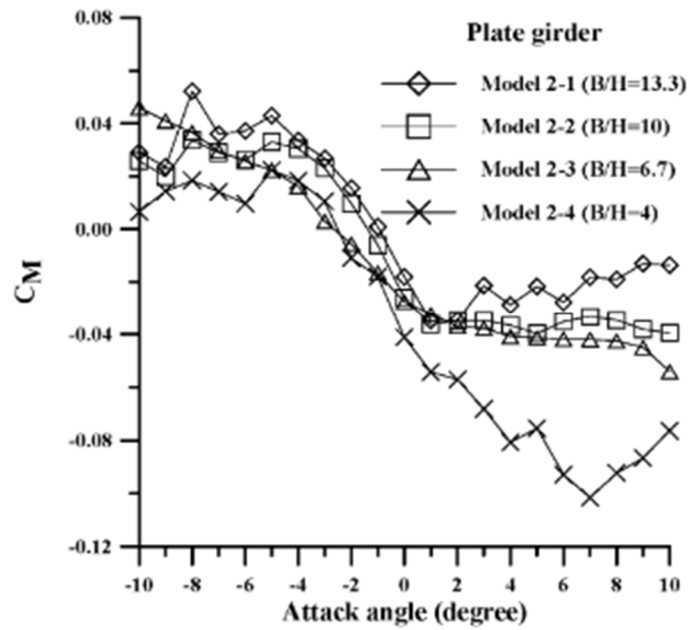


Figure E. 4: Torsional coefficients (Lin *et al.*, 2005).

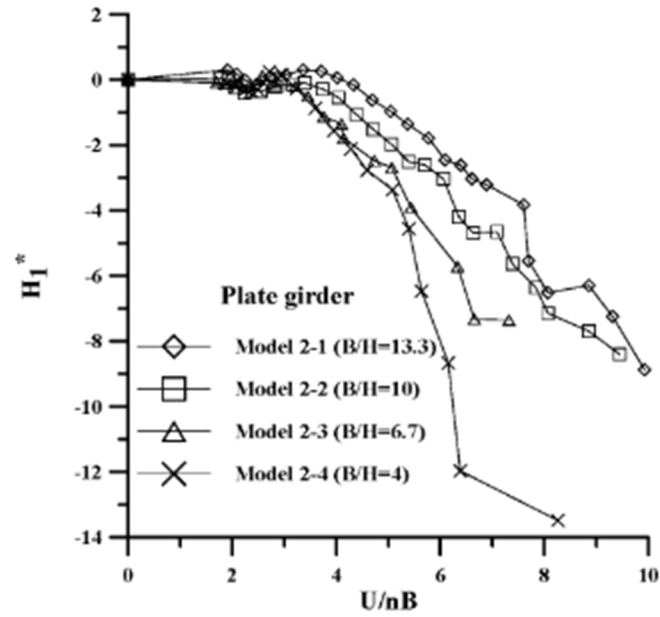


Figure E. 5: Flutter derivative H_1^* (Lin *et al.*, 2005).

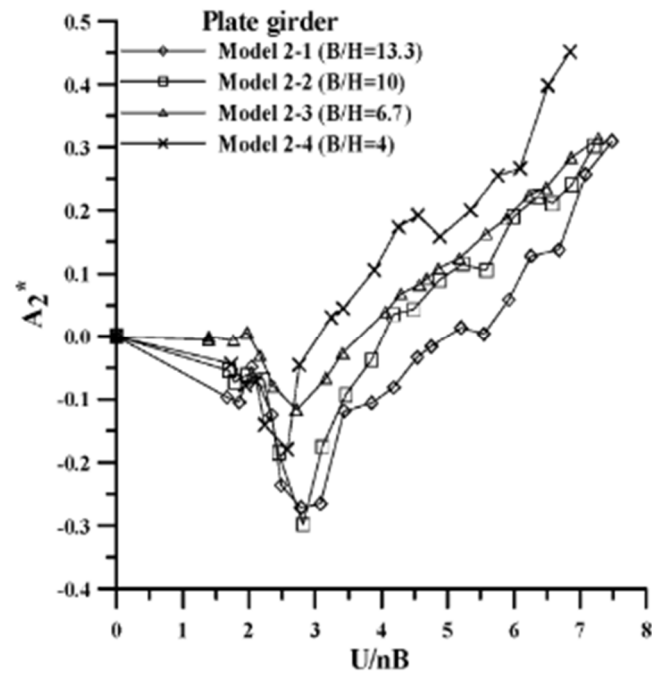


Figure E. 6: Flutter derivative A_2^* (Lin *et al.*, 2005).

References

- Lin, Y.Y., Cheng, C.M., Wu, J.C., Lan, T.L., Wu, K.T. 2005. Effects of deck shape and oncoming turbulence on bridge aerodynamics. *Tamkang Journal of Science and Engineering*, 8(1): 43–56.

Curriculum Vitae

Name:	Carolina Almeida Novaes dos Santos
Post-Secondary Education and Degrees:	<p>Federal University of Rio de Janeiro Rio de Janeiro, RJ, Brazil March 2006 – February 2011 B.S. Civil Engineering</p> <p>Federal University of Rio de Janeiro Rio de Janeiro, RJ, Brazil March 2011 – March 2013 M.Sc. Civil Engineering</p>
Honours and Awards:	<p>Academic Dignity Cum Laude Degree 2011</p> <p>National Council for Scientific and Technological Development (CNPq) PhD Scholarship March 2015 – February 2017</p>
Related Work Experience	<p>Teaching Assistant The University of Western Ontario Fall Term 2016, Fall Term 2017, Winter Term 2018</p> <p>Civil Engineer Controllato – Design, Monitoring and Control of Structures Rio de Janeiro, RJ, Brazil March 2011 – October 2014</p>
Publications:	<p>Santos, C.A.N, El Damatty, A.A., Pfeil, M.S., Battista, R.C., 2019. Structural Optimization of Two-Girder Composite Cable-Stayed Bridges under Dead and Live Loads. Canadian Journal of Civil Engineering. Manuscript revisions in progress.</p>